Mechanical Development of Thermosets During Cure

By

John Puentes

A dissertation submitted in partial fulfillment of

the requirements for the degree of

Doctor of Philosophy

(Mechanical Engineering)

at the

UNIVERSITY OF WISCONSIN-MADISON

2017

Date of final oral examination: 05/04/2017

This dissertation is approved by the following members:

Tim A. Osswald, Professor, Mechanical Engineering
Natalie Rudolph, Assistant Professor, Mechanical Engineering
Lih-Sheng Turng, Professor, Mechanical Engineering
Roderic S. Lakes, Professor, Engineering Physics
Daniel J. Klingenberg, Professor, Chemical and Biological Engineering

Acknowledgements

Many thanks to the collaborators of this project. These include: Alexander Chalupka for the partnership on the kinetic and mechanical analysis of this work, Lorenz Wruck for the collaboration on the Raman spectroscopy, José Colón for the partnership in the mechanical analysis, Brian LaQua and Lucas Iervolino for the collaboration on the warpage measurements, Darcy Davis and Keith Dahl for their collaboration on warpage modeling, and Nora Catalina Restrepo for the mentorship and guidance exploring the complexity of thermosets.

I would also like to thank several faculty and committee members. I took my first lecture in polymer processing with professor Tom Turng. Professor Daniel Klingenberg provided mentorship in transport phenomena. Many of the ideas of this work started by sitting in the lectures of professor Roderic Lakes, thank you for your detailed guidance in many of the technical aspects of this study. Professor Natalie Rudolph has served as a mentor, friend, and role model. Thank you for starting this project and for the trust along the way. No words can express my gratitude with my advisor, professor Tim A. Osswald. Thank you for opening the doors of your lab, lectures, and home, and for the life lessons.

I also want to thank the readers and editors of this manuscript, for your patience and feedback, Thomas Pfeifer, James Baek, Alec Redmac, Whitney Gent, and David Pratt. Thank you to the listeners in the difficult times, thank you for the encouragement, Camilo Pérez, Luisa López, Roberto Monroy, Andrew Schmaltzer, James Baek and Kyle Busch. Thanks to my family for their support and encouragement. Thank you to Emilia Puentes for the graphic design assistance in many graphs and the style of this work. Emilia, you are hope, compassion, and unconditional love. As my soulmate, I am reminded of the beauty of life through your essence. Thank you.

Abstract

Novel experimental and modeling techniques to quantify and correlate the kinetic and mechanical development of thermosets during cure are evaluated in this work. Commercial epoxy adhesives and prepregs are analyzed using standard protocols and improved protocols proposed here. First, the use of initial fast ramps in heat flux differential scanning calorimetry (DSC), up to 500 K/min, was used to follow the isothermal kinetic development of adhesives. More complete kinetics were captured while mitigating cure during the heating step. This was achieved with the optimization of the electronic furnace parameters. The enthalpy spike at the dynamic-to-isothermic transition remains an issue. Preliminary empirical shifts are proposed to compensate the signal lag. This method was used to represent the kinetics in the time-temperature-transformation (TTT) diagram including correction for filler, moisture, and pre-cure history. The formal kinetic method was used giving a simpler model compared to the conventional Kamal-Sourour equation. Second, the moduli development was captured from the gel point up to the fully cured state in a single DMA three-point bending test. A new sample was used by sandwiching a partially cured plate between two fully cured plates of adhesive. Kinetic, viscosity, gel point and shrinkage information were used to delimit and select parameters, the upper, and lower bounds of the moduli. Sandwich beam elastic theory was used to quantify the moduli of samples during cure. This method reduced beam compliance and eliminated signal noise. The previous techniques still measured kinetic and mechanical development using different instruments, masses, sample geometries, and conditions. Third, to solve this problem, an in-situ method attaching ultrasonic transducers and a Raman probe to a mold chamber was used. The degree of cure and moduli were measured simultaneously giving a closer interpretation of the cure-mechanical development interaction. Raman spectroscopy captured more reaction at the initial and propagation stages compared to DSC analyses. It also measured more accurately the end stage governed by diffusion mechanisms. This work concluded

by exploring warpage measurements using a laser measurement device. The method allowed for the capture of a 3D rendering of the mold and the final component. More accurate warpage was quantified for the case of angle distortion in L-shaped parts. The angle distortion was found to strongly depend on the profile thickness. Steps towards implementing the results of this work in a numerical simulation of warpage of composite parts are detailed.

Contents

List of Figures

List of Tables

Chapter 1

Introduction and Motivation

Thermoset adhesives and composites are widely used in the automotive and aircraft industry. Of all polymers produced currently, 88 % correspond to thermoplastics and 12 % to thermosets (see Fig. 1.2) [1]. Construction and building materials cover 30 % of thermoset applications, with electronic, marine, and pipe combined representing 34 % (See Fig. 1.1) [1]. Transportation is the second-largest application with 24 %, exhibiting faster growth promoted by the use of composite components in lightweight automotive and aircraft applications.

Epoxy is considered a high-end thermoset due to its high strength and elastic modulus, excellent performance under fatigue, high toughness, low creep, and high thermal resistance. From the array of thermosets, epoxy resins consist of about 5.3 % of the market [1]. Epoxy adhesives are used in the bonding of a variety of components, such as honeycomb structures, or with metals. Epoxy is also used as the matrix of composites reinforced with fibers, for example to produce airplane fuselages, automotive panels, and bicycle frames.

The successful production of thermoset components and bonding relies on the understanding of the kinetics behavior. A poor understanding can cause component defects such as warpage, delamination, and defective assemblies. Current markets trend towards producing thinner adhesives and prepregs with higher glass transition temperatures, and exhibit higher impact resistance [2–4]. This aims to satisfy the demand for higher tolerances, shorter cycle times and improved mechanical performance. The complex chemistry and behavior of these formulations demand a reevaluation of the standard testing protocols.

The objective of this work is to modify and expand experimental and modeling techniques to quantify the kinetic, thermal, and mechanical behavior of thermosets during cure.

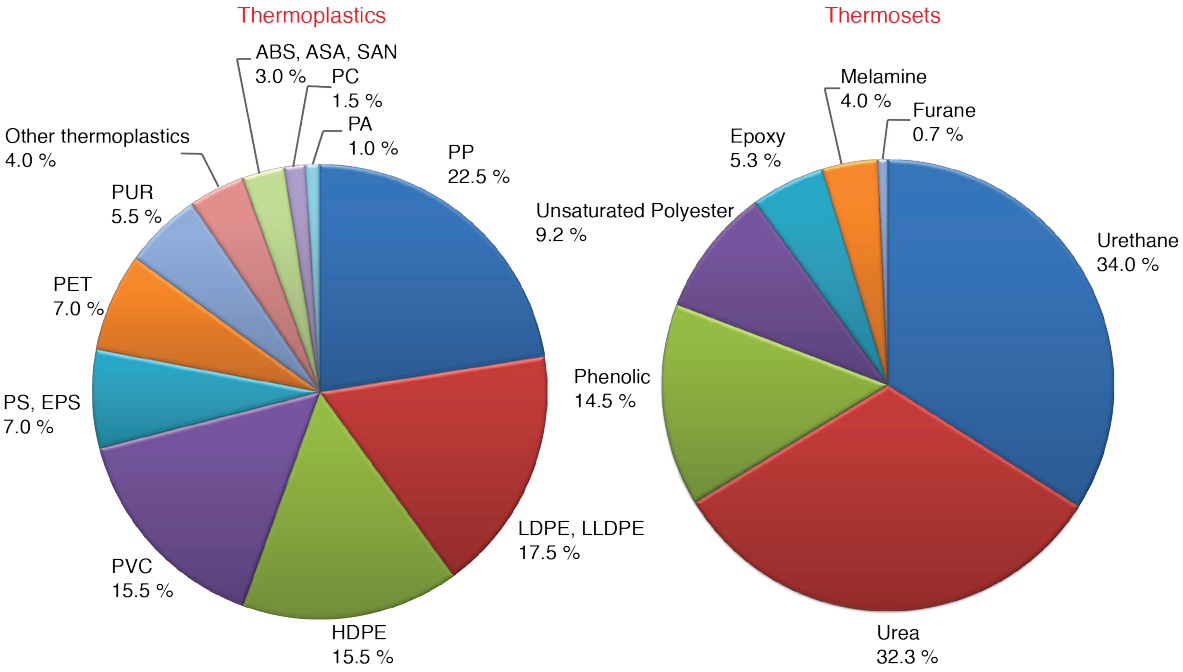

Figure 1.1: Break down of the 2011 world thermoplastic (2012) and thermoset (2010) polymer production in major areas of application. Used with permission from Osswald [1].

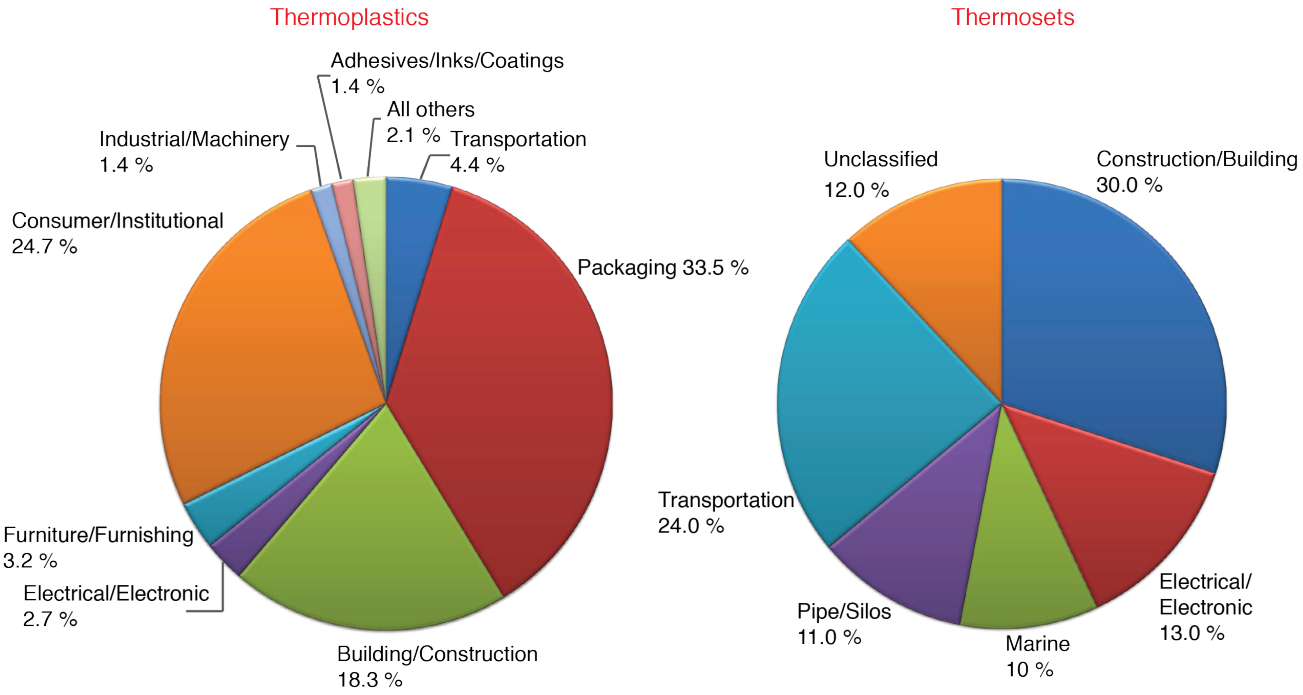

Figure 1.2: Break-down of the world polymer production in major thermoplastic (2012) and thermoset (2010) polymer categories. Used with permission from Osswald [1].

Chapter 2 shows a novel protocol to quantify isothermal kinetics of thermosets via Differential Scanning Calorimetry (DSC) using initial heating rates up to 500 K/min. The goal is to eliminate loss of data due to curing in the transition from heating to the isothermal cycle during testing. Chapter 3 uses the fast ramp method developed in Chapter 2 to measure and model the kinetics of two commercial adhesives. The method includes correction for filler, moisture, and precure history. The kinetics results are summarized in the Time-Temperature-Transformation (TTT) diagram, giving preliminary manufacturing recommendations.

Based on the kinetic analysis, Chapter 4 presents a modified technique to measure the modulus continuously, from the gel point up to the fully cured state in Dynamic Mechanical Analysis (DMA). The idea is a sandwiched beam composed of two outer plates for structural stability and a core made of the partially-cured epoxy that will be measured during curing. An evaluation of the improvement compared to discrete DMA protocols and better trend characterization is described.

Even with the proposed techniques, the correlation of kinetic and mechanical development remains a challenge. Chapter 5 breaks from modifying standard protocols, and presents an alternative that can capture kinetic and mechanical development simultaneously. An in-situ method attaching ultrasonic transducers and a Raman probe to a chamber is explored. The technique allows the simultaneous characterization and connection of curing and the mechanical transition from liquid to gel and solid.

Chapter 6 explores an alternative to measured warpage in thermoset composites. A 3D rendering of an L-shaped component and mold is obtained using a Laser scanner technique. The technique allows us to compare the dimensions of a location on the part with the mold to quantify warpage. Initial steps towards using the models gathered in Chapters 2-5 are described in Chapter 7 as part of the future work to simulate warpage in L-shaped components.

Chapter 2

Quasi-Isothermal DSC Testing of Epoxy Adhesives using Initial Fast Ramps

Three major factors decrease the accuracy of the cure measurement in standard-isothermal testing using Differential Scanning Calorimetry (DSC). First, cure occurs during the heating step. Second, data is lost during the stabilization period between the dynamic and isothermal step. Third, the baseline selection requires a modification to the protocol. Chapter 2 explores the use of initial fast ramps as an alternative method to decrease heating time and loss of data. The use of fast ramps has been avoided in the characterization of thermosets due to overshoot that occurs between the dynamic and isothermal step, which is troublesome for systems with autocatalytic kinetics. By mitigating these factors, a quasi-isothermal protocol was developed. Therefore, more complete cure kinetics were captured with the implementation of fast heat-flux DSC to decrease the ramp time and through the optimization of furnace parameters to decrease stabilization time and temperature overshoot.

The data suggested this quasi-isothermal analysis more accurately measured the isothermal curing kinetics of the DA 409 epoxy adhesive manufactured by Adhesive Prepreg for Composite Manufacturers (A.P.C.M. LLC) at 110, 115 and 120 °C for fast ramps of 175, 350 and 500 K/min compared to the traditional ramp of 5 K/min. The enthalpy spike at the dynamic to isothermal transition remains an issue; however, an empirical shift can be used to compensate for the enthalpy signal lag. This technique shows the potential to produce a quasi-isothermal cycle, eliminating the loss of data in the initial stage of the reaction.

2.1 Introduction

Understanding cure kinetics of thermosets, including epoxies, is critical to continue the advancement of lightweight manufacturing with prepreg materials [2, 5, 6]. Spectrochemical [7–11], mechanical [12–16], and thermal [17–21] analysis have all been used to monitor curing reactions. One of the most common, which dates back to the 1960s is Differential Scanning Calorimetry (DSC), which measures the heat released during the exothermic reaction [22–24] from which both the cure rate and the degree of cure as a function of time and temperature can be determined.

There are numerous protocols for isothermal DSC [18, 20, 25–27], one of which was developed at the Polymer Engineering Center by Hernandez-Ortiz and Osswald in 2002 [28, 29]. This method was based on the principle that the behavior of a thermoset under an isothermal state can be assessed by combining results from non-isothermal and isothermal DSC scans. The method was further improved by Restrepo-Zapata et al. [30–33], which will be the starting point of this work and referred to as the 'core' method. One unifying aspect of all these methods is how to address the reaction that occurs during the non-isothermal period. For example, Fava placed the sample and increased the temperature manually as quick as possible to reach a constant temperature [22], and Restrepo-Zapata et al. used non-isothermal tests to account for the reaction that occurred in the ramp regime [31].

With state-of-the-art heat-flux DSC technology, ramps of up to 500 K/min are possible [34], which allows for a new solution to this problem. The ramp time from 25 to 125 °C can be decreased from 20 min for a heating rate of 5 K/min to 12 s, which is two orders of magnitude smaller. However, fast DSC has been hampered by temperature overshoots and long stabilization times at the transition between the dynamic and isothermal step, which offsets the gains of a short ramp time. Therefore, applications of fast DSC for polymeric materials have been limited to crystallization kinetics [34–40].

This study explores an improvement of the core protocol for isothermal DSC scans using initial heating rates of up to 500 K/min. With modifications to the furnace control parameters, the issues of stabilization time and temperature overshoots were nearly fully mitigated, which produced quasi-isothermal cycles by eliminating the loss of data during the heating step. The elimination of the baseline to calculate the exothermal reaction (degree of cure) was evaluated as well. Epoxy film

adhesive DA 409 was analyzed with both the core method and for fast ramp rates of 175, 350 and 500 K/min to determine the benefits of the new approach. The method outlined here is the basis to the analysis shown in Chapter 3, where the kinetics and processing window of epoxy adhesives DA 408 and DA 409 are fully characterized in the time-temperature-transformation (TTT) diagram.

2.2 Materials and Methods

2.2.1 Materials

A heat activated epoxy film, DA 409, manufactured by Adhesive Prepreg for Composite Manufacturers (A.P.C.M. LLC), typically used to bond composites, metal onto metal and honeycomb structures was analyzed. It has an open thermoplastic knit for bond-line thickness control, as seen in Fig. 2.1.

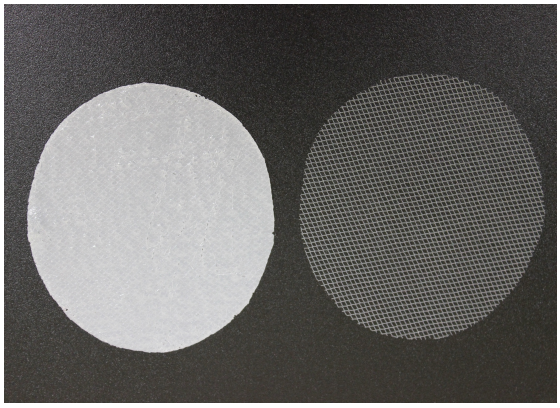

Figure 2.1: Epoxy film adhesive DA 409. From left to right, adhesive with the inseparable knit, and thermoplastic knit after dissolving the epoxy film in acetone.

Based on the MSDS, adhesive DA 409 had a content by weight of 90 % epoxy resins (Bisphenol A), 6 % cyan guanidine and 4 % amines, the last two acting as hardeners. Cyan guanidine, or dicyandiamide (DICY) is typically used as a powder-dispersed hardener in thin films because of its high exothermic effect. It is typically used as a hardener for high temperature curing resins between 160 and 180 °C, resulting in a long curing process. DICY forms crystals with a melting point around 210 °C. The reaction of bisphenol-A (DGEBA) and the amines is the typical network formation of epoxy resins, where epoxy and amine groups are linked (see Fig. 2.2).

Adhesive DA 409, as most commercially available adhesives, come with a filler, in the form of

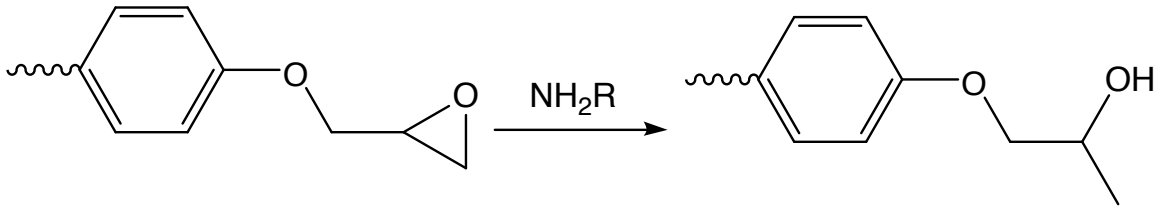

Figure 2.2: Formation of bonds during curing of epoxy resins using amine [41].

reinforcement (fibers), or a thermoplastic knit for bond-line thickness control. A protocol, provided in the next sections, was developed to eliminate the influence of the filler in the characterization of the thermoset.

2.2.2 Sample Preparation

Circular samples were cut from the film adhesive (in a precuring stage-prepreg stage) inside a freezer at -18 °C (0 °F), with the mass kept between 5 ± 0.2 mg. Samples were then placed into Netzsch Concavus® pans with pierced lids, and weighed. Before testing, each sample was equilibrated at room temperature (22 °C) over a 2 h period, then weighed again to control and eliminate measurement errors due to varying initial temperature and moisture influence. The tests were performed within the first two months of the 12-month shelf life of the adhesive to eliminate pre-curing stage variations. All the following tests were executed on a NETZSCH DSC Polyma 214®.

2.2.3 Filler Content

To quantify the mass content of filler (thermoplastic knit, member of the nylon family), 50 mm samples were cut, weighed, and placed in a sealed container filled with acetone for 15 min. Once the epoxy dissolved completely, the knit was dried and measured (see Fig. 2.1). A nylon knit content of 1 to 1.5 % by weight was measured, which agreed with the manufacturer's value of 1 %. The specimen mass was corrected in the DSC software to compensate for the thermoplastic knit.

A thermal characterization of the knit was performed. Two consecutive heating and cooling scans were executed as following: first, the sample was heated from 30 to 280 °C at a rate of 10 K/min, then cooled to 30 °C at a rate of 20 K/min. This procedure was repeated. The thermoplastic

knit showed a melting temperature, T_m, of 222.0 °C and a crystallization temperature, T_c, of 175.4 °C. These temperatures were outside of the range of the isothermal scans, but would have influenced the non-isothermal scans if the mass correction for filler was not applied.

2.2.4 Core DSC Protocol

Samples were first tested using non-isothermal scans. Based on the analysis of the non-isothermal results, uncured adhesive samples were tested under a non-isothermal/isothermal cycle. The method was based on two consecutive DSC scans. The first scan—heating, dwell time, heating, cooling—heated the uncured sample to the isothermal state, and quantified the exothermal reaction and the residual cure. The second scan followed immediately. It used the same thermal cycle of the first scan, but in the fully cured sample giving the exact baseline at the conditions tested.

Non-Isothermal Scans

Non-isothermal scans were performed at four heating rates 1, 2.5, 5 and 10 K/min in triplicate. These heating rates were selected based on the recommended manufacturing cycles used to produce thin plates as seen in Fig. 2.3—this analysis neglected the influence of processing pressure (recommended as 2 bar (30 psi)), and the results are not valid for thick parts. In the first scan, samples were heated from 30 to 270 °C and cooled to 30 °C at a rate of 20 K/min. The second scan followed immediately using the same thermal cycle. These results were used to quantify four parameters: the total heat released during the reaction, Q_T, the dependency of Q_T on the heating rate, the isothermal interval to be tested, and the loss of data during a ramp cycle before reaching the isothermal state.

Isothermal Scans

Samples were tested at three temperatures 110, 115, and 120 °C, which was selected based on the non-isothermal analysis. In the first heating scan, samples were heated from 30 to either 110, 115 or 120 °C at 5 K/min. The samples were held at a constant temperature for 1 h, then heated to 270 °C at 5 K/min (to quantify the residual cure), and cooled to 30 °C at 20 K/min. The second heating scan followed immediately using the same thermal cycle. Fig. 2.4 shows a diagram of the

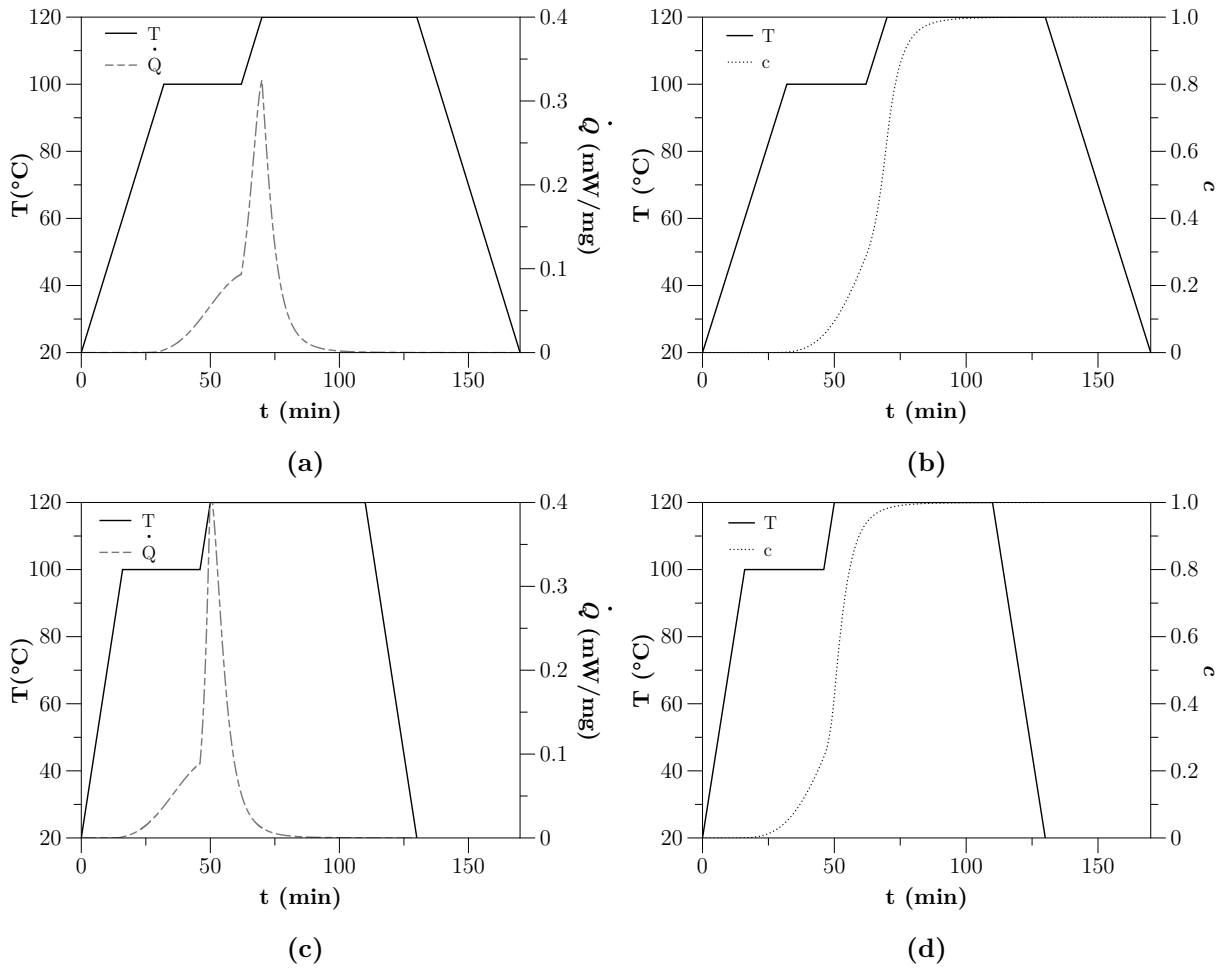

Figure 2.3: Manufacturing cycle used to produce thin parts with epoxy DA 409: (a) $\dot{Q}$ and (b) c during a 2.5 K/min heating/cooling ramp, and (c) $\dot{Q}$ and (d) c during a 5 K/min heating/cooling ramp.

core method for the isothermal cure of DA 409 at 110 °C using an initial heating rate of 5 K/min. The first cycle captures:

a. The heating ramp (possible loss of information).

b. The exothermal reaction (degree of cure).

c. The residual cure.

and the second cycle captures:

A. The baseline for the heating ramp step.

B. The baseline for the exothermal reaction.

C. The baseline for the residual cure.

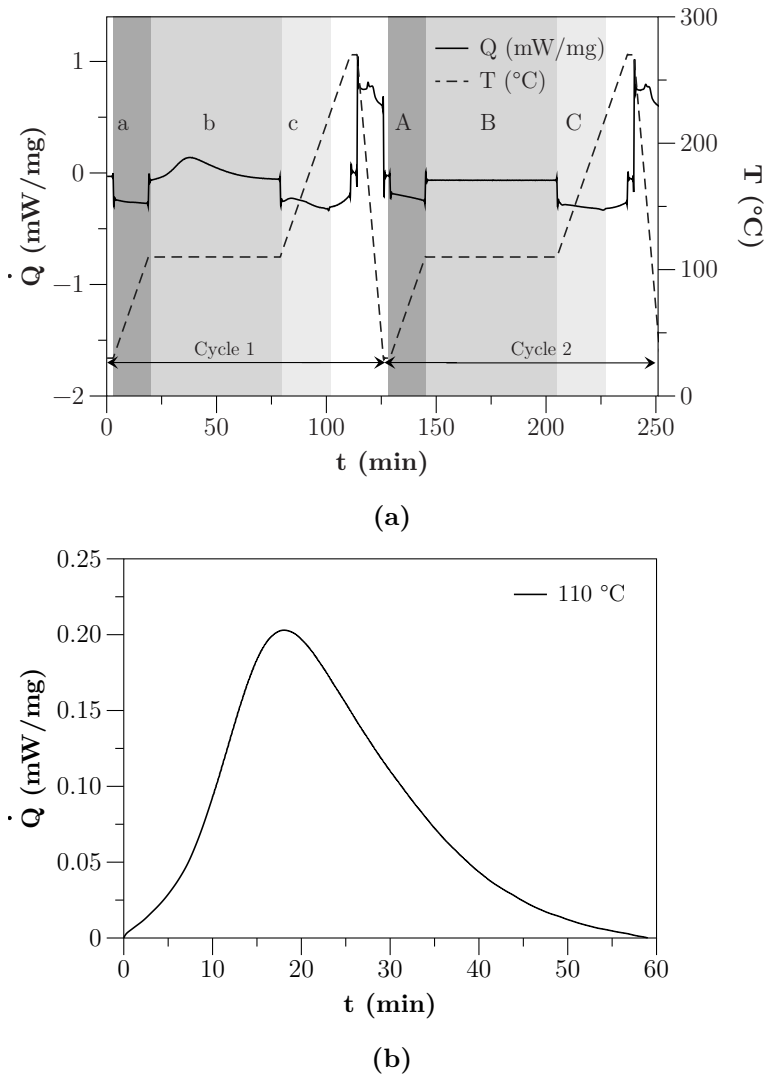

Figure 2.4: Isothermal cure reaction of epoxy film DA 409 at 110 °C: (a) core method with an initial heating rate of 5 K/min, and (b) $\dot{Q}$ versus t after baseline subtraction (region B subtracted from region b).

2.2.5 Improved DSC Protocol

For the fast DSC, the only modification to the protocol was increasing the ramp rate for the two heating steps to 175, 350 or 500 K/min. In theory, if a quasi-isothermal state is reached, no data is lost during the initial heating ramp, and a baseline is not needed. This means that the non-isothermal scans and the second cycle could be eliminated.

2.3 Results and Discussion

2.3.1 Core DSC Protocol

Non-Isothermal Scans

The total heat released, Q_T, was 295 ± 8 J/g at the four heating ramps tested. Q_T showed a slight linear increase with the increase of the heating rate. To simplify the analysis of the results, Q_T was considered constant. The results from the heating scan at 1 K/min were used to select the temperatures tested in the isothermal protocol as seen in Fig. 2.5(a) [42].

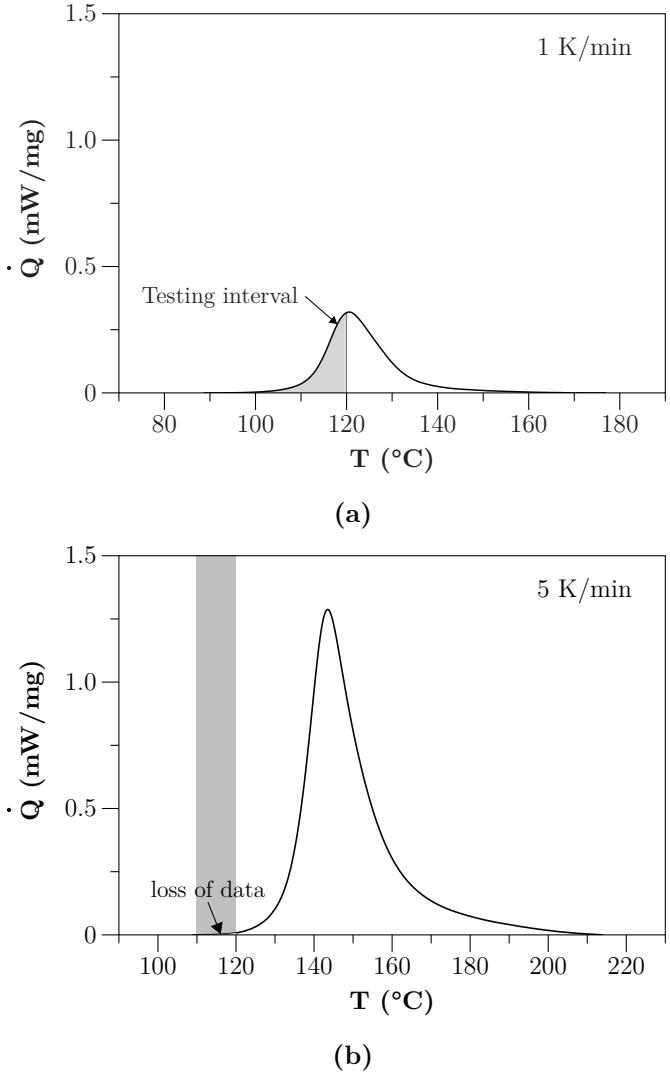

Figure 2.5: Selection of temperatures for the isothermal scans based on non-isothermal tests: (a) isothermal testing interval, and (b) data lost during the heating step.

Over the first third of the area under the curve $\dot{Q}$ versus T was covered [42]. From this area, three temperatures were selected for the isothermal scans, 110, 115 and 120 °C. These temperatures are important in the manufacturing cycle since most of the reaction occurs at these temperatures (refer to Fig. 2.3).

An initial heating rate of 5 K/min for the isothermal scans was selected based on the manufacturing cycle shown in Fig. 2.3 [43]. The instantaneous heat, from 30 to 110, 115 or 120 °C at 5 K/min was 0.017, 0.034 and 0.28 J/g respectively. This corresponded to a degree of cure, c, of $3.7\text{x}10^{-5}$, 0.014 and 0.1 %. Epoxy film DA 409 exhibited a c of less than 1 % during this initial ramp for the three temperatures tested (see Fig. 2.5(b)). Since less than 1 % of data is lost during the initial ramp, epoxy DA 409 is an ideal candidate to test the differences between slow and fast initial heating rates. The differences will be mainly due to the protocol itself and not to the reactive behavior of the material.

This small c quantified during the ramp period of an isothermal scan is not the rule for many thermosets. Highly reactive systems can exhibit a significant c in a 19-min time of temperature rise at a 5 K/min rate. A consequence is that a significant part of the reaction occurs in the non-isothermal state, leading to the incorrect isothermal calculation of c and the incorrect selection of processing conditions.

Isothermal Scans

The first cycle was baselined using the second cycle, and the data was then normalized choosing the initial time as the time when the constant temperature was reached (stabilization time in the transition ramp-isothermal segment). Fig. 2.6 shows the results for the three temperatures tested after subtracting the 16-18 min of the initial ramp time and shifting the initial time to zero. Notice that between 1-108 s of information were lost in the core protocol during the baseline subtraction, and during signal stabilization.

Only the scan at 110 °C exhibited a residual cure of 9 % (27 J/g) since this temperature was below the glass transition temperature at the fully cured state, T_{g_1}, (111.3 °C) (refer to Chapter 3 for the T_g analysis).

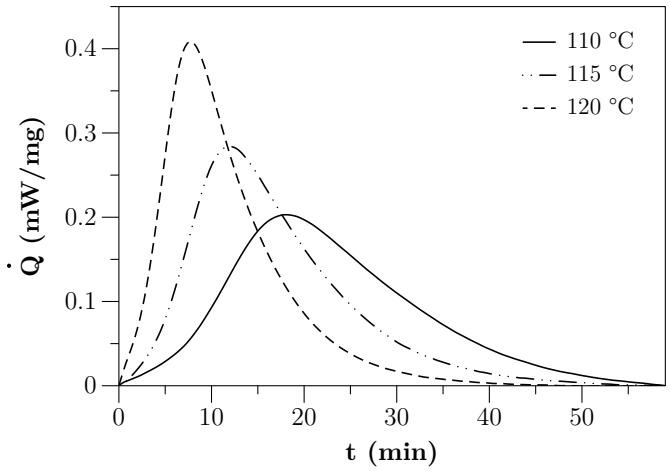

Figure 2.6: $\dot{Q}$ versus t using an initial heating rate of 5 K/min.

2.3.2 Isothermal Scans using Initial Fast Ramps

The core isothermal method depends on non-isothermal DSC scans to select the temperatures tested and to measure the loss of data during the initial heating rate. It also needs a second cycle to baseline the data. Two options to shorten and improve the protocol are the use of initial fast ramps or the preheating of the furnace to the desired temperature before placing the sample and reference pan. Fast ramps are avoided due to temperature overshoot during the transient state before the instrument stabilizes at a constant temperature. This overshoot accelerates the reaction, which leads to incorrect cure data. Fig. 2.7 shows the results for an 110 °C scan using the method proposed here.

Elimination of Temperature Overshoot

When using fast or very slow heating/cooling rates the electronic parameters of the DSC furnace are modified to eliminate temperature delay or overshoot [35]. This calibration varies with the application, material and rates tested. Table 2.1 summarizes the regulation parameters used to optimize the transition from fast heating to the isothermal state for epoxy DA 409. The parameters X_p, T_n, and T_v are PID electronic variables that regulate the response time to temperature changes for the furnace and sample in the transition region tested. Fig. 2.8(a) shows the effect of the temperature overshoot, if the parameters optimization is not applied. It was validated that with the proper optimization of furnace and sample parameters, the temperature overshoots produced

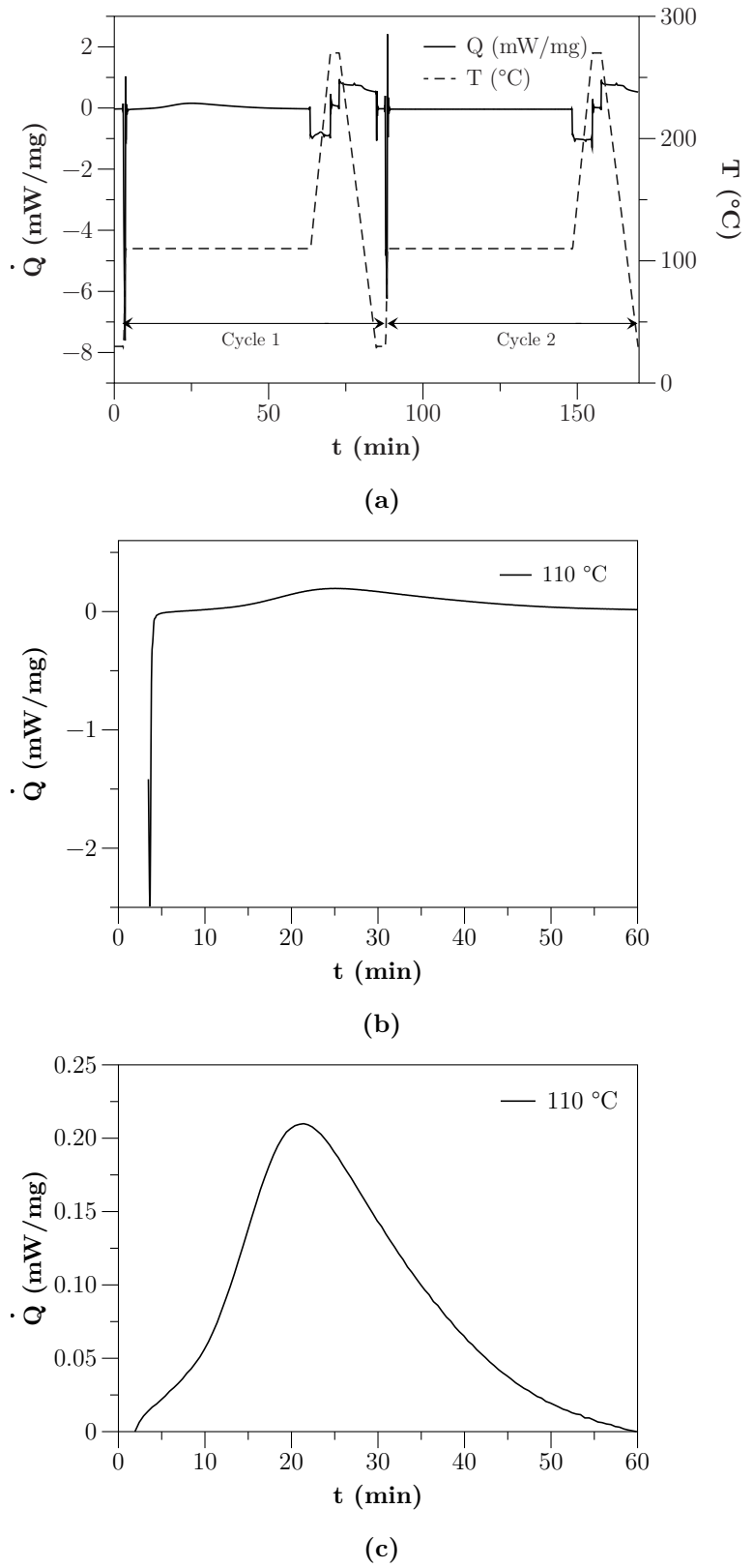

Figure 2.7: Isothermal scan at 110 °C with an initial heating rate of 175 K/min: (a) modified DSC cycle with an initial fast ramp, (b) $\dot{Q}$ versus t after subtracting the time of enthalpy stabilization, and (c) $\dot{Q}$ versus t after baseline subtraction.

during fast ramps were greatly reduced, as seen in Fig. 2.8(b).

Table 2.1: Furnace parameters used to eliminate temperature overshoot in the NETZSCH DSC Polyma 214 during the testing of film adhesive DA 409.

Parameter	Definition	Furnace	Sample
X_p	Proportional Part	4.5	3.75
T_n	Reset time	4.0	4.0
T_v	Derivative time	4.0	3.5
STC	Off for all heating ramps		
Autocooling	Off		

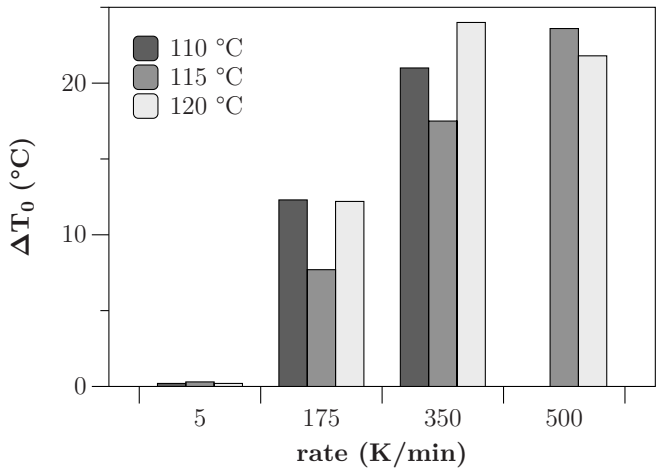

(a)

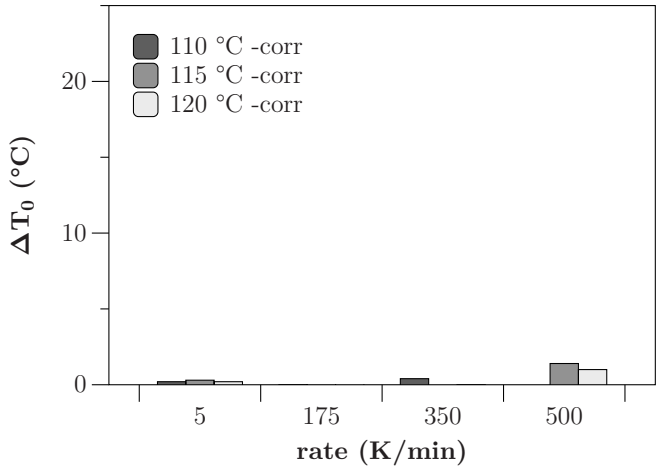

(b)

Figure 2.8: Temperature overshoot, ΔT_o, in the transition from heating to the isothermal segment: (a) no optimization was applied, and (b) optimization of the furnace electronic parameters was applied.

Enthalpy and Heating Rate Adjustments

Fig. 2.7(a) showed a spike in the enthalpy signal during an initial fast ramp. After the enthalpy stabilizes, it is difficult to choose the initial point where the data is valuable. The alternative was to use the second cycle to baseline the data. But this effect cannot be completely eliminated with the baseline, as seen in Fig. 2.7(b). This residual enthalpy spike is related to the specific heat capacity, C_p, and the stabilization time of the DSC system. C_p is slightly lower for uncured than for fully cured thermosets, and this is scaled up using high heating rates. In this method, samples are uncured during the first scan and fully cured during the second scan (baseline), causing the residual enthalpy peak observed.

The stabilization time for the enthalpy signal is also different for the first and second cycle. One can attempt to solve this problem by performing a C_p calibration with a standard material such as sapphire for different thicknesses. However, the differences in the thermal behavior of sapphire and epoxies will add another error into this calibration higher than the second ramp correction.

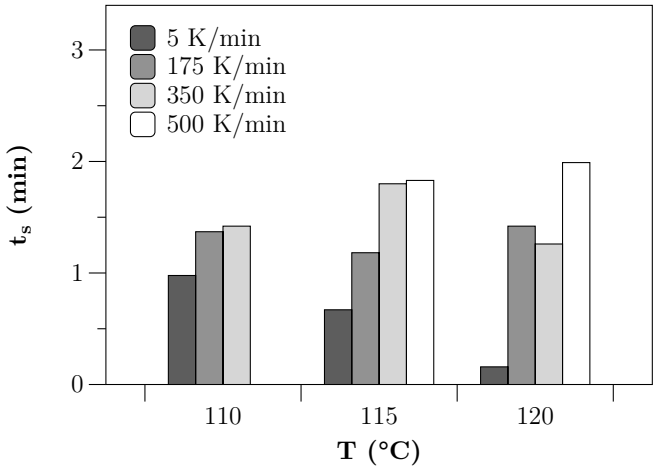

Figure 2.9: t_s of the DSC system for the different temperatures and heating rates tested.

Fig. 2.9 shows the stabilization time, t_s, of the system. It was found that the need for the second cycle to baseline the data remains if the appropriate enthalpy and heating rate optimization is not found. t_s ranged between 40 to 120 s, limiting this method to systems that do not exhibit a significant reaction during the first 1-2 min. t_s increased with the increase of the heating rate as seen in Fig. 2.9. If fast ramps are used, the heating rate should be selected based on the influence of t_s on the data collection and degree of cure.

One criterion to assess the reliability of t_s is to compare Q_T during the reaction. If this point is chosen correctly, Q_T of the isothermal scans using initial slow and fast ramps will agree. Fig. 2.10 shows Q_T for the different heating rates tested. Comparing the results of with the 5 K/min tests, the difference ranged from 0.5 to 7 %.

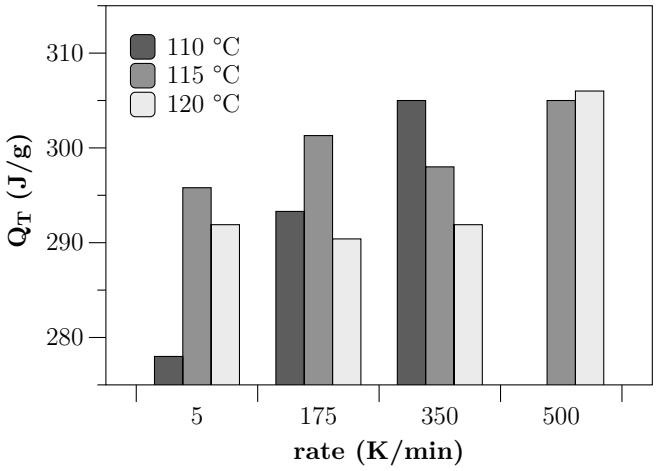

Figure 2.10: Q_T for the different temperatures and heating rates tested.

Data Normalization

For the remaining analysis, the data was baselined using the second cycle, and the time for stabilization of the enthalpy instability was substracted, which differed for every case, as seen previously in Fig. 2.9. Fig. 2.11 summarizes the results after the normalization. Notice that the 500 K/min ramp was not included for the 110 °C results. Netzsch DSC Polyma® 214 has a minimum step time of 10 s. A change in temperature of 80 K (from 30 to 110 °C) at 500 K/min cannot be tested because it will happen in 9.6 s.

Fig. 2.11 shows that the enthalpy signal for the fast ramps lagged the slow ramp scan. Every DSC device has a time lag when capturing sample's changes, due to the tolerances of electrical components [44]. To get accurate results a tau-R correction, the correction of the time constant and the thermal resistance between, sensor, pan, and sample are implemented. Here, when the program temperature is reached after the fast ramp, the sample, the pan, and the furnace's lag to the sensors is increased. This affects the enthalpy signal (exothermal reaction) in the testing of thermosets. An additional thermal resistance of the system is the not-ideal contact between sample

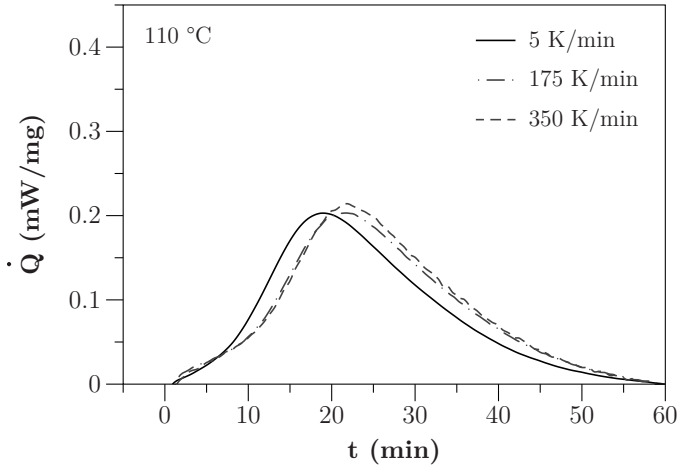

(a)

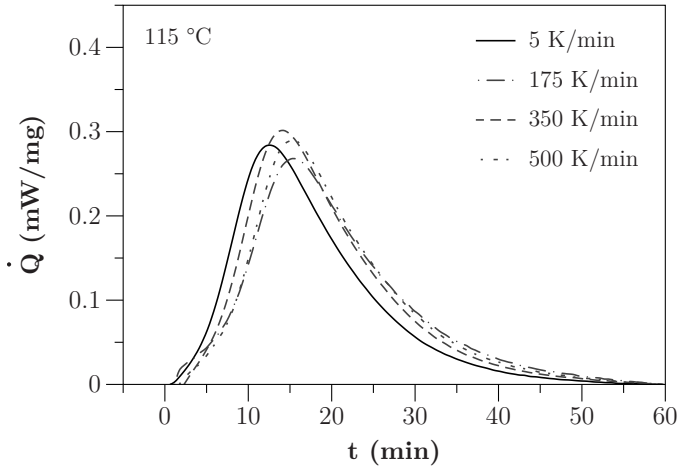

(b)

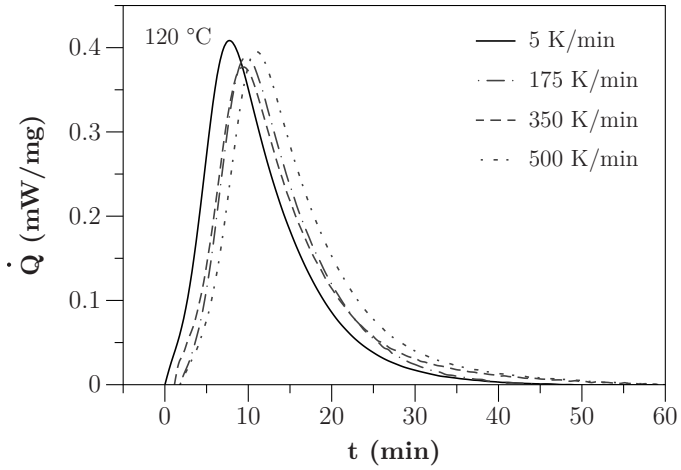

(c)

Figure 2.11: $\dot{Q}$ versus t for the different temperatures and heating rates tested.

and pan especially with adhesives that have a high porosity. In this study, the time at which the maximum heat flow value, $\dot{Q}_{peak}$, is reached, t_p, was used to shift the enthalpy signal. Fig. 2.12 shows t_p for the different heating rates.

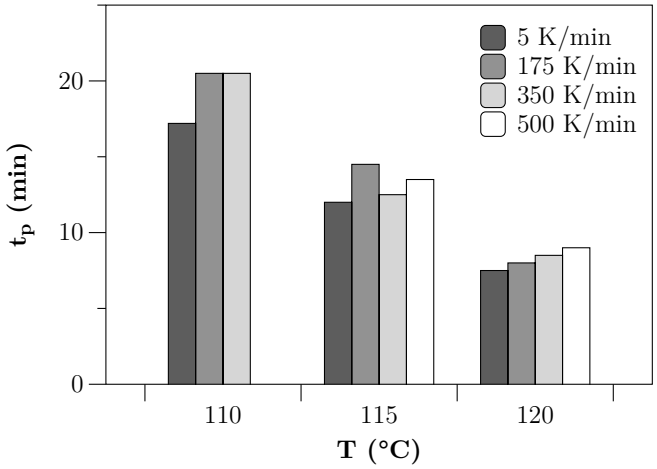

Figure 2.12: t_p for the different temperatures and heating rates tested.

Fig. 2.13 shows the data after shifting the scans with an initial fast ramp (see Fig. 2.11) using t_p of the initial heating rate of 5 K/min. A small difference was observed at the beginning of the reaction, but overall the data agrees for all cases.

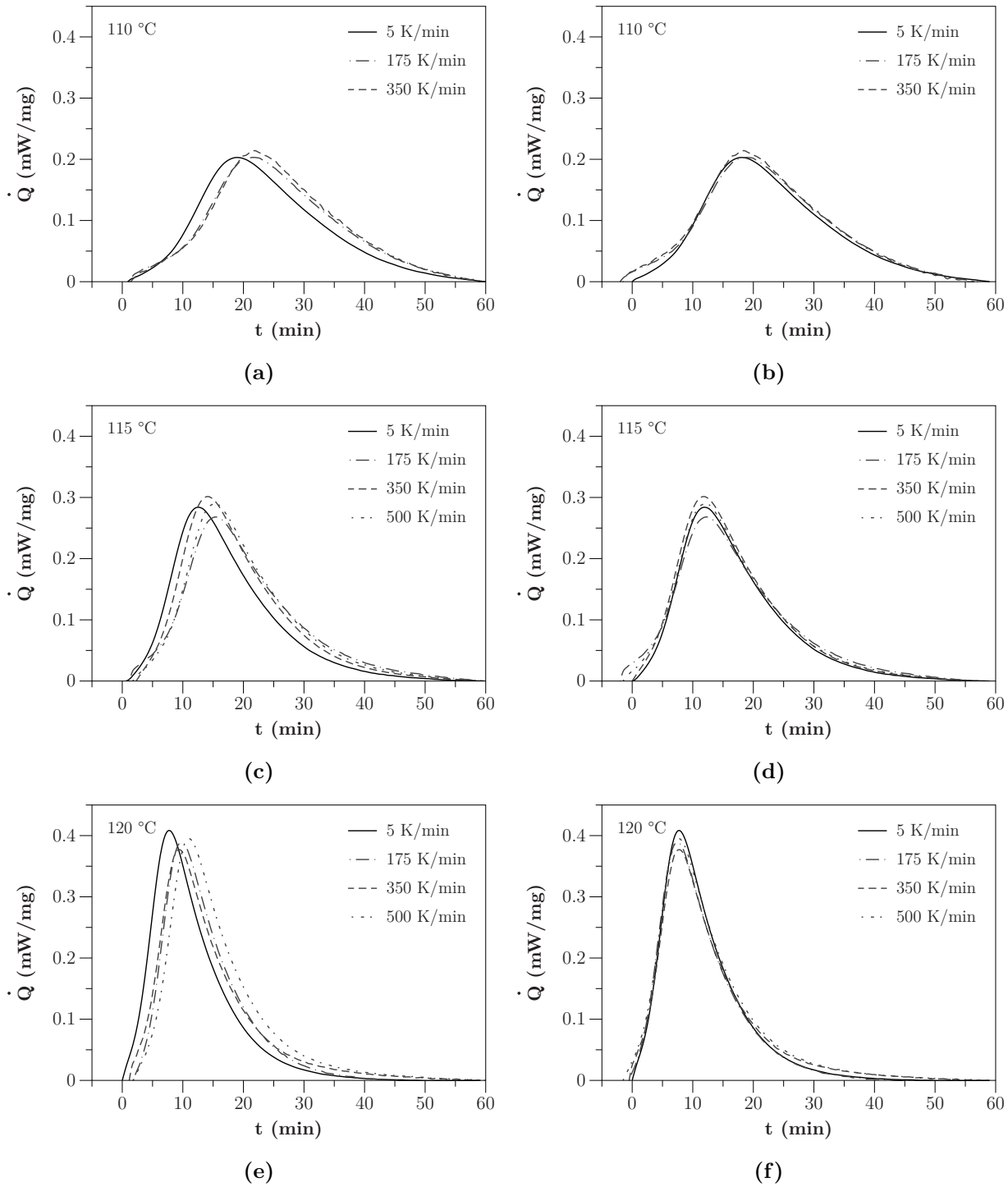

Figure 2.13: Comparison of the exothermal response using slow ramps (5 K/min) versus fast ramps (up to 500 K/min) at the beginning of isothermal scans.

2.4 Conclusions

A novel method to analyze thermoset adhesives in a quasi-isothermal state was developed and evaluated. Initial heating rates up to 500 K/min were used. The results were compared to a core method that uses an initial heating rate of 5 K/min. In the core method, the material takes between 17 and 19 min to reach the isothermal conditions. With a fast ramp, the isothermal condition was reached between 10 and 31 s. The results showed that with the proper optimization, initial fast heating rates could be used to characterize a thermoset reaction in a quasi-isothermal state.

The optimization of electronic parameters of the furnace for the adhesive and conditions tested eliminated temperature overshoot. The problem of an enthalpy spike was not eliminated. The use of a second thermal cycle on a fully cured sample was still needed to find the correct baseline. Even after the baseline subtraction, a residual enthalpy spike remained. This is due to differences in C_p for uncured and fully cured material, combined with the stabilization time of the system. However, this can be accounted for with an empirical data normalization. The stabilization time, t_s, was used to choose the beginning of the data eliminating the residual enthalpy spike. A thermal lag of the enthalpy signal was observed for the fast ramp method. The time at which Q_{max}, for the 5 K/min tests was reached was used to normalize the enthalpy signal. This empirical shift worked for the adhesive under study. After the optimizations and post-processing of the data, the scans using an initial slow and fast ramp showed excellent agreement. Future work will include the study of slower rates, between 50 and 150 K/min. A new study looks for the possibility to preheat the furnace before placing the reference and sample pan. The goal is to obtain a quasi-isothermal state and evaluate the possibility to eliminate instabilities in the enthalpy signal and the need for a baseline (second cycle). Future work also includes a transient energy balance to quantify the stabilization time of the geometry and conditions tested.

Chapter 3

TTT-diagram of Epoxy Film Adhesives using Quasi-Isothermal Scans with Initial Fast Ramps

The characterization of film adhesives is challenging because they required freezer storage, contain an inseparable filler—thermoplastic knit or carbon fiber reinforcement, and are heat activated systems in a pre-cured state with unknown chemistry. A testing protocol that eliminates these potential sources of error in epoxy characterization is proposed. Chapter 3 presents a method to generate time-temperature-transformation (TTT) diagrams of epoxy film adhesives via Differential Scanning Calorimetry (DSC). Non-isothermal and isothermal DSC scans are used to capture the reaction and the glass transition temperature. The use of an initial fast ramp—up to 500 K/min—in the isothermal scans is explored for the first time. This technique shows the potential to produce a quasi-isothermal cycle, eliminating the loss of data in the initial stage of the reaction.

The total heat released, Q_T, the activation energy, E, and the fractional kinetic parameter, A, are captured via Friedman and Ozawa-Flynn-Wall methods. The Kamal-Sourour model and the formal kinetic model are fit to find an equation for the rate of cure, dc/dt. The simplest model that accurately captures the reaction, a parallel two-step model A $\rightrightarrows$ B, is outlined. The glass transition temperature is modeled via DiBenedetto's equation to include the diffusion-controlled mechanism. The TTT-diagrams of two commercial adhesives, DA 408 and DA 409, are shown with an analysis of processing optimization.

The use of quasi-isothermal scans with initial fast ramps combined with the correction for filler, moisture, and pre-curing history can be applied to characterize fast curing thermosets, complex B-stage resins, and thermoset composites. The modeling results can also be used in numerical

studies of residual stresses and dimensional stability in the manufacturing of thermoset composites.

3.1 Introduction

Epoxy adhesives exhibit a high strength and modulus, perform well under fatigue, have high toughness, and low creep [5]. Applications include the bonding of composites, honeycomb structures, and metal to metal components. In composite laminates, these thermoset formulations can be used to impregnate a fiber reinforcement producing a prepreg (partially cured pre-impregnated laminate), where an initial cure occurs during the production process. These sheets or tapes, commonly having a unidirectional continuous fiber orientation, can be stacked on top of one another at room temperature or elevated temperature, depending on the required tackiness. The stacking sequence or ply book determines the orientation of the layers, resulting in composites with tailored properties [6].

Manufacturing efforts are directed to lightweight composites for their excellent fuel economy and to meet environmental regulations. Therefore, metal counterparts are being replaced by composite laminates in the aircraft and automotive markets. Aircraft manufacturing processes using thermoset prepregs include vacuum molding in an autoclave, automated tape layup (ATL), and automated fiber placement (AFP) [6]. In the automotive sector, fast curing formulations are required to meet the demands of mass production. Processes such as prepreg compression molding and a variation of resin transfer molding (RTM) are used in this sector [5].

The method and analysis proposed here is relevant as the market produces thinner adhesives and prepregs with a higher glass transition temperature, that perform at higher temperatures, and exhibit higher toughness and impact resistance [4]. Snap-cure prepregs (cure achieved within minutes) are being introduced for structural body and aesthetic parts in automobiles [2, 5]. The complex and often unknown chemistry of these thermosets requires a re-evaluation of the standard testing and modeling protocols. The optimum processing cycles and parameters are selected based on the kinetic reaction. This chemical reaction depends on time, thermal history, material properties, and geometrical conditions. The TTT-diagram maps the degree of cure and physical transitions of a thermoset, and it is used to evaluate the processing window [33].

The construction of the TTT diagram starts with the characterization of the reaction that requires an experimental and modeling approach. Differential Scanning Calorimetry, DSC, is one

of the techniques used to experimentally quantify the rate of cure and degree of cure as a function of time and temperature. Calorimetry is a technique that quantifies the heat absorbed or released by a substance undergoing a physical or a chemical change [45]. This change of internal energy at constant pressure is the enthalpy, H. The cure of a thermoset lowers the enthalpy and is classified as an exothermal process. These enthalpy changes are measured by the calorimeter that registers the diference of the heat flow, $\dot{Q}$ (energy per unit time per unit mass), from a baseline. In the baseline, no reaction or transition occurs, and it is assumed that the heat of reaction or transition or both is equal to zero at the baseline [45].

The heat released during the exothermal reaction of a thermoset is assumed to be directly proportional to the rate of cure [46]. The rate of cure, dc/dt, is modeled as the ratio of the instantaneous heat rate, $\dot{Q}$ (energy rate per unit mass), to the total heat released during the reaction per unit mass, Q_T (see Eq. 3.3).

$$\frac{dc}{dt} = \frac{\dot{Q}}{Q_T} \tag{3.1}$$

The degree of cure, c, is modeled as the ratio of the instantaneous heat, Q (energy per unit mass), to the total heat released, Q_T (see Eq. 3.2).

$$c = \frac{Q}{Q_T} \tag{3.2}$$

Three procedures are often used to model the kinetics [47]. In these theories, the temperature and degree of cure dependency are split and considered independent. The temperature dependence is expressed as a reaction rate, K_T, modeled as an Arrhenius function, and the degree of cure as a function, $f(c)$, which describes or fits the kinetic mechanism (see Eq 3.3).

$$\frac{dc}{dt} = K_i(T) f(c) \tag{3.3}$$

with

$$K(T) = Ae^{\left(-\frac{E}{RT}\right)} \tag{3.4}$$

where A is the frequency factor, E is the activation energy, R is the universal gas constant, and T is the temperature.

The first approach uses overall rate law simplified models such as the Kamal-Sourour model [24] shown in Eq. 3.5, with K_1, the rate constant that accounts for the catalytic and initial reactivity, K_2, the rate constant related to auto-catalytic effects, and m and n, the orders of the reaction. This is a phenomenological model widely used to fit thermoset kinetics. Several in-house codes and software have implemented this model [29, 31, 48, 49]. Recent literature reported that to achieve a proper fit with this model, most of the parameters should be specified as parabolic functions of the temperature except for the activation energy, E, that is fixed as a constant value [31].

$$\frac{dc}{dt} = (K_1 + K_2 c^m)(1 - c)^n \tag{3.5}$$

The second approach uses the integral iso-conversional method by Ozawa-Flynn-Wall or the differential iso-conversional method by Friedman [50–52]. This method determines the activation energy, E, and the fractional kinetic parameter, A, quantified directly from several non-isothermal or isothermal DSC curves [42, 47]. These parameters are obtained without a kinetic model [53].

The third approach, or formal kinetic model, describes the kinetics using a single or multiple-step processes (parallel, independent, competitive or consecutive steps) with constant activation parameters [42, 47]. In this method, a statistical analysis suggests the model that best describes the experimental data out of a set of equations tested. Software such as NETZSCH Thermokinetics 3 incorporates the last two methods. Table 3.1 summarizes the models tested in this study, individually or in combination, using the formal kinetic method.

Table 3.1: Types of reactions tested for the adhesives of study individually or in combination. Models based on the Thermokinetics 3 database [53].

Model	Type of reaction
$(1 - c)$	first order
$(1 - c)^2$	second order
$(1 - c)^n$	nth order
$(1 - c)^n c^m$	nth order autocatalysis according to Prout-Tomkins
$(1 - c)^n (1 + K_{cat} c)$	nth order autocatalysis

In thermosets with partial diffusion control, such as in epoxy systems, a correction to the reaction rate is performed, obtaining an overall rate constant using the principle proposed by Rabinowitch [54].

$$\frac{1}{K_i} = \frac{1}{K_{c_i}} + \frac{1}{K_d} \tag{3.6}$$

K_i is the total rate constant of the ith reaction, K_{c_i} is the Arrhenius rate constant of the chemical reaction controlled by the kinetic conditions, and K_d is the diffusion rate constant.

The kinetic modeling accounting for diffusion is used to construct the TTT-diagram proposed by Gillham et al. [17, 55–58]. Fig. 3.9 shows a theoretical (TTT) diagram.

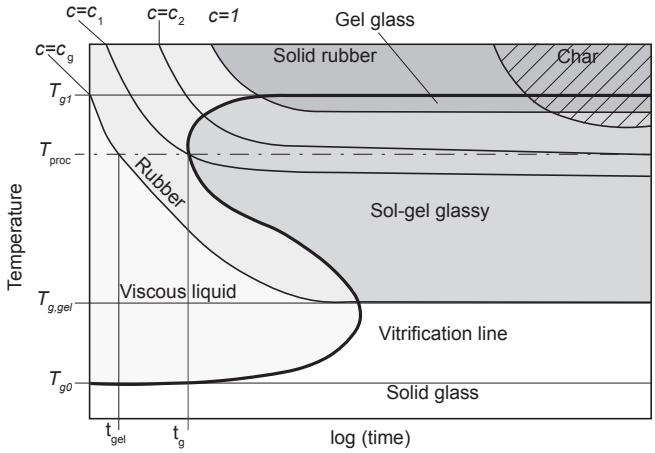

Figure 3.1: Schematic of the TTT-diagram. Used with permission from Osswald [46].

This diagram maps the interrelations between material properties and changes in a material during an isothermal cure as a function of time. It marks the main phase changes of a thermoset:

1. Gelation ($T_{g,gel}$): formation of an infinite molecular network followed by a rise to long range elastic behavior in the macroscopic fluid [56].

2. Vitrification ($c = c_g$): state where T_g rises to T_{proc}, delaying the chemical reaction [56].

3. Full cure ($c = c_1$).

4. Devitrification: T_g decreases during an isothermal cycle as in chart degradation [56].

Material states depicted in the diagram include liquid, solid glass, sol/gel-rubber, gel-rubber, sol/gel-glass, gel-glass, and char. The glass transition temperature T_g of the material is used as a parameter to monitor the curing reaction [31]. The changes in the material during isothermal

cure are described by contours of the time reaching one of the above states. The thermomechanical properties of the resin change with every transition.

This study outlines an experimental and modeling method to construct the TTT-diagram of film adhesives. Commercial film adhesives DA 408 and DA 409 are tested. The experimental method includes a correction for filler, the influence of moisture content, freezer storage and pre-cured stage. The use of an initial fast ramp in isothermal DSC scans proposed in Chapter 2 is evaluated here. Quasi-isothermal scans are obtained improving the accuracy of the prediction. This technique shows potential to eliminate loss of data in isothermal DSC scans. Several modeling procedures are described, showing the advantages of the formal kinetic model. A parallel two-step model with diffusion correction is used to graph the TTT-diagram to fully understand the behavior of the adhesives under analysis. Processing recommendations for the studied adhesives are outlined.

The results presented here are used in Chapter 4 to develop a proper chemo-rheological analysis of epoxy DA 409, which includes the quantification of the gel point, chemical shrinkage, viscosity and moduli and their correlation with the degree of cure.

3.2 Materials and Methods

3.2.1 Materials

Two heat activated epoxy films, DA 408 and DA 409, manufactured by Adhesive Prepreg for Composite Manufacturers (A.P.C.M. LLC) were analyzed. As described in section 2.2.1 in Chapter 2, these film adhesives have an open thermoplastic knit for bond-line thickness control (see Fig. 2.1). The two epoxy formulations were also acquired as unidirectional carbon fiber prepregs—DA 409U/G35 150 and DA 408U/G35 150 respectively, with a resin content of 48 % by weight. These adhesives have a shelf life of 12 months at -17.8 °C or 20 days at 25 °C.

3.2.2 Sample Preparation

The protocol described in section 2.2.2—cutting, storage, mass and thermal equilibrium control—was used to prepare the samples for the non-isothermal and isothermal DSC analysis. The method eliminated errors due to freezer storage conditions, pre-curing history, and moisture effects.

3.2.3 Methods

Filler Content

In this study, the materials were tested with the nylon scrim rather than with carbon fiber as usually reported in the literature [59]. The steps shown in section 2.2.3—separation of epoxy/nylon knit via dissolution in acetone, and evaluation of melting, T_m, and crystallization temperatures, T_c, of the nylon knit—were applied to correct for the influence of the filler content. T_m and T_c of the nylon knit were outside of the range of isothermal scans tested for both epoxy systems. The correction eliminated the effect of T_m of the filler in non-isothermal epoxy scans. This error was visualized in 2014, in my collaboration with Knott [60], as a small enthalpy hump. This hump could lead to poor baseline selection and the inaccurate prediction of Q_T.

Degradation Temperature

Before the DSC analysis, both materials were characterized with thermogravimetric analysis (TGA) on a NETZSCH TG 209 F1 Libra, under a dynamic linear ramp to quantify the degradation temperature. This instrument has a resolution of 0.1 μg. The tests were performed under a nitrogen atmosphere, from 30 °C to 700 °C at a ramp of 2.5 K/min. The mass was kept between 4–5 mg. Fig 3.2 shows the results from the analysis performed with the NETZSCH Proteus 6.1 software. Based on the onset temperature, T_A, according to ISO 11358, both epoxy systems exhibited a degradation temperature at 344 ± 0.5 °C. However, mass loss began at around 280 °C, which was used as the upper temperature limit for the DSC scans.

DSC Method

Here we extended and further optimized the experimental method proposed by Hernandez-Ortiz and Osswald [28, 29], and later improved by Restrepo-Zapata [30, 31, 33, 61, 62]. This method to obtain TTT-diagrams is based on non-isothermal and quasi-isothermal DSC measurements. The glass transition temperature, T_g, is required to model partial diffusion control. This method was used to characterize polyester [28], linseed based epoxy [30,31,61], and EPDM rubber [33,62]. This study shows that their method works for epoxy film adhesives with the proper modifications.

This study evaluated the optimization of the quasi-isothermal protocol presented in chapter 2.

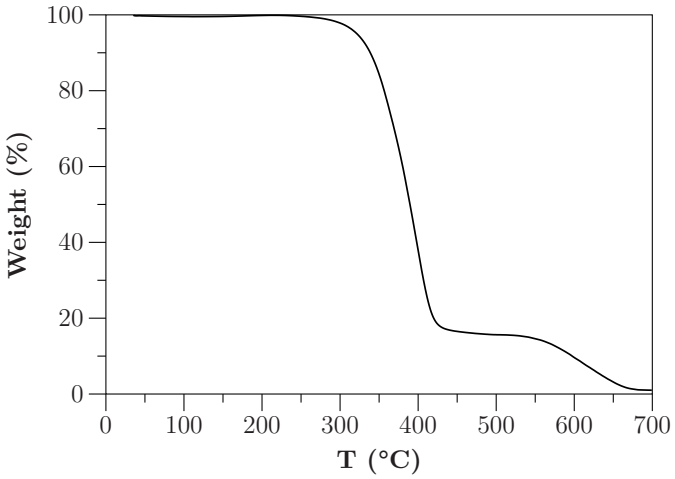

Figure 3.2: Dynamic TGA curve for adhesive DA 408.

State of the art DSC technology includes heating ramps up to 500 K/min, reaching an isothermal stage within seconds. This could eliminate problems concerning loss of data in the ramp stage before the isothermal cycle. Careful attention was paid to reducing the thermal overshoot produced by the slow response of the equipment, which has been reported as counterproductive [45]. The specimen's delayed heat-released caused by a fast ramp was corrected. Temperature, enthalpy and heat flux calibrations were executed according to NETZSCH guidelines. Below is a detailed explanation of the method.

Non-Isothermal Scans

Non-isothermal scans were performed at four heating rates 1, 2.5, 5 and 10 K/min, based on the manufacturing cycle, and to analyze data within at least one order of magnitude in between the lowest and highest heating rate [42]. Samples were tested in two-steps. In the first heating scan, the sample was heated from 30 °C to 270 °C, and cooled to 30 °C at a rate of 20 K/min. The second heating scan followed immediately using the same thermal cycle. This helped to assess the fully cured stage of the samples—no residual cure is captured—and to obtain a baseline for the particular thermal program.

The Glass Transition Temperature

T_g, was the material property used to assess the curing reaction [31]. T_g of the adhesives was measured during the 5K/min non-isothermal scans, reducing testing time. Sample mass was kept between 8–12 mg for this test. T_g for the unreacted network (prepreg stage in this study), T_{g_0}, was measured in the first heating cycle starting at -30 °C for the 5 K/min test. Although 20 K/min is the recommended rate for T_g measurements [45], the DSC's resolution gave accurate results at 5 K/min.

The precured stage of the adhesives within the first month of production was chosen as the zero degree of cure. T_g of the fully reacted network, T_{g_1}, was measured in the second heating cycle—fully cured sample subjected to a second heating scan. The physical aging of the adhesive was not included—the value of T_{g_1} in epoxy resins further increases due to physical aging [63]. Isothermal scans were used to quantify T_g inbetween the two extremes, T_{g_0} and T_{g_1} [31]. This eliminated the use of multiple instruments and sample sizes in the characterization. The isothermal temperature (processing temperatures, T_{proc}) was assumed equal to T_g, reaching a maximum degree of cure calculated from the ratio of the total degree of cure to the residual degree of cure.

Isothermal Scans

The results from the heating scan at 1 K/min were used to determine the interval for the isothermal protocol. The first third of the area under the curve Q vs T was covered [42]. This eliminates errors caused by signal correction in the initial stages of the reaction [42]. In this work, T_{g_1} was used as the limit of the interval, which gives a temperature interval of about 25 K. In isothermal cycles exceeding T_{g_1}, the diffusion mechanism plays a minor role—the curing reaction occurs mainly due to the chemical reaction. To construct the TTT-diagram, isothermal scans were performed up to T_{g_1}.

Four temperatures 80, 90, 100, and 105 °C for adhesive DA 408, and 80, 90, 100, and 110 °C for adhesive DA 409 were tested. In the first heating scan, the sample was heated from 30 °C to the respective isothermal temperature using slow/fast ramps. The samples were held between 1 to 6 h for high and low temperatures respectively. Samples were then heated up to 270 C at a rate of 5 K/min and cooled to 30 °C at a rate of 20 K/min. The second heating scan followed immediately

using the same thermal cycle. Fig 3.3 shows a diagram of the method using a 5 K/min for an iso scan at 110 °C (refer to section 2.2.4 for a detailed explanation of the method). The jumps in every transition represent the stabilization period of the instrument.

For the isothermal scans, two methods were compared. The first method used a 5 K/min ramp to reach the isothermal stage, and the second method used fast ramps of 175, 350 and 500 K/min. This study aimed to evaluate fast ramps as a method to eliminate loss of data during the ramp stage in isothermal scans.

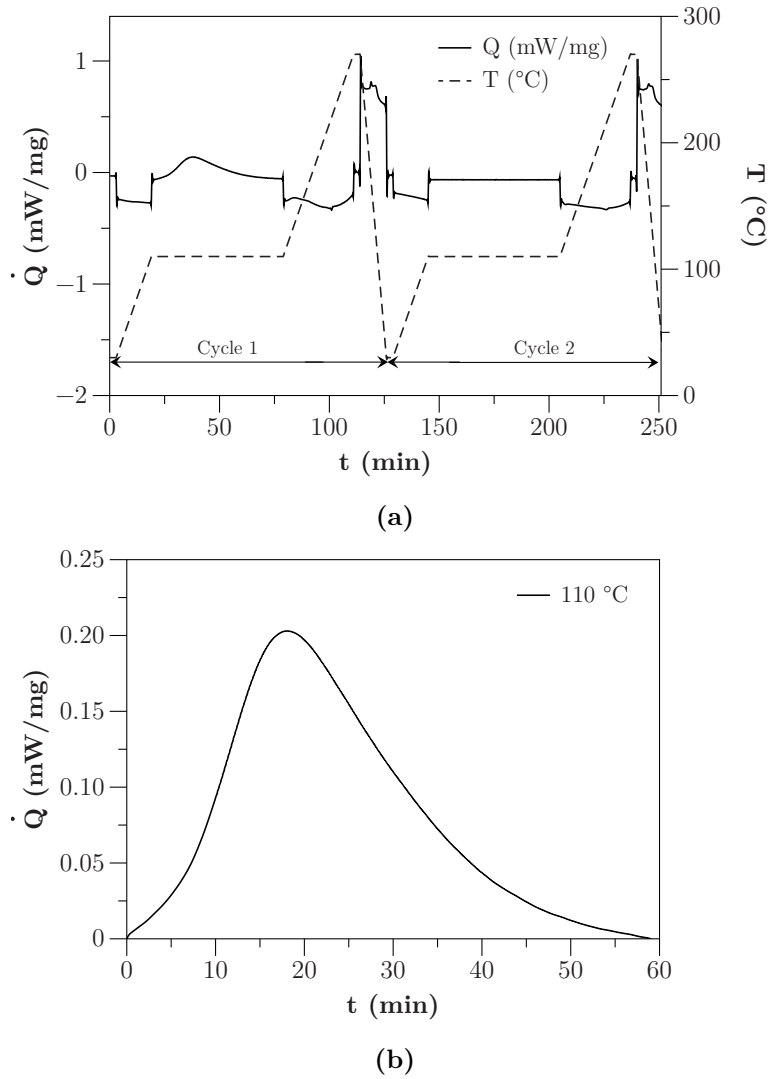

Figure 3.3: DSC method to quantify the rate of cure: (a) first cycle including the exothermal reaction and second cycle showing the baseline, and (b) $\dot{Q}$ versus t after baseline subtraction and data normalization.

3.3 Results and Discussion

For all samples and conditions tested, the baseline (second scan) properly closed and coincided with the first scans. This proved to be an accurate and reliable protocol for the characterization of film adhesives and prepregs that require freezer storage and include a filler. The experimental method presented here is not restricted to a modeling tool.

In the following analysis, the raw data from the DSC scans was post-processed in Proteus 6.1 software, and modeled via a Friedman and Ozawa-Flynn-Wall methods and a formal kinetic model with NETZSCH Thermokinetics 3 software. The Kamal-Sourour model was implemented for additional comparison on IBM SPSS software. T_g and the residual cure were quantified to assess the importance of the diffusion mechanism.

3.3.1 Non-Isothermal Scans

The total heat released, Q_T, was quantified from the non-isothermal scans, and gave insight into the dependency of the heat released to the heating rate. Q_T for adhesives DA 408 and DA 409 was 292 ± 8 J/g, and 295 ± 8 J/g respectively. From the non-isothermal scans, the first activation energy, E_1, and pre-exponential factor, A_1, were estimated with the use of model free methods (ASTM E 698) [53]. E_1 and A_1 were 106.1 KJ/mol and 11.35 1/s for adhesive DA 408, and 89.25 KJ/mol and 8.58 1/s for Adhesive DA 409. These values were used as the initial values for all the fittings.

The parameters of the Kamal-Sourour model were found based on T_g and the residual cure. T_g rises slower than T_{proc} in the non-isothermal scans indicating that the chemical reaction was the governing mechanism. No residual cure was observed under the heating rates tested for both adhesives. Non-isothermal data was then fit without correction for diffusion.

In the formal kinetic model, a series of reaction types present in epoxy systems—autocatalytic and n-order reaction—were tested for the two adhesives of study (see Table 3.1). The models were fit to the experimental data, individually or in a combination. The best model statistically for both, dynamic and isothermal data, was a two consecutive step model represented as A $\xrightarrow{1}$ B $\xrightarrow{2}$ C, seen in Eq 3.12 to 3.13 in the appendix.

However, several models showed a good agreement with the experimental data. One of those

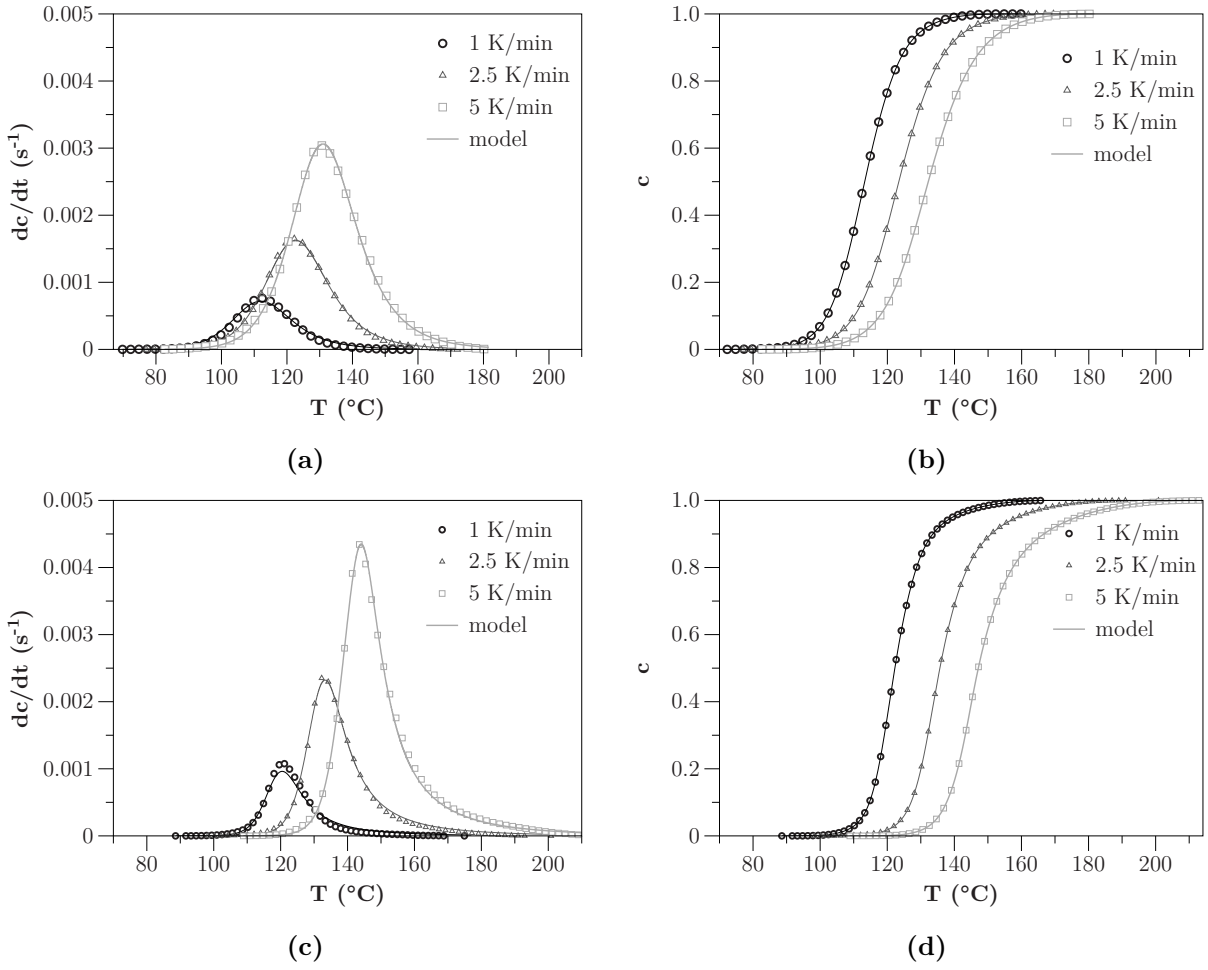

Figure 3.4: Non-isothermal DSC fittings: (a) dc/dt and (b) c for epoxy DA 408; (c) dc/dt and (d) c for epoxy DA 409. The diffusion-controlled reaction mechanism was not included here.

models was a parallel two-step model, A $\rightrightarrows$ B (see Eq 3.7). The first step was an nth-order autocatalysis according to the Prout-Tompkins equation, and the second step was an nth-order reaction.

$$\frac{dc}{dt} = K_1 c^m (1-c)^{n_1} + K_2 (1-c)^{n_2} \tag{3.7}$$

K_1 and K_2 are the kinetic controlled rate constants for steps one and two respectively, n_1 and m are the order of the reaction for the first step, and n_2 is the order of the reaction for the second step. Fig 3.4 shows the accurate fitting of the parallel two-step model for the non-isothermal results of both adhesives, without diffusion correction. The above results applied to the Kamal-Sourour model as well (constant coefficients and no diffusion correction). Table 3.2 summarizes the fitting parameters.

Table 3.2: Regression parameters and statistics for epoxies DA 408 and DA 409. The values correspond to the non-isothermal fittings using a parallel two-step model.

Parameters	Epoxy DA 408	Epoxy DA 409
$\lg(A_1)$ (s^{-1})	11.4984	9.6059
E_1 $(KJmol^{-1})$	103.6431	89.1401
n_1	1.7228	2.3443
m	0.4848	0.8157
$\lg(A_2)$ (s^{-1})	8.7463	2.1501
E_2 $(KJmol^{-1})$	105.0261	88.7121
n_2	1.7228	1.9134
Weighed least squares	0.8242	2.6779
Mean of residues	0.0191	0.0181
Correlation coefficient	0.992	0.998

3.3.2 Glass Transition Temperature

Values for T_{g_0} and T_{g_1} were calculated based on the midpoint temperature method (ASTM D3418) [64, 65]. The values calculated for adhesive DA 408 were T_{g_0} equal to -1.6 °C and T_{g_1} equal 105.3 °C. For adhesive DA 409, T_{g_0} was equal to -5.6 °C and T_{g_1} was equal to 111.1 °C. Several points in between T_{g_0} and T_{g_1} were obtained from the isothermal scans for both adhesives. The model proposed by DiBenedetto [66], given by Eq. 3.8, was implemented.

$$T_g = T_{g_0} + \frac{(T_{g_1} - T_{g_0})\lambda c}{1 - (1 - \lambda)c} \tag{3.8}$$

The parameter λ is defined as $\lambda = \Delta C_{p_1}/\Delta C_{p_0}$, with ΔC_p defined as the difference of the heat capacity in the glassy and rubbery state for the uncured, ΔC_{p_0}, and fully cured, ΔC_{p_1}, networks. In this analysis, λ was a fitting parameter found through non-linear regression. λ values for DA 408 and DA 409 were 1.497 and 1.178 respectively. Fig 3.5 shows the excellent agreement between the model and the experimental data.

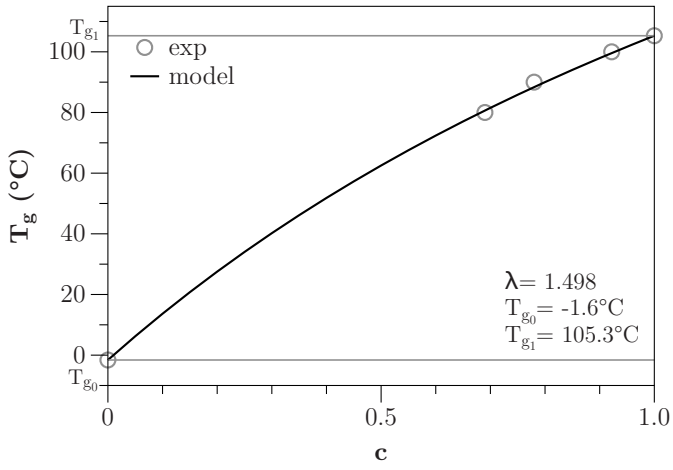

(a)

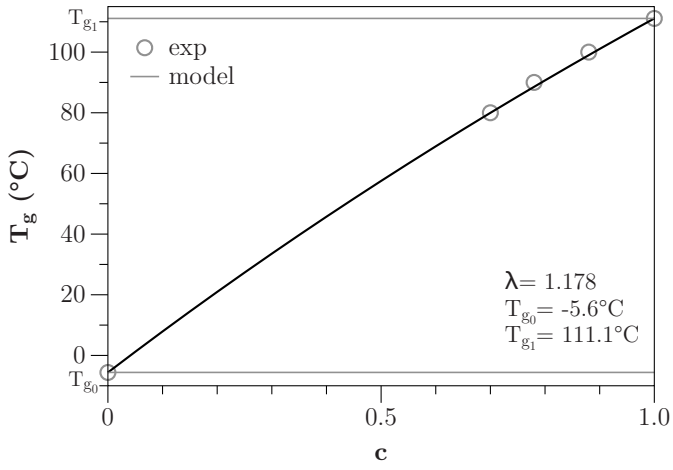

(b)

Figure 3.5: Experimental T_g and numerical fitting using DiBenedetto's equation: (a) epoxy DA 408, and (b) epoxy DA 409.

3.3.3 Isothermal Scans

An initial fast ramp could eliminate loss of data in the heating step before the isothermal cycle. However, the use of a fast ramp must be done with caution. The electronic parameters of the oven were modified to eliminate a temperature overshoot. This was accomplished by following the guidelines provided in chapter 2. The samples showed a thermal delay that requires time optimization factors to shift the scans. The shifting was done based on the peak of the reaction and the initial time.

A scan with an initial ramp of 5 K/min was used as the baseline. A change in the curves was observed at the beginning of the reaction for scans below T_{g_1}, where the thermal optimization should be further evaluated. Fig 3.6 shows the results before and after shifting the data. The same equation was valid to model the data with initial slow and fast ramp.

The parameters obtained in the non-isothermal fitting were used as the initial guess for isothermal scans below T_{g_1}. All samples below T_{g_1} exhibited residual cure. No residual cure was captured for samples tested above T_{g_1}. Here, T_g rises slower than T_{proc} at the beginning of the reaction, and was equal or higher in the last stage. The appropriate diffusion correction was then applied [31].

Flammersheim and Opfermann showed that, using the formal kinetic model, the kinetics can be predicted from isothermal and non-isothermal data simultaneously or interchangeably [42]. They modeled resins where the reaction was chemically dominated for both non-isothermal and isothermal regimes, or partial diffusion was relevant in both non-isothermal and isothermal data [42].

In the present study, the non-isothermal scans exhibited a small contribution of the diffusion mechanism at the heating rates tested. In contrast, the diffusion mechanism was more significant in all the isothermal scans below T_{g_1}. Modeling mixed data of scans with and without significant diffusion influence can lead to the diffusion mechanism being hindered. If a single model is found that predicts all the data accurately, the addition of this model into a FEA residual stress analysis will be more complex. Since one of the purposes of this study was to find a model that can follow the kinetic reaction, and that can be easily added to a residual stresses study in FEA, dynamic and isothermal scans were modeled independently.

Diffusion correction was required for the isothermal data as expected. Fig 3.7 shows the fit of a simpler parallel two-step model, similar to the equation presented in the non-isothermal scans

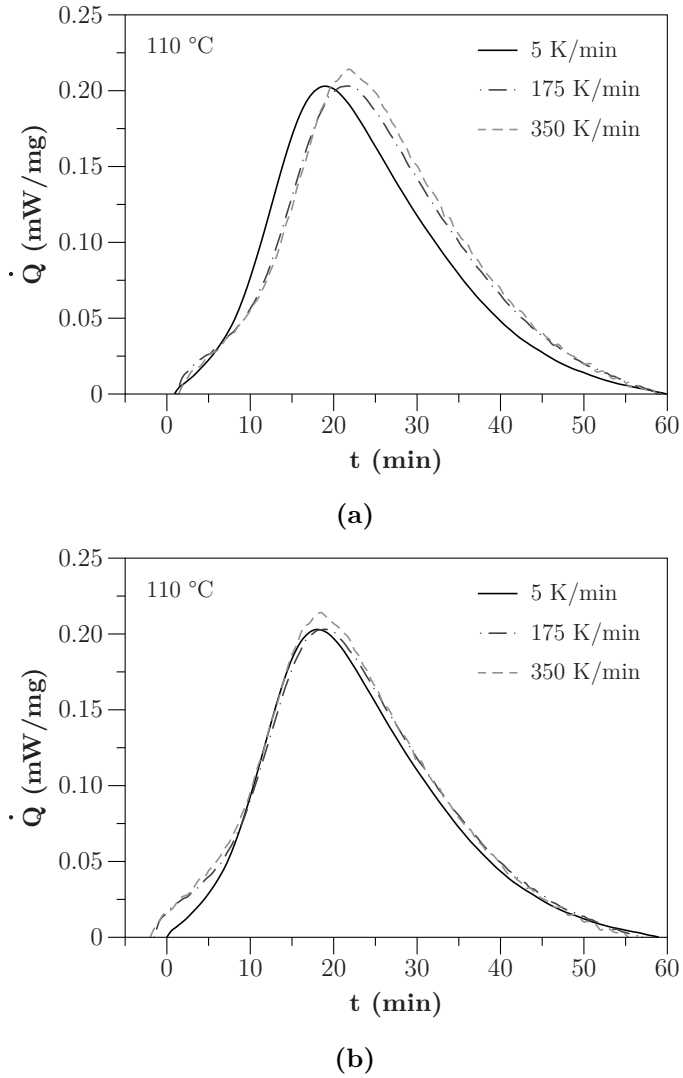

Figure 3.6: DSC method using initial fast ramps in epoxy DA 409 at 110 °C: (a) non-shifted data, and (b) shifted data using the initial time and peak time.

(see Eq 3.7). The model accurately followed the experiments capturing the partial diffusion in both adhesives. When attempting to model the isothermal scans with the Kamal-Sourour model, a correction for diffusion was required, and most coefficients were given as linear or parabolic functions of the temperature. Consequently, that model was not reported here, since the aim was to identify the simplest model.

Here, to capture partial diffusion control, the rate constant was modified based on the model proposed by Rabinowitch [54], shown previously in Eq. 3.6. For T $>T_g$, the rate constant under diffusion control, K_d, was modeled with the WLF type equation by Wise et al. [67]. Since the WLF type equation is used for analysis above T_g [47], an Arrhenius type equation was used to model K_d

for T<T_g. When T is equal to T_g, K_d is equal to the coefficient $K_d(T_g)$.

$$K_d = K_d(T_g)e^{-\left[\frac{C_1(T-T_g)}{C_2+T-T_g}\right]}, \quad T>T_g \tag{3.9}$$

$$K_d = K_d(T_g)e^{-\left[\frac{E_d}{R}\left(\frac{1}{T}-\frac{1}{T_g}\right)\right]}, \quad T<T_g \tag{3.10}$$

With

$$\frac{E_d}{R} = \frac{C_1 T_g^2}{C_2} \tag{3.11}$$

where $K_d(T_g)$ is the diffusion coefficient at the glass transition temperature, T_g, and C_1 and C_2 are the coefficients of the WLF equation. Here, K_d varies for every reaction step added to the model, and C_1 and C_2 are the same for all reaction steps. The initial guesses for the diffusion parameters were based on the work of Flammersheim and Opfermann [47], with C_1 and C_2 starting as 40 and 52 K respectively, and the lg($K_d(T_g)$) equal to -4.42 s^{-1}. Table 3.3 summarizes the fitting parameters. Fig. 3.8 shows the degree of cure prediction for both adhesives under isothermal conditions using the coefficients in Table 3.3. The effect of diffusion below T_{g_1} is seen in both epoxies as well as the chemical reaction control above T_{g_1}.

Table 3.3: Regression parameters and statistics for epoxies DA 408 and DA 409. The values correspond to the isothermal fitting using a parallel two-step model.

Parameters	Epoxy DA 408	Epoxy DA 409
lg(A_1) (s^{-1})	11.7188	9.7001
E_1 ($KJmol^{-1}$)	104.1055	90.1885
n_1	1.2025	1.1929
m	0.4749	0.7156
lg(K_{d_1}) (s^{-1})	-1.8399	-0.8458
lg(A_2) (s^{-1})	20.9656	2.1235
E_2 ($KJmol^{-1}$)	178.4024	88.2790
n_2	5.0224	0.8310
lg(K_{d_2}) (s^{-1})	-2.7956	-4.4182
C_1	22.4681	19.0081
C_2 (K)	61.1754	67.1888
Weighed least squares	0.2491	0.1215
Mean of residues	0.0049	0.0047
Correlation coefficient	0.9976	0.9983

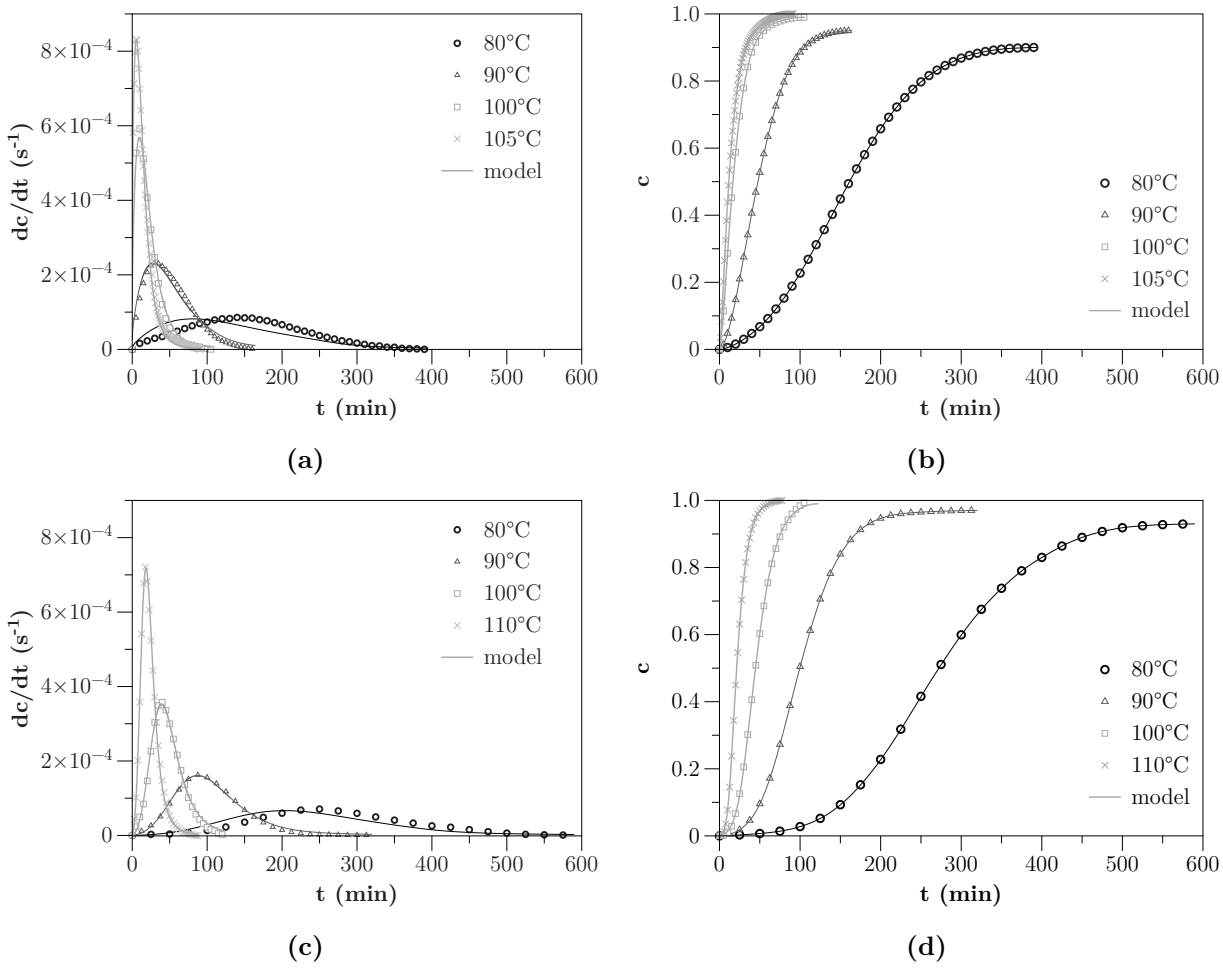

Figure 3.7: Isothermal DSC fittings: (a) dc/dt and (b) c for epoxy DA 408; (c) dc/dt and (d) c for epoxy DA 409. A parallel two-step model with diffusion correction was used.

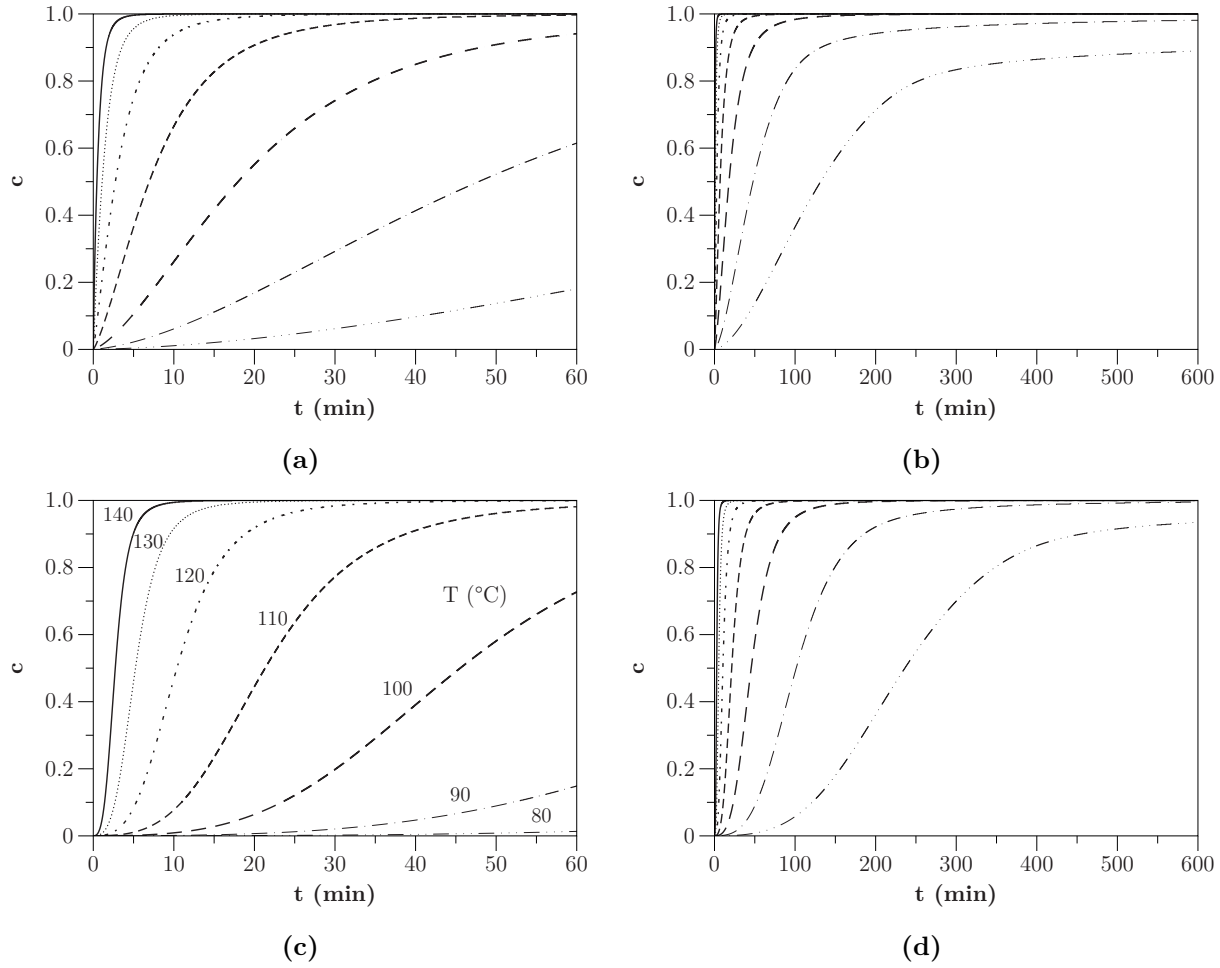

Figure 3.8: c prediction under isothermal conditions using parallel two-step model: (a)-(b) DA 408 (T_{g_1} of 105.3 °C), and (c)-(d) DA 409 (T_{g_1} of 111.1 °C).

3.3.4 TTT Diagram

The next step was to construct the TTT diagram for both adhesives using the parallel two-step model described in Table 3.3. Fig 3.9 shows the different thermal and reactive behavior of these two films with similar composition but different chemistry and physical properties. This diagram can be used to assess storage temperature and processing cycles for these adhesives.

Based on the results shown in Fig 3.9, the processing cycle and cure times for adhesive DA 409 recommended by the manufacturer can be optimized. This material reached a degree of cure of 99 % at 120 °C for 45 min (the manufacturer recommends 1h). The gel point was observed near the 12 min mark suggested by the manufacturer (10.5 min in the TTT-diagram). The discrepancy can be related to the method used to quantify the gel point.

The experimental and numerical results for adhesive DA 408 deviated from the manufacturer's valuesx. Using a cure cycle of 95 °C for 1 h, a degree of cure of 93 % was reached. The samples were structurally stable but with potential to cure further. Reasons for the discrepancy are the manufacturer's processing temperature is lower than T_{g_1} (105.3 °C), and pressure cannot be included in a DSC analysis (the manufacturer recommends a processing pressure of 30 psi). Cruz showed that the pressure and geometry of the part affect the reaction rate constants, distance between neighboring molecules, and molecular mobility [11]. The gel point was reached after 10.2 min at 105 °C.

The study of these two adhesives showed the influence of the glass transition temperature in processing and thermal cycles that affect residual stress build-up during manufacturing. The TTT-diagram then was used to select and optimize processing temperatures and to eliminate the risk of having under cured components. Adhesive DA 408 should be processed at 95 °C for 100 min or 105 °C for 60 min to reach a degree of cure of 99 %.

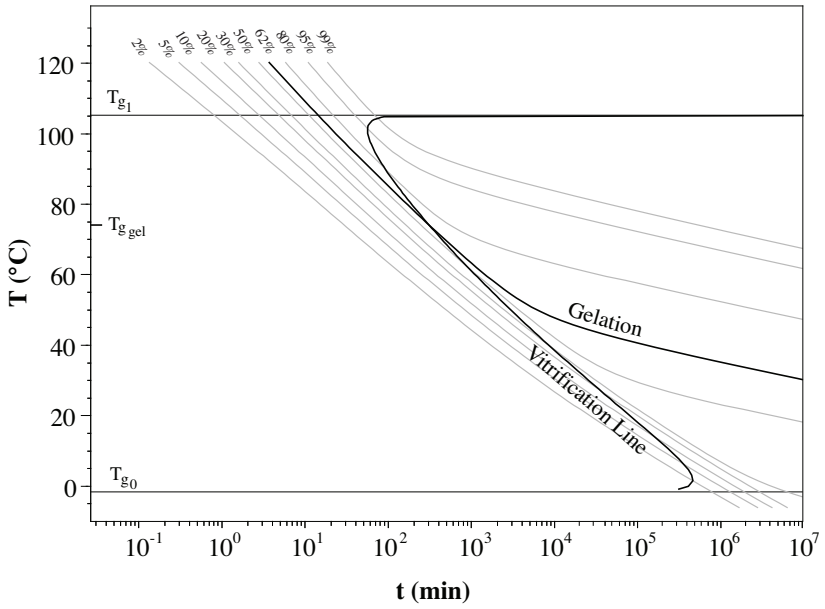

(a)

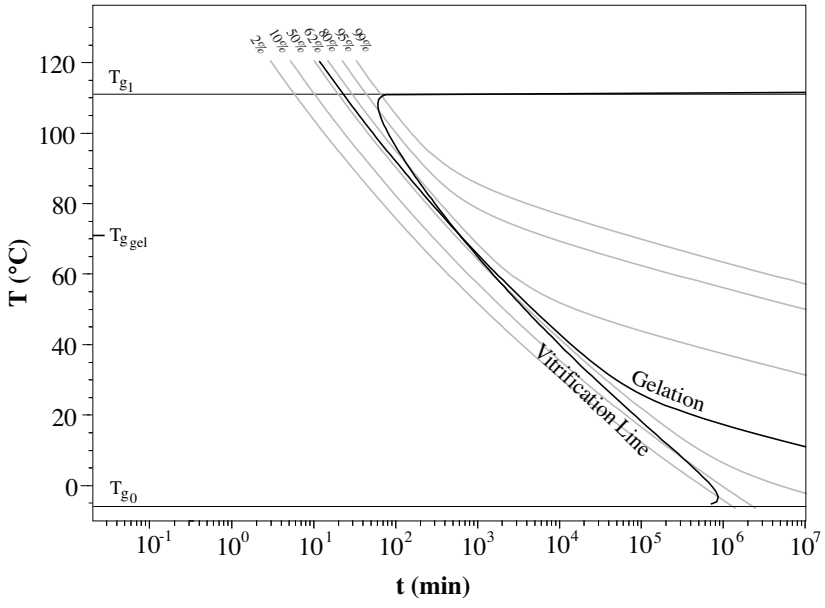

(b)

Figure 3.9: TTT-diagram of adhesives (a) DA 408 and (b) DA 409 using a parallel two-step model.

3.4 Conclusions

A method to construct the TTT-diagrams of film adhesives was outlined for commercial epoxy films DA 408 and DA 409. The method included a protocol to quantify the degree of cure of adhesives that require freezer storage. The filler was weighed after dissolving the adhesive in acetone, and a mass correction was applied in the DSC scans of the adhesive. A DSC analysis of the filler showed that the melting and crystallization temperature of this nylon were far from the temperature range of the exothermal reaction of study.

Vacuum sealed storage, and a period of 2 h of equilibration in between the test and the freezer storage, eliminated the influence of moisture. Testing the adhesives within the first two months of the shelf life gave accurate results where the influence of the pre-curing stage was not observed. The accurate overlapping of the reaction curves and baselines, and the repeatability proved the robustness of the steps proposed. This method can be used to characterize other fillers such as the reinforcement fibers as well.

The use of an initial fast ramp worked to characterized adhesives DA 408 and DA 409 in a quasi-isothermal stage. The method required an optimization in the electronic parameters of the oven to eliminate temperature overshoot. The data was shifted based on the initial and peak time to account for the thermal delay of the sample. The data was baselined using a scan at 5 K/min. A change in the curves was observed at the beginning of the reaction for slow and fast ramps reaching a temperature below T_{g_1}. This method can be applied to various fast curing thermoset systems.

A formal kinetic model gave a simpler yet accurate model to fit the kinetics. The results presented here corresponded to a parallel two-step model, with diffusion correction for the isothermal scans. The Kamal-Sourour model and the formal kinetic model showed no difference modeling the non-isothermal data. However, the Kamal-Sourour model required variable parameters changing with temperature in the isothermal scans and was not reported here because of its complexity.

Future efforts should study the influence of a 1 % wt. thermoplastic filler versus a 52 % wt. carbon fiber reinforcement in the exothermal reaction and thermal behavior of adhesives. Methods to predict the pre-curing stage should also be explored. The numerical stability of the models used should be evaluated in thermal cycles outside of the range tested. Also, a single model that represents all the regimes can be evaluated, assessing the numerical complexity of implementing

this model in FEA with additional physics.

The use of fast ramps has potential in the characterization of fast curing thermosets. The study of complex B-stage resins and thermoset composites can be approached with the method outlined as well. The modeling results will be added to numerical studies of dimensional stability in the manufacturing of composite laminates.

3.5 Appendix

Table 3.4: Regression parameters and statistics for epoxies DA 408 and DA 409. The values correspond to the non-isothermal fittings using a two consecutive step model, A $\xrightarrow{1}$ B $\xrightarrow{2}$ C.

Parameters	Epoxy DA 408	Epoxy DA 409
$\lg(A_1)$ (s^{-1})	13.4933	7.5050
E_1 $(KJmol^{-1})$	119.2157	89.0244
n_1	0.96020	1.0579
$\lg(K_{cat_1})$	0.2391	2.2880
$\lg(A_2)$ (s^{-1})	8.5115	3.2869
E_2 $(KJmol^{-1})$	82.4586	42.9352
n_2	1.3408	1.4871
Fraction of consecutive reaction (fr)	0.1166	0.2980
Weighed least squares	0.1658	0.3286
Mean of residues	0.0053	0.0063
Correlation coefficient	0.9998	0.9997

Table 3.5: Regression parameters and statistics for epoxies DA 408 and DA 409. The values correspond to the isothermal fittings using a two consecutive step model, A $\xrightarrow{1}$ B $\xrightarrow{2}$ C.

Parameters	Epoxy DA 408	Epoxy DA 409
$\lg(A_1)$ (s^{-1})	19.8997	7.9340
E_1 $(KJmol^{-1})$	161.1264	89.0244
n_1	0.6583	0.8073
$\lg(K_{cat})$	-0.5066	2.0441
$\lg(K_{d_1})$ (s^{-1})	-4.4200	8.3505
$\lg(A_2)$ (s^{-1})	6.1754	5.7860
E_2 $(KJmol^{-1})$	65.8456	63.8236
n_2	0.9085	0.8077
$\lg(K_{d_2})$ (s^{-1})	-1.7472	-2.0814
C_1	18	13.9478
C_2 (K)	68	91.3205
Fraction of consecutive reaction (fr)	0.0726	0.0959
Weighed least squares	0.2361	0.0324
Mean of residues	0.0048	0.0024
Correlation coefficient	0.9974	0.9996

$$\frac{dc_C}{dt} = \frac{dc_{A,B}}{dt} fr + (1 - fr)\frac{dc_{B,C}}{dt} \tag{3.12}$$

$$\frac{dc_{A,B}}{dt} = K_1 c_{A,B}^{n_1}(1 + K_{cat} c_{B,C}) \quad and \quad \frac{dc_{B,C}}{dt} = K_2(1 - c_{B,C})^{n_2} \tag{3.13}$$

Chapter 4

Moduli Development of Epoxy Adhesives during Cure

Quantifying the modulus development during cure of adhesives and prepregs is complex due to the resin's behavior. First, each phase and transition needs a careful selection of frequency, strain and thermal cycles. Second, between the gel point and the degree of cure at which resins are typically demolded, the material has a high compliance, causing excessive noise in data. Third, samples are made using multiple layers, which can cause delamination. Lastly, the data analysis and finding of trends is difficult because most tests are performed at discrete cure values.

A testing protocol to detect the moduli changes in one experiment is presented. Adhesive DA 409 was analyzed using the kinetic, viscosity, gel point, and shrinkage information to delimit and select the parameters for the moduli tests. The frequency and strain of each property were selected based on dynamic strain and frequency sweeps. First, the gel point was measured using three methods; the cross-over of storage and loss moduli, the point where the complex viscosity reached industry accepted values, and the intersection of the dissipation factor at multiple frequencies. The gel point was found between 56 and 63 % cure. Second, the viscosity was measured in a parallel plate rheometer, under isothermal and non-isothermal cycles, and fitted using the Castro-Macosko model. Third, the linear shrinkage was measured in a DMA in compression using zero strain to eliminate displacement due to compression loads. The total shrinkage was 4.34 %, with most of the shrinkage occurring in the liquid viscoelastic region. A linear relationship between shrinkage and cure was observed.

Lastly, the modulus was measured in a DMA in a three-point bending test. With this new protocol, the modulus was measured from the gel point up to the fully cured state by sandwiching a partially cured beam between two fully cured plates. The high compliance and noise were mitigated

with this sandwich sample. An effective modulus of the three plates was obtained. The modulus of the partially cured beam was extracted using the elastic sandwich beam theory. This method shows potential in the testing of thermoset composites and films.

4.1 Introduction

Quantification of mechanical properties in the different phases and transitions of a thermoset during cure is required to assess manufacturing protocols. The production of composite components and adhesive bonding requires a detailed knowledge of the thermoset resin. As mentioned in the scope of this work, a poor understanding can cause component defects such as warpage, delamination, poor mechanical performance and incorrect fitting in assemblies. Modeling has been used as a predictive engineering tool to optimize and eliminate risk factors because of the thermoset behavior during the processing of a component. Modeling of thermoset composites focuses on the prediction of process-induced residual stresses, which requires a detailed kinetic and mechanical characterization. Chapters 2 and 3 presented the kinetic characterization of commercially available resins. This chapter details the mechanical characterization of the same adhesives.

The focus of this chapter is the characterization of the modulus. A mix of empirical and experimental models have been used and they are divided into elastic and viscoelastic approaches. The following models have related the modulus to the degree of cure using elastic theory.

Levistky and Shaffer proposed a reaction dependent elastic model for Poisson's ratio [68, 69]. They studied the thermal stresses developed in the processing of thermosets. The model included a mixture of reacted and unreacted material. Levitsky and Shaffer assumed a constant bulk modulus, K, and described a Poisson's ratio function of the material state (reacted or unreacted), ν, as shown in Eq. 4.1.

$$\nu(t) = \frac{3K - 2G_{\infty}c(t)}{6K + 2G_{\infty}c(t)} \tag{4.1}$$

G_{∞} is the shear modulus of the fully cured resin, and c is the degree of reaction or solidification. Lindrose published a study on monitoring moduli changes in curing epoxies via ultrasonic waves. Lindrose suggested that Shaffer and Levitsky's assumption of constant bulk modulus for curing epoxies was not correct [70].

Osswald proposed an empirical linear dependency of the elastic modulus, E, and ν with c to include mechanical property development in compression molding of thin and thick sheet molding compound (SMC). The model had three regions; fluid like behavior until a c of 5 %, linear growth of E and ν between 5 and 80 % cure, and a constant E and ν above 80 % when the material reached its final strength based on Barone and Caulk's work [71]. Fig 4.1 shows Osswald's model.

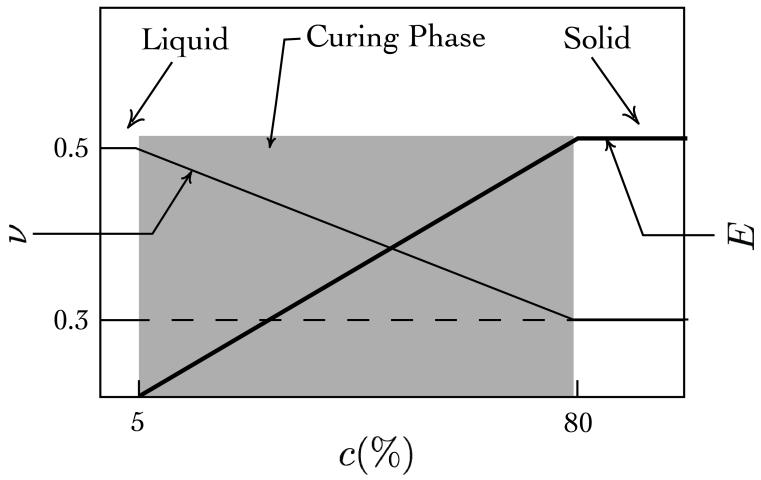

Figure 4.1: Approximation of Poisson's Ratio, ν, and elastic modulus, E, versus c. Adapted and translated from the original slide of a presentation given at the IKV: Institute of Plastics Processing at RWTH Aachen [72].

This empirical model has been used in shrinkage and warpage prediction in SMC and glass mat thermoplastic (GMT) plates [73–77]. Golestenian and El-Gizawy also used this model in a numerical method to investigate residual stresses in thermoset composites reinforced with fiber woven mats [78]. Although modeling the fiber undulation and the resin interaction is a challenging for these composites, they reported good results.

The bounds and linearity proposed by Osswald do not always apply. The gel point and structural integrity change based on the material. Resins are designed to gel and solidify at higher or lower values based on their application. For example, Ramis et al. reported a non-linear relationship of a normalized modulus and c until 75 % cure, followed by a linear relationship between 75 and 100 % cure [21]. They studied thermoset powder coating (TGIC). Ruiz and Trochu also reported a non-linear correlation between E and c in an E-glass/T580-63 glass/polyester composite [79]. They performed a three-point bending test on beam samples. First, they tested fully-cured samples at

different temperatures, and then they repeated the protocol for partially-cured samples relating both results. They fitted the results of E versus c using hyperbolic cosine laws and shift factors for c and T_g.

Hahn and K. S. Kim studied residual stress development at different curing stages for the T300/3501-6 graphite/epoxy [80]. They used the thermochemical data reported by Lee et al. [81]. For the mechanical testing, they partially cured unidirectional and cross-ply strips, and cooled them down to room temperature at a rate of 3 K/min. The laminates were then subjected to a tensile test. They measured the transverse, E_2, and longitudinal, E_1, moduli for five discrete curing points. E_2 slightly changed over time and was not studied further, whereas E_1 showed a big dependency to c. These authors used a linear-elastic constitutive model to relate to c, as shown in Eq.4.2.

$$\frac{E_2(t)}{E_2^{\infty}} = f(c) = c \tag{4.2}$$

where E_2^{∞} is the transverse modulus of the fully cured material. ν was considered constant and the shear modulus was not included in the analysis. This data and method neglected the temperature influence on property development and should be carefully reevaluated for heat-activated thermosets.

Bogetti and Gillespie presented another constitutive model in their work on process-induced stresses in thick thermoset composites [82]. They reported a mathematical model for the cure shrinkage and the cure-dependent elastic modulus of a CYCOM 4102 polyester with 54 % by volume of E-glass, and AS4/3501-6 graphite/epoxy [81] (67 % by volume of fibers), both previously measured by other researchers. They assumed E and ν development began at the gel point and stops when diffusion dominated over the chemical reaction. They proposed a c-mixing rule model for the resin modulus during cure. They compared their model to Hahn and K. S. Kim's experimental results [80] and obtained good agreement. Their work shows the importance of both thermal and chemical shrinkage. These shrinkages modify the specific volume as the part cures, becoming a source of internal loading. Poisson's ratio was assumed constant, and the shear modulus was calculated based on the isotropic material relation with E and ν. Their model of the cure-dependent modulus gave similar results to those of Levitsky and Shaffer [68, 69], who considered a constant bulk modulus and changed Poisson's ratio in their constitutive model. Bogetti and Gillespie's model

assumed that the modulus and cure shrinkage remained constant once the reaction is dominated by diffusion.

Johnston collaborated on a finite element program, now COMPRO, for the prediction of residual stresses and deformation induced in autoclave manufacturing [83]. One of the outcomes of his work were two elastic models for E and ν including processing temperature and T_g dependencies. The cure dependency was implicitly included through T_g. First, Johnston added a T-shift to Bogetti and Gillespie's model [82]. For the second model, Johnston approximated the mechanical development of thermosets as a cure-hardening process that can be divided into linear segments monotonically increasing (this was analogous to the work of Chapman et al. that related E versus crystallization in thermoplastic composites [84]). All the segments were considered elastic, neglecting viscoelastic relaxation.

To validate his work, this author used experimental data from the AS4/8552 graphite/epoxy composite. In his research, collaborators tested rectangular samples in dynamic torsion using a rheometer. The tests were done at multiple strains as the samples cured isothermally. The samples were made with unidirectional prepregs. This author superposed values of E from the rheometry test with values of c from a DSC test, both experiments ran under the same conditions. When using this model, the segments are not enough to capture all the changes, and the model does not include frequency dependency. This model has been used in its original form or with adaptations in the prediction of deformations in autoclave processing [85], for studies of thin and thick RTM parts, and analysis of the spring-forward effect on part corners [86]. Johnston's model has been adapted to include more segments and more complex relations between T_g and c [87, 88]. The extended model requires up to nine parameters.

Khoun et al. reported experimental methods to quantify properties of thermosets used in composites [89]. They studied CYCOM 890 RTM epoxy resin. To measure mechanical properties, these researchers adopted DMA in three-point bending mode, and rheometer in the solid-state torsion mode [79, 83, 87]. They used Johnston's extended equation to model the modulus development during cure. Overall, the model captured the main transitions, but was not able to capture the smooth modulus development between these transitions.

Several viscoelastic models have also been studied. Dillman and Seferis studied dynamic mechanical properties of thermosets as a function of viscoelastic and kinetic parameters [90]. The

result was a viscoelastic model that includes the kinetic effect of the curing reaction, and temperature and frequency dependencies. They based their model on the analogy between dynamic mechanical relaxation and dielectric relaxation [91]. To validate the model, they subjected partially cured plates of a TGDDM/DDS epoxy system to DMA. The tests were performed at four isothermal temperatures and at a frequency within the linear-viscoelastic region (LVR). Analogous to dielectric studies, the authors coupled kinetic parameters to this model. Dillham and Seferis' model is a generalization of the Standard Linear Solid model for non-reactive systems, or the so-called single relaxation time model. This model was developed to capture kinetic analysis of dynamic mechanical data, and it accounts for the frequency dependency. This equation predicts modulus' values at different frequencies.

White and Hahn studied residual stresses in thermoset composites [92, 93]. Two publications, one on a process model [92], and another one on experimental validation [92], summarized their results. The model, targeted to thin asymmetric-laminates, included chemical and thermal strains. The transverse compliance J_{22} was considered linear-viscoelastic with cure-dependent parameters, whereas E_{11}, E_{22} and the major Poisson's ratio ν_{12} were considered elastic and cure dependent (J_{22} was based on Schapery's model [94]). These authors tested IM6/3100 graphite/bismaleimide using an intermittent cure technique similar to that of Hahn and K. S. Kim [80]. A series of tensile tests and creep tests showed E_{11} and E_{22} increase with c, whereas ν_{12} decreases. The model showed a good fitting of the experimental results, with a variation on the later cure stage.

Y. K. Kim and White studied the viscoelastic behavior of Hercules 3501-6 epoxy system during cure [95]. They tested the stress relaxation response for five degrees of cure between 0.57 and 0.98 on a DMA. Stress relaxation of each degree of cure was recorded for several temperatures. Master curves and shift factors for the five cure stages using time-temperature superposition were presented. They explored two constitutive models: a power law model and a discrete exponential (Prony) series. The authors concluded that the power law model did not accurately describe stress relaxation of this material for a wide temperature range. Fittings with the exponential Prony series were in good agreement with the experiments. These authors reported that the degree of cure highly affected the stress relaxation, especially above the gel point. Y. K. Kim and White showed applications of this constitutive model in later publications [96–98].

Other relevant publications including viscoelastic models are the work of Wang et al. [99],

O'Brien et al. [100], and Prasatya et al. [101], and Ruiz and Trochu [79].

Despite the number of models and approaches presented, no consensus on the experimental and analytical approaches has been reached, and the new material developments make it more difficult to do so. One of the biggest challenges is to find a continuous protocol to follow the modulus throughout the entire reaction. The delimitation of the bounds; beginning and end of the modulus, and their role in the selection of frequency, strain, load and thermal cycles is also another challenge.

To this effort, the focus here is to capture the modulus by identifying the properties and transitions in the liquid and gelation states. The method includes sample preparation to reduce compliance, selection of frequency and strain for each test, and temperature cycles based on a kinetic analysis reported previously (see Chapter 3) and the manufacturing conditions of components with this material. The use of a sandwich sample to capture the modulus development in one test is evaluated. This technique shows the potential to simplify discrete sample protocols of the modulus where multiples tests are performed at discrete curing values. The benefits and recommendations for potential improvements of this method are outlined.

4.2 Materials and Methods

4.2.1 Sample Preparation

Three different types of samples were prepared using epoxy adhesive DA 409 to study the complex viscosity, shrinkage, and complex moduli, respectively. The samples were produced by stacking several layers of adhesive DA 409, each with a thickness of 0.152 mm, cut to the required geometry outlined below. All the dimensions were selected using a plot of the sample thickness versus complex moduli by TA Instruments, which gives a recommended range of dimensions based on the instrument operating range [102, 103]. Before testing, each sample was equilibrated to room temperature, 25 °C, over a 3 h period. The manipulation of the samples replicated the standard analysis performed in DSC to match the sample pre-cured state and thermal history across all testing protocols (refer to Chapter 3).

Viscosity and Shrinkage Samples

The complex viscosity was measured in circular disks with thickness 1 ± 0.1 mm and a diameter of 25 mm. The chemical shrinkage—assumed as the through thickness shrinkage in this work—was measured in rectangular plates with dimensions of 14 x 12 x 5.2 mm. The chemical shrinkage was measured in adhesive DA 409 and in unidirectional carbon fiber-epoxy prepreg DA 409U/G35 150 samples. All the samples were made of uncured film for the viscosity and shrinkage analysis.

Moduli Samples

The moduli were measured in rectangular beams fully cured and partially cured up to the gel point with dimensions 44.0 x 12.7 x 1.75 mm. The gel point, c_{gel}, was obtained from the complex viscosity tests. Samples of adhesive DA 409 and unidirectional carbon fiber-epoxy prepreg DA 409U/G35 150 were tested. The sandwich beams were tested with the fibers aligned in the transversal direction where the epoxy modulus development during cure is more significant. The composite modulus is dominated by the stiffness of the fibers when they are aligned in the longitudinal direction [104].

Samples were manufactured using two techniques; the vacuum bagging technique in a convection oven, under 0.09 MPa (13.4 psi) negative gauge pressure, and compression molding. Using the vacuum bagging technique, thickness variation and a semicircular profile were observed for these small samples, and thus these samples were discarded. The compression technique gave an even thickness profile and therefore these samples were used for the analysis presented here. The temperature ramp used was predicted based on the experimental and modeling results of the kinetics analysis presented in Chapter 3. The partially cured samples were removed once the sample reached c_{gel} and immediately frozen to assure that the degree of cure matched the kinetics analysis. The fully cured samples were removed later and cooled down at a 5 K/min rate to reduce warpage effects. Fig. 4.2 shows the processing cycle for the fully and partially cured beams.

First, rectangular beams were made for the fully cured analysis. A new sample preparation method was developed for the partially cured samples. At c_{gel}, the adhesive and prepreg did not have enough strength to withstand a load without permanently deforming and stretching. To solve this problem, the partially cured, yet tacky and compliant, beams were placed in between two plates of a stiffer material. This sandwich beam reduced the material and structural compliance

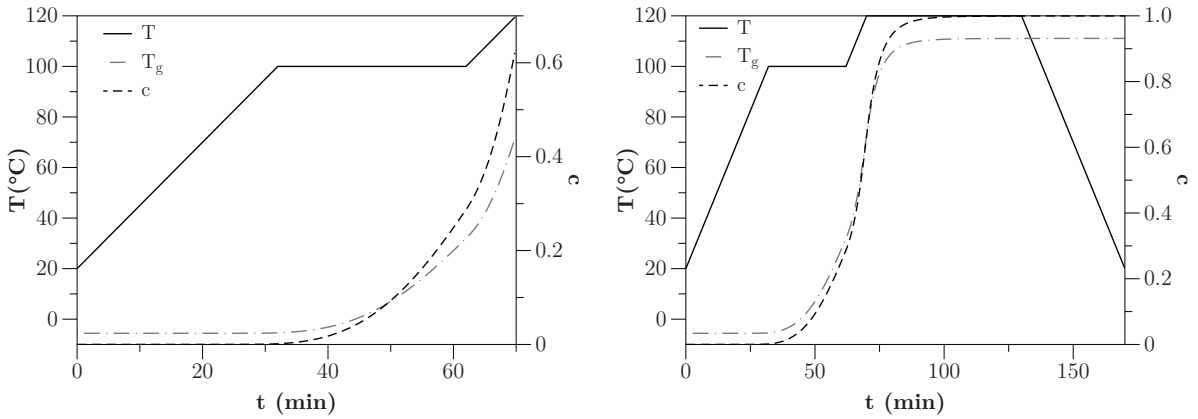

Figure 4.2: Manufacturing cycle used to make rectangular beams for three point bending test of: (a) partially cured samples, and (b) fully cured samples.

of the samples, minimizing the high noise to signal ratio due to the resolution of the DMA testing frame. Four type of beams were tested in this study. The four trials consisted of partially cured prepreg DA 409U/G35 150 placed in between beams made of:

a. Thermoplastic plates

b. Fully cured mix activated epoxy plates (system 2000 epoxy resin mixed with hardener 2020 both from Fibre Glast Development Corporation).

c. Steel plates

d. Fully cured plates of epoxy DA 409.

4.2.2 Viscosity and Gel Point Test

The uncured disks with thickness 1 ± 0.1 mm and diameter 25 mm were tested on a TA Instruments ARES-LS2 Advanced rheometer. The elastic and storage shear moduli, G' and G'', and complex viscosity, η^*, were characterized as a function of time, temperature, and heating rate. The tests were performed in 25 mm parallel plates coated with mold release Frekote® 700-NC to allow sample removal.

First, dynamic-strain sweep tests were executed to ensure that all the rheological measurements were within the linear viscoelastic region (LVR). For this test, the temperature was set to 25 °C, and

the frequency was varied between 1 to 10 Hz. Consequently, a 1 % strain and a frequency of 1 Hz were selected for the dynamic temperature ramp and time sweeps. Second, dynamic temperature-ramp tests were performed to characterize the temperature and heating rate dependency of the viscosity. The temperature was varied from 30 to 180 °C at a rate of 1, 2.5, and 5 K/min. Lastly, dynamic time-sweep tests were performed at 100, 120, and 140 °C between 20 and 80 min heating the sample from 40 °C at a rate of 5 K/min.

4.2.3 Shrinkage Test

The uncured plates with thickness 5.2 ± 0.1 mm were tested on a TA Instruments RSA III DMA. Samples were tested in the compression mode in the 8 mm parallel disks. DMA in compression mode has been reported as a method to quantify through thickness shrinkage in composites [104–106]. In this study, tests were done at a frequency of 1 Hz, in the auto tension adjustment mode, with a constant static force of 0.02 N and a sensitivity of ± 1 mN. In this mode, the instrument adjusts the gap to maintain a constant compressive force. A zero strain was set to eliminate gap changes due to the dynamic load. Samples were heated from 30 to 120 °C in 1 min and held there for 80 min. The instrument took 4-5 min to stabilize. A better approach would be to preheat the DMA before testing. The analysis was performed at a constant temperature. A preliminary analysis assumed that the thermal expansion coefficient, α, of the instrument and sample did not change at a constant temperature, and that α of the sample did not change with c. With this protocol, the gap compensation was only due to through thickness shrinkage.

4.2.4 Moduli Test

Three-point bending tests with a 25 mm span were performed. The fully cured beams were characterized first. Similar to the viscosity protocol, several strain sweeps were executed to find the LVR region. For this test, the temperature was set to 25 °C, and the frequency varied between 1 to 10 Hz. Consequently, for the fully cured samples, a strain of 0.002 %, a preload between 0.2 and 0.3 N, and a frequency of 1 Hz were selected for the temperature ramp and time sweeps. Temperature sweep tests were performed to evaluate the dependence of the moduli to the temperature for a fully cured sample. The temperature varied from 30 to 180 °C at a rate of 5 K/min. Based on the temperature sweep results, dynamic-time sweep tests were performed below T_{g_1} at 100, 105, and

110 °C between 20 and 100 min for the four types of partially cured beams.

4.3 Results and Discussion

The selection of the testing frequency included the kinetics behavior and the viscoelasticity. The manufacturing of components made of adhesive DA 409 and prepreg DA 409U/G35 150 via vacuum bagging in an oven is on the order of magnitude of 10^1 to 10^2 min (between 60 and 130 min). However, the viscosity is reached between 22 and 75 min at the temperatures tested, and the exponential growth occurs within minutes or seconds (see Fig. 4.3(b)). The data collection of reactive systems in a rheological analysis is in the order of 10^{-1} to 10^1 s (between 0.06 and 10 s; 0.1-15 Hz) to eliminate loss of data. Higher frequencies capture more data in a short period of time but shift rheological values to higher magnitudes, compared to the static case. This requires a shift, for example, with the frequency-temperature superposition principle—this principle does not always apply particularly during a phase change at the temperatures tested [107] . A test done at a small frequency would give values closer to static conditions, but it could cause significant loss of data. The frequencies selected were a tradeoff between these competing situations.

Also, the analysis presented here assumed that the LVR of adhesive DA 409 at a constant degree of cure—uncured for the viscosity tests and fully cured for the moduli tests—was representative of all the states during the progression of the reaction. Further analysis of the relation between linear viscoelasticity and the degree of cure could improve the accuracy of this analysis.

4.3.1 Gel Point

Three criteria were applied to quantify c_{gel} of DA 409 [108] as seen in Fig. 4.3. First, c_{gel} was identified as the cross-over of G' and G'' using the Tung and Dynes method in the dynamic temperature ramp tests [109]. The crossover was captured at 148.5 °C using a 5 K/min ramp measured at 1 Hz, giving a c_{gel} of 56 %. The gel point value given by this test is frequency dependent [110].

Second, c_{gel} was quantified as the point where the viscosity reached a value between 10^3 and 10^4 Pa-s, assuming that in that region the adhesive no longer flows [108]. In the dynamic time sweep tests, this viscosity range was reached at 72.4, 28.3, and 21.8 min for the 100, 120, and 140 °C test respectively, as seen in Fig 4.4(b). This second criteria gave a gel point at a c of 63 %.

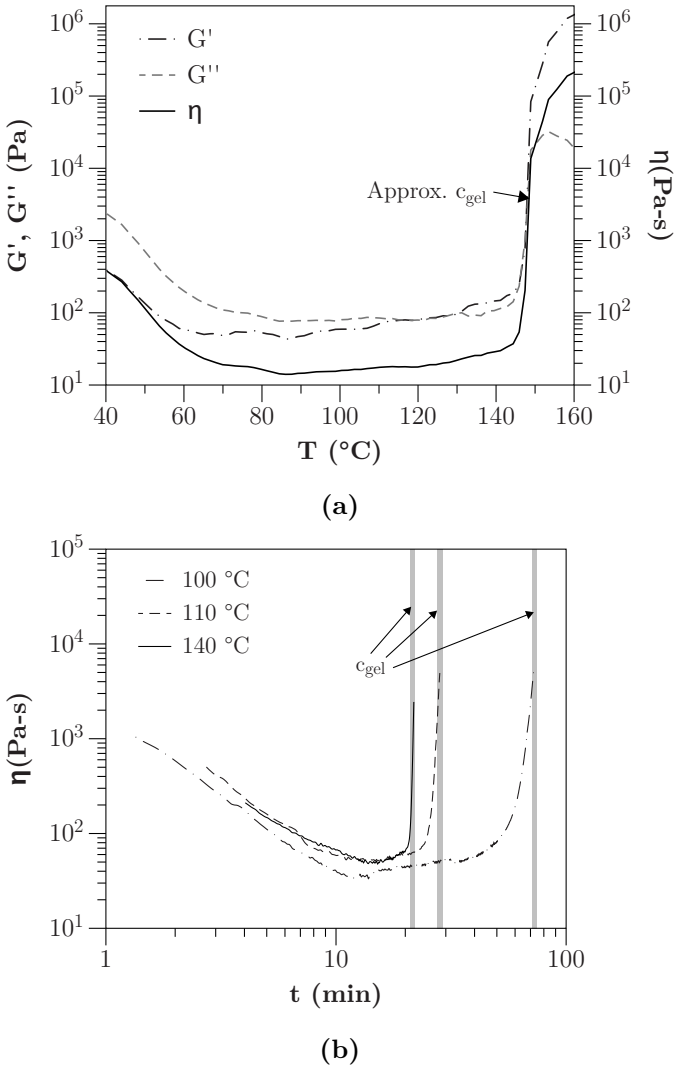

Figure 4.3: c_{gel} of epoxy DA 409: (a) G'-G'' cross over, and (b) η rise—a dynamic–isothermal cycle was used with an initial heating rate of 5 K/min.

Third, the frequency independent c_{gel} proposed by Winter and Chambon [110, 111] was emulated. This criterion uses the crossing of tan δ curves obtained in various simultaneous frequency sweeps, giving a more accurate gel point. To approximate the effects of a multi-wave sweep test, two dynamic temperature ramp tests at 0.1 and 1 Hz were performed. The tan δ values for both frequencies were plotted over time. This gave a c_{gel} of 62 %. A c_{gel} between 62 and 63 % was chosen for the rest of the analyses. This range fits within the reported data in studies of epoxy systems.

4.3.2 Viscosity

Fig. 4.4 shows the viscosity of epoxy DA 409 for the temperature and time sweep tests. The viscosity decreased at the early stage of the reaction with the temperature increase reaching minimum values between 10 and 50 Pa-s. After the minimum viscosity region, η_{min}, the viscosity rose exponentially as the molecular weight increased the during the kinetic reaction [33]. Above 2443 to 8958 Pa-s, the network exhibited gelation followed by the development of the solid moduli, which was measured in the DMA. For the geometry and rheometer transducers used, the maximum G^* value that could be measured was 60.3 MPa. Moduli values of the adhesive tested were in the range of 8 to 15000 MPa limiting the analysis to the liquid viscoelastic region.

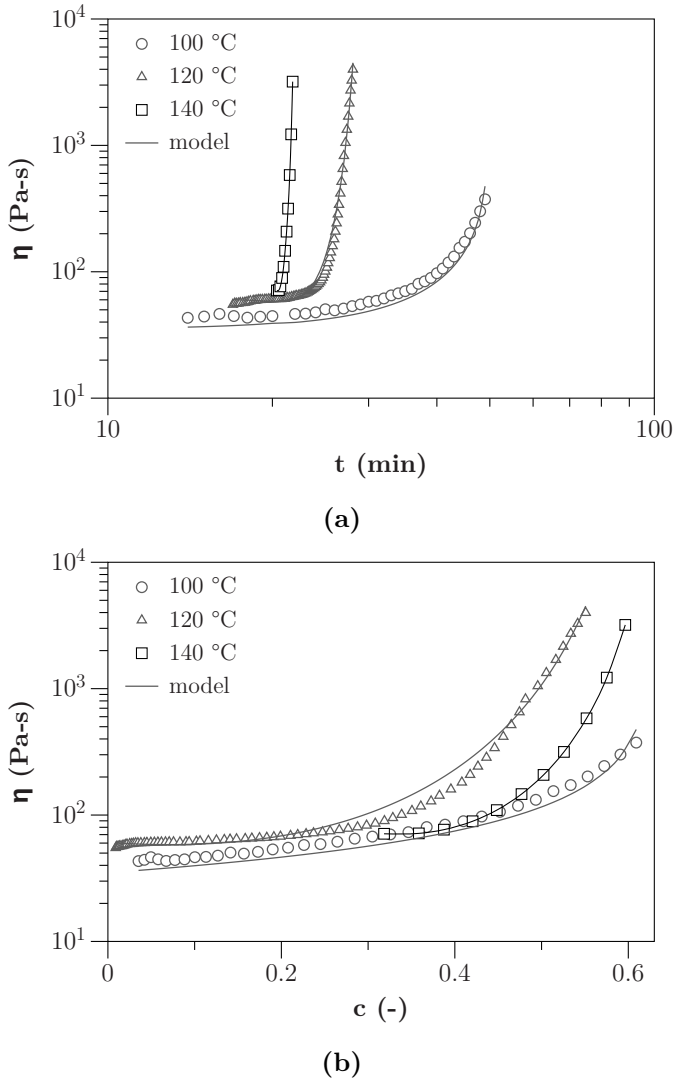

Figure 4.4: Viscosity of epoxy DA 409 as a function of (a) time and (b) cure for various temperatures.

Table 4.1: Parameters of the Castro-Mackosco model used to fit the isothermal portion of the viscosity curves.

Parameter	100 °C	120 °C	140 °
η_0 (Pa-s)	34.96	60.73	723.26
E_a (J/mol)		90000	
c_{gel} (-)		0.63	
c_1 (-)	0.7334	-0.6913	-7.648
c_2 (-)	0.0525	5.023	13.67

The rheological results gave values of the viscosity over time and temperature history. The kinetic analysis was then used to obtain the viscosity development as a function of the degree of cure. Curves of viscosity and degree of cure over time were then superposed to generate a graph of η versus c. Fig. 4.4 shows the numerical fit using the Castro-Mackosco model [112] and the coefficients are summarized in Table 4.1. Notice that the modeling was only performed in the isothermal region which changes the coefficients, specially for 140 °C were the analysis started at a c of 30 %.

The minimum viscosity result (see Fig. 4.4(a)) can be used to modify the manufacturing process of samples and composite components in this study. A pressure reduction in the processing cycle before reaching the minimum viscosity could give significant benefits. It can avoid squeezing out all the resin, which could induce dry fibers and uneven consolidation of the composite due to the lack of resin. It can also prevent undesired flow that could produce uneven thickness and fiber/matrix content in the final part. The optimization of the heating rate can reduce the porosity in adhesives. A longer minimum viscosity region will induce the required flow to eliminate porosity. A flow region that balances the elimination of porosity and produces even thickness profiles can be studied with the kinetic and rheological models presented in this work. Further porosity and flow studies will be required for this purpose.

4.3.3 Shrinkage

The shrinkage was accurately measured in the carbon fiber epoxy sample, DA 409U/G35 150, without modifying the DMA setup, as seen in Fig. 4.5. A chemical shrinkage of 4.34 % was captured using equation 4.3 [48, 113, 114].

$$\varepsilon_v = \left[1 + \frac{1}{3}\left(\frac{h - h_0}{h_0}\right)\right] - 1 \tag{4.3}$$

ε_v is the volumetric shrinkage, h_0 is the initial gap, and h is the actual gap. The shrinkage exhibited a linear dependency with the degree of cure. As seen in Fig. 4.5, a c_{gel} of 62 % corresponded to a shrinkage of 2.63 %, which is 60.5 % of the total shrinkage. The rapid increase of shrinkage occurred in the liquid viscoelastic region. The sample shrank 1.71 %, in a slower fashion, in the solid viscoelastic region where the stiffness grows.

During the stiffness growth, the residual stresses are caused by the competing mechanisms of chemical shrinkage, stiffness growth, and stress relaxation. If the stiffness increases faster than the shrinkage, residual stresses during processing could cause crack propagation. The interaction shrinkage-stiffness growth is a topic of further study [82].

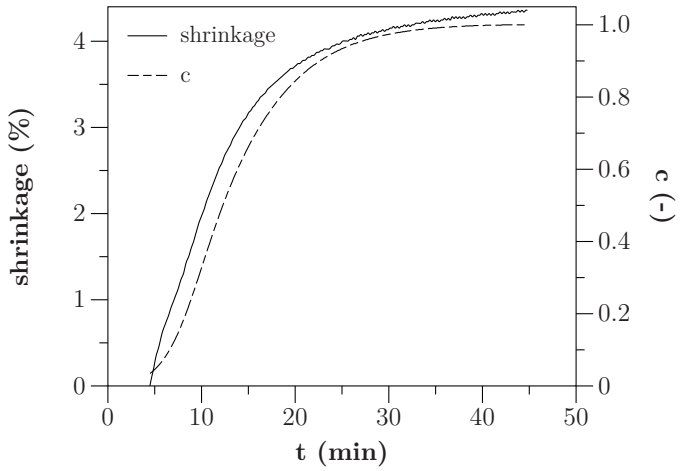

Figure 4.5: Calculated volumetric shrinkage of composite DA 409U/G35 150. Test performed at 120 °C.

The epoxy DA 409 sample dripped when it reached the minimum viscosity making this result unreliable. Osmeda recently reported a solution to this problem by attaching a piston-type cell to the DMA [104]. This device encloses the sample with a degassing unit eliminating gap errors due to radial flow, and it also compensates for potential air entrapment. The fibers in this composite were sufficient to restrict the resin flow in the DMA however in compression, composites with lower viscosity values of the matrix will require an enclosed system.

Also, it is important to assure bonding and contact between plates before testing, because gaps and voids will alter the gap change results. The zero-strain eliminated compression due to dynamic

stresses. The instrument took 4-5 min to stabilize in the transition from heating to isothermal state. Preheating the DMA before testing could eliminate this temperature instability. The gap change was measured after the stabilization of the transition from heating to the isothermal segment. The gap change in the composite then only combined the chemical shrinkage and the consolidation of the composite laminates [104, 115]. The gap change can be divided in two stages: long before gelation chemical shrinkage and laminate consolidation play a role, and after that point only chemical shrinkage is present [115].

The shrinkage of the composite along the fiber direction is constrained by the stiffness of the fibers and it was assumed equal to zero in this work. This assumption does not significantly decrease the accuracy of the warpage calculations according to results by Ersoy et.al [106]. This preliminary study only tested the shrinkage at the processing temperature. A complete study of the shrinkage at different temperatures and ramps could be performed to better understand the contraction in the solid viscoelastic region. This could allow the optimization of temperature ramps to reduce dimensional stability of final components. The evaluation of the thermal expansion coefficient is part of further work to suplement this analysis.

4.3.4 Moduli

Fully Cured Sample

The temperature dependency of epoxy DA 409 and prepreg DA 409U/G35 150 are shown in Fig. 4.6. The storage modulus of the fully cured composite with the fibers aligned in the transverse direction was between 12 and 15.7 GPa below 95 °C. The modulus decayed rapidly after 95 °C to a value of 4 GPa at 120 °C—processing temperature. The glass transition temperature of the fully cured composite, T_{g_1}, was between 111.6 and 117.0 °C using the peak of tan δ criteria. This value agreed with a T_{g_1} of 111.1 °C measured in DSC (see Chapter 3). The strength added by the fibers eliminated compliance effects that cause high deviations in T_{g_1} measurements via DMA. Some of the high values were result of a shift due to frequency dependency and variations in sample geometry. E'_∞ for epoxy DA 409 was between 1.59 and 1.69 GPa. The storage modulus decreased to 1.31, 1.25, and 0.95 GPa for 100, 105, and 110 °C respectively. This value will serve as the baseline to correlate the final modulus of the partially cured samples at the respective temperatures. The

modulus dropped to 0.19 GPa at 120 °C which is the manufacturing temperature.

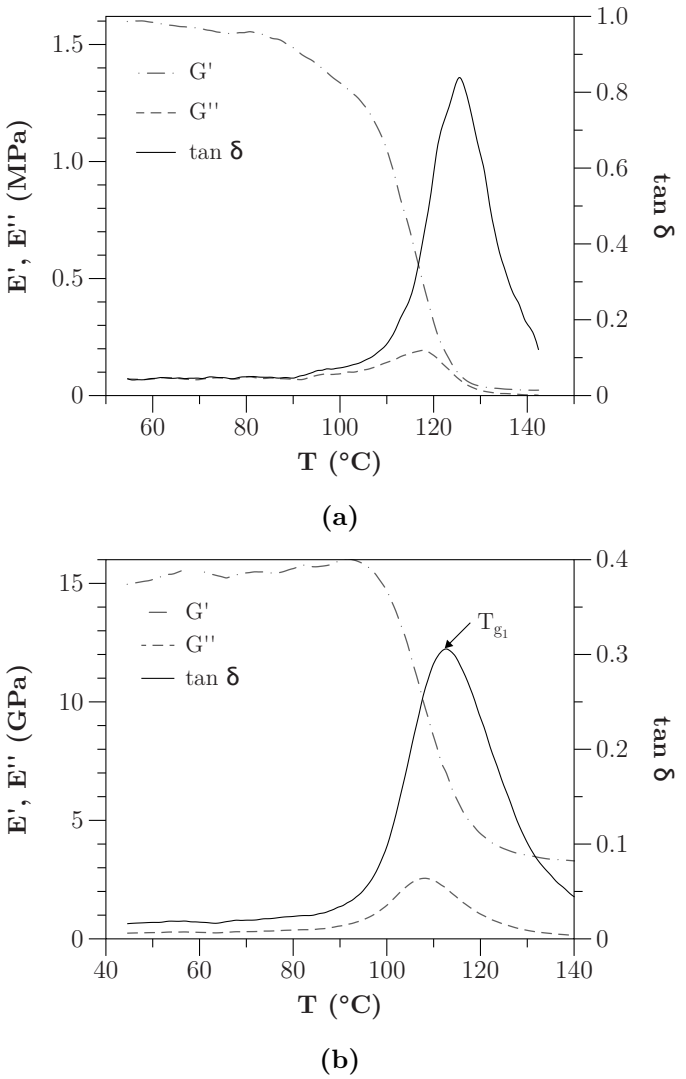

Figure 4.6: E', E'' and tan δ in three point bending of fully cured: (a) epoxy beam DA 409, and (b) carbon fiber/epoxy beam DA 409U/G35 150.

Partially Cured Sample

The new sample protocol required a careful analysis of the outer plates used to hold the partially cured sample as seen in Fig. 4.7. The sandwich beam with thermoplastic outer plates (a) gave a high noise-to-signal ratio value because at the temperatures tested the beam compliance was higher than the recommended range for the instrument. Also, during cure this sandwich beam was permanently deformed. The beam with epoxy 2000 outer plates (mix activated system) (b) exhibited the same problems as the thermoplastic case; compliance outside the recommended range

and permanent deformation of the beam. Delamination also occurred in this sample. The limiting adhesion and compliance requirements in this sample can be explained by the low T_{g_1} of epoxy 2000, which is 82 °C. The elastic modulus of this epoxy decreased significantly even at the lowest temperature tested of 100 °C.

The steel plates (c) gave better results but showed two limitations. First, the modulus was under predicted in samples with poor bonding, causing separation of the partially cured samples from the steel plates. Second, the modulus was over predicted for samples with proper adhesion because of the contribution of the steel stiffness. Using the bending theory in sandwich beams, the modulus can be corrected by subtracting the contribution of the steel. The values were within the expected range after correcting for the steel component. However, the most accurate and consistent results were obtained using fully cured plates of DA 409 as stiffener (d) and these results are reported here.

A schematic of the sandwich beam is shown in Fig. 4.8. The modulus was calculated using the method presented in Wang et al. [116], who measured the modulus development of an adhesive plate within two wood plates. During the test a load, P, and deflection, Δ, was applied at the center of the sandwich beam with a phased angle δ. The storage component of the sandwich beam stiffness, C', is given by

$$C' = \frac{P'}{\Delta} \tag{4.4}$$

The stiffness of the beam can be related to the material properties and dimensions of the cured and uncured resin using the sandwich beam solution by Adams and Weinstein [117]. For this solution, the dynamic stiffness, K, for the sandwich beam where no shear transfer, K, and complete shear transfer, K_T, in the interface is transmitted are included as shown in Eqns. 4.5 and 4.6.

$$K = E'_u I_u + 2E'_c I_c \tag{4.5}$$

$$K_T = E'_u I_u + 2E'_c I_{u-c} \tag{4.6}$$

E'_c, E'_u, I_c, and I_u are the storage modulus and the moment of inertia for the fully cured and uncured resin plates respectively. The moment of inertia was computed using Eq. 4.7 substituting,

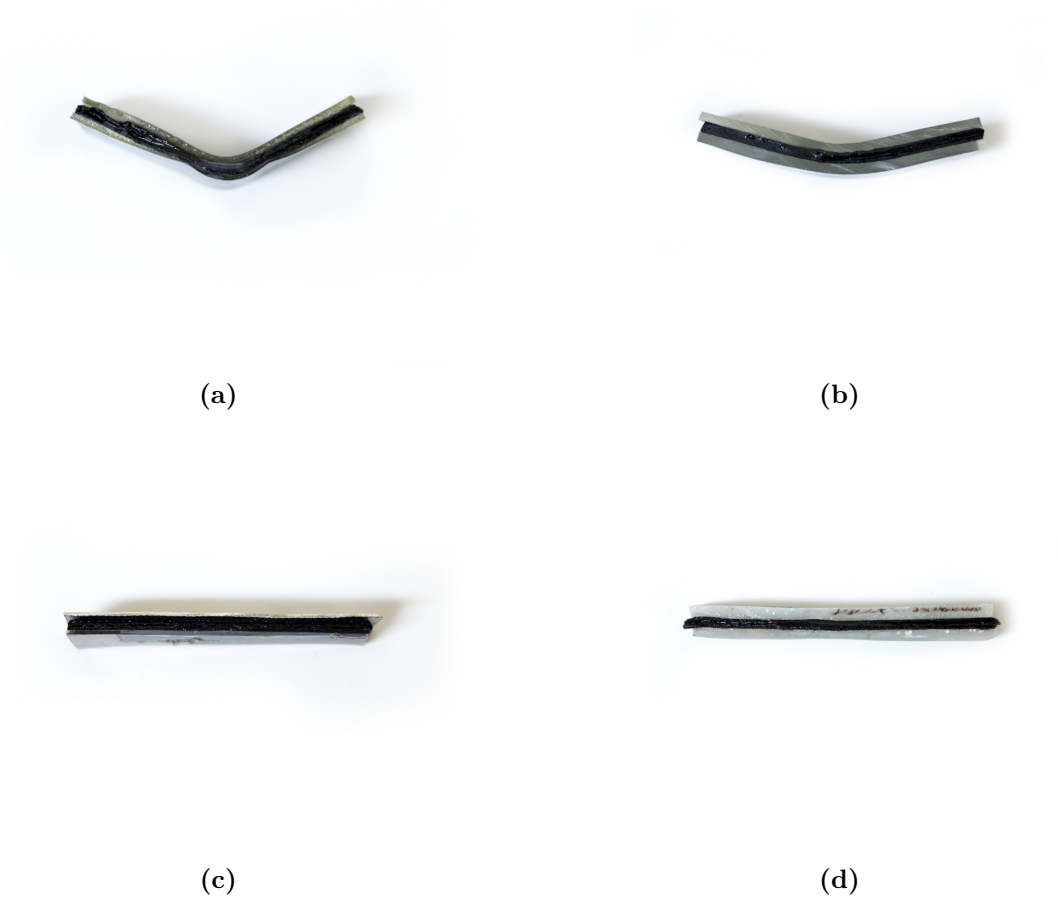

(a) **(b)**

(c) **(d)**

Figure 4.7: Deformation of sandwich beam after three point bending test with different types of outer plates: (a) polypropylene, (b) fully cured two-part epoxy (system epoxy 2000), (c) steel, and (d) fully cured epoxy adhesive (adhesive DA 409).

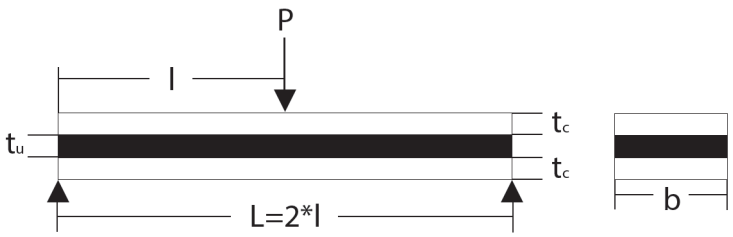

Figure 4.8: Three-point bending setup; t_u is the thickness of the uncured plate and t_c is the thickness of the fully cured plate.

t and h with the thickness of the uncured and fully cured resin plates, respectively. The fictitious variable I_{u-c} includes the shear effect of the total bonded sample.

$$I = \frac{bt^3}{12} \tag{4.7}$$

$$I_{u-c} = \frac{bt^3}{12} + \frac{bt(h+t)^2}{4} \tag{4.8}$$

Applying Adams and Weinstein's procedure [117] for a sandwich beam, it is possible to relate the composite stiffness, C'_u, with the shear storage modulus of the partially cured plate, G'_u, using equations 4.9-4.11.

$$C' = \frac{P'}{\Delta} = \frac{6K_T}{l^3(1+M)} \tag{4.9}$$

$$M = \frac{3(K_T - K)}{l^3 K\gamma^2}\left(l - \frac{tanh\gamma l}{\gamma}\right) \tag{4.10}$$

$$\gamma^2 = G'_u\left(\frac{2K + (t+h)^2 E'_c bh}{KE'_{ht}}\right) \tag{4.11}$$

where M and γ are variables to simplify the expression. The shear modulus of the partially cured plate, G'_u, can be related to the storage modulus, E'_u, assuming isotropic behavior.

$$E'_u = 2(1+\nu_u)G'_u \tag{4.12}$$

ν_u is the Poisson's ratio of the partially cured plate. Following the same procedure as Wang et al. [116], the shear modulus was calculated using the Matlab interpolation function. First, a linear vector from 1 Pa to 1 GPa was created considering the output data from the DMA test. Second, the values of the shear modulus were inserted into Eqns. 4.9-4.11 to calculate the vectors $\bar{\gamma}$, $\bar{M}$ and $\bar{C}'$. The results gave a relation between $\bar{C}'$ and $\bar{G}'$. Using the experimental values of the beam stiffness and the values calculated using the assumed shear modulus, the shear modulus of the partially cured plate was computed using the interpolation function within Matlab. For further details refer to [116].

Figs. 4.9 and 4.10 show the moduli developing during cure under three isothermal conditions. The competing thermal and kinetic effects are shown [79]. The beginning of the test showed a slow growth of E'_u where the temperature effect dominates. The results showed that with an increase in the tested temperature the initial modulus is lower. This was followed by a rapid increase that ended in a plateau, which is more noticeable at 110 °C—this temperature was 11 degrees below T_{g_1}, therefore the plateau was diffusion dominated causing a residual cure. The final cure value only reached a c value of 97.4 % at 100 °C. The final moduli values were offset from the analysis of E' of a fully cure sample shown in Fig. 4.6.

Tests were performed below T_{g_1} (111.1 °C) because the mechanical development is highly dependent of T_g [79]. Ruiz et al. reported data discrepancies in three point bending test of partially cured sample tested above T_{g_1} [79]. The sample preparation proposed here could be use to correct for this problem, further studies will include testing of samples above T_{g_1}.

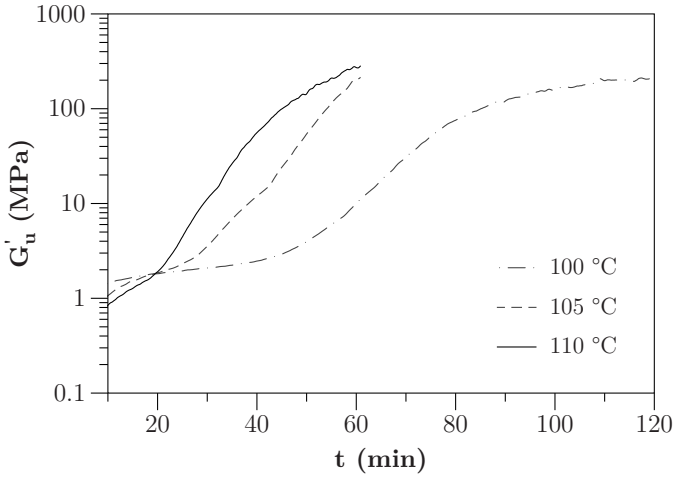

Figure 4.9: Calculated G'_u from three point bending data of the partially cured plate.

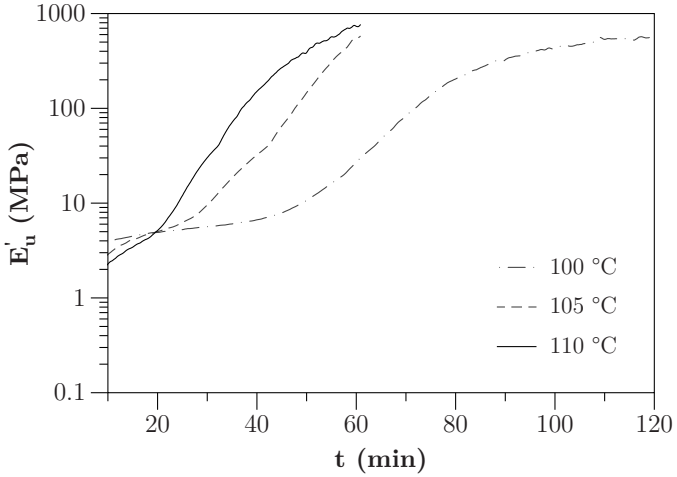

Figure 4.10: Calculated E'_u from three point bending data of the partially cured plate.

4.4 Conclusions

A method to continuously capture the modulus development of thermosets during cure was presented. The modulus was captured in three-point bending from the gel point up to the fully cured state in one experiment. A new sample preparation was used by sandwiching a partially cured plate between two fully cured plates. The preliminary results were promising in quantifying the modulus at all states in one sample avoiding testing at discrete curing values.

This sandwich beam decreased the compliance of the sample and eliminated permanent deformation at the beginning of the test near the gel point. The corrected selection of the outer plates was evaluated. The best result was given by plates of the same epoxy adhesive in the fully cured state. The result was an effective modulus of the three plates. Preliminary analysis using sandwich beam theory allowed the extraction of the modulus of the partially cured plate. Further evaluation of this simplified elastic theory is needed including the effect of the soft state in the deformation when transferring shear between layers. A viscoelastic analysis could also be performed to quantify relaxation effects.

The viscosity and gel point served as the lower bound of the moduli test, and fully cured samples were used to obtain the upper bound. The gel point and viscosity results agreed with the reported literature. The degree of cure was connected to the analysis of all the mechanical properties evaluated, showing the advantages of relating kinetic and mechanical analysis when assessing property development. The disadvantage of using different geometries, masses, and instruments remains when testing thermosets via DMA and DSC. A novel approach to this challenge is presented in the next chapter.

The shrinkage development and the effect on potential residual stress build-up were discussed. The interaction of the chemical shrinkage and moduli development and their role in residual stress build-up are still open to further discussion.

This method can be implemented to properly prepare thermoset and composite samples and select testing conditions such as frequency, strain, and temperature cycles based on the kinetic, viscosity, gel and shrinkage analysis.

Chapter 5

Ultrasound Wave Propagation Combined with Raman Spectroscopy to Monitor the Development of Thermosets during Cure

The mechanical and kinetic development of thermosets during cure is difficult to correlate with standard tests. First, the degree of cure, shrinkage, and moduli are measured in independent tests using different sample geometries and masses. Second, some tests only measure values at discrete points of thermal and cure history without matching a manufacturing process. Lastly, these independent results are correlated assuming equal thermal history in all tests. Chapter 4 evaluates the simultaneous measurement of kinetic and mechanical changes with a set-up attaching ultrasonic transducers and a Raman probe to a chamber.

First, a mixed activate epoxy was tested in a room temperature set-up. The time of flight of longitudinal and transversal waves was measured at a frequency of 1 MHz. The thickness and density changes were correlated to the chemical shrinkage measured with an LVDT sensor, calculating the wave speeds and moduli. Simultaneously, Raman spectroscopy was used to quantify the degree of cure based on the intensity of the oxirane ring vibration at 1255 cm^{-1}, and normalized using the CH in bending in backbone at 1186 cm^{-1} which is constant throughout the reaction. Center shift and peak broadening were offset using a cumulative peak definition of $\pm$ 5 cm^{-1}.

The methodology was extended using a mold-type chamber including temperature and pressure effects up to 0.25 MPa. Two heat activated epoxies were evaluated. Piezoelectric properties of the ultrasonic transducers limited the wave analysis at high temperatures. In all tests, the degree of cure calculated from Raman spectroscopy agreed with a DSC analysis with Raman spectroscopy

reporting higher values in the initial and propagation stages. Both tests combined gave insight into cure-dependent changes of mechanical properties, with the potential to monitor multiple property changes in real time on a manufacturing process.

5.1 Introduction

High-volume industries, like the automotive industry, continue implementing fiber reinforced thermosets for their thermal stability, mechanical strength and light weight properties [2]. The complex warpage behavior due to curing limits the spread of applications with thermoset composites. A major cause of warpage is the development of the mechanical properties with the degree of cure. Efforts focus on characterizing the cure dependency of properties like the moduli and chemical shrinkage in the composite matrix (thermoset). Accurate models that describe these properties are used to predict and prevent dimensional instabilities (warpage) in the final components.

Measuring the moduli involves thermo-chemical analyses and mechanical testing as described in Chapters 2-4. A thermo-chemical analysis quantifies time and thermal history changes in the molecular structure, and mechanical testing captures the temperature, time and frequency dependency of the moduli. These changes cause phase transformations that modify material and mechanical properties. Mechanical properties are related to thermo-chemical history through four variables: the degree of cure, c, the glass transition temperature, T_g, the gel point c_{gel}, and chemical shrinkage, Δv.

Conventional protocols have the disadvantage that every variable is measured using different instruments, sample masses, geometries and conditions. For example, c is measured using differential scanning calorimetry (DSC) or Raman spectroscopy, T_g is measured via DSC or DMA, whereas c_{gel} is measured using a rheometer. The shrinkage is quantified volumetrically in a pycnometer or dilatometer or through thickness in a rheometer, DMA or with an LVDT sensor [113]. Another disadvantage is that the moduli can only be measured at discrete cure stages in tensile tests (elastic assumption) or dynamic mechanical analyses, DMA (viscoelasticity is included). At the end, these independent thermal and mechanical tests should be correlated.

In-situ characterization via non-destructive tests is a promising alternative to conventional tests and thermo-chemical analyses. Continuous measurements of multiple properties save characteri-

zation time and enhance the understanding of the cure dependent changes in thermosets and the corresponding composites. Ultrasound wave propagation, for example, is used in composite manufacturing as a non-destructive testing method to quantify and evaluate material properties and microstructure. The ultrasonic signal is used to control porosity, voids, and to predict cracks and defects in parts. Additionally, the viscous damping, elastic and shear moduli can be inferred using ultrasound wave propagation. This application in polymer measurements is dated as early as 1946-52 [118]. In thermoset composites, ultrasound wave propagation has also been used for cure monitoring [119–121], online process monitoring of polymer composites production [122], and as in-situ non-invasive mechanical characterization [123]. Recent work by McHugh reported ultrasound as a high-frequency DMA technique for polymer characterization [124]. McHugh suggested the need of combining wave analysis with kinetic models for cure prediction [124].

Raman spectroscopy is another in-situ technique used in composites to characterize the chemical composition and curing. Studies in epoxy systems include in-situ curing monitoring using fiber-optic Raman spectroscopy at room temperature [9], monitoring the evolution of different reactive species [10], and the weakening of the Raman signal due to temperature effects [125]. Recent work by Cruz showed the advantages of Raman spectroscopy over DSC in the characterization of unsaturated polyester and epoxies including pressure and temperature effects [11, 126, 127].

Another improvement to conventional protocols are devices that gather more information measuring several material properties in one test. Examples are the pressure-volume-temperature (PVT) devices such as the GNOMIX high-pressure dilatometer (PVT apparatus) and PVT-c proposed by Saraswat et al. and Nawab et al. respectively [128, 129]. To this effort, we have recently reported a preliminary study combining Raman spectroscopy and ultrasound wave propagation to characterize epoxy systems [130]. A similar combination was reported in the medical field in 2000 by Romen et al. [131]. They studied coronary arteries using intravascular ultrasound (IVUS) to analyze the arterial wall structure and potential intravascular deposits, and Raman spectroscopy to get a chemistry spectrum of the cholesterol content.

The combination of ultrasound wave propagation and Raman spectroscopy will be studied here to get simultaneous insight on the degree of cure and mechanical properties. Two set-ups are presented. First, a cylindrical chamber was made for measurements in mix-activated systems that cure at room temperature. To compensate the shrinkage of the resin before it reaches the gel point,

an open reservoir was added in one of the acrylic disks. The open reservoir allows measurements with the modular Raman probe, and the ultrasonic transducers are placed in the acrylic disks.

Second, a heated measuring mold was made to monitor isothermal and dynamic curing conditions. This mold also has access for the modular Raman probe and the ultrasonic transducers. In both measurement devices, the Raman-spectroscope enables the quantification of low frequency transitions in the molecules (vibrations, rotations, etc) [132], and the ultrasonic transducers quantify the time of flight of longitudinal or transversal waves through the material as it cures. Both measurements allow the correlation of c with the mechanical property development of the material. The chemical shrinkage was measured in an independent test, with the use of an LVDT sensor for the mix activate systems and via DMA in compression mode for the heat activate systems (see Chapter 4). Three epoxy resins are measured by DSC and by the proposed approach. The results are compared and the accuracy of the new approach is evaluated.

5.2 Materials and Methods

5.2.1 Materials

Three epoxy systems were tested in this study. The first material tested was system 2000 epoxy resin mixed with hardener 2020 both from Fibre Glast Development Corporation. Epoxy 2000 is a mixed activated thermoset that cures at room temperature; it is used as a bonding matrix of a fiber reinforcement for structural applications. The mix EP 2000/2020 has a density of 1135 kg/m^3. The next two materials tested were epoxy film adhesives DA 408 and 409 from Adhesive Prepregs for Composite Manufacturers (A.P.C.M. LLC). Both epoxies are heat-activated systems used in bonding of composites and as the matrix of unidirectional carbon fiber prepregs. The density of DA 408 and 409 is 1150 kg/m^3.

5.2.2 Sample Preparation

For the mix-activated system, 26 g of epoxy 2000 were hand-mixed with epoxy hardener 2020 in a ratio 100:27 by weight (3:1 by volume) for 2 min to allow proper dispersion. The mixture was then poured into the chamber and placed in a vacuum chamber for 3 min at a vacuum pressure of 0.092 MPa (0.92 bars). This step removed bubbles induced in the mixing process. Data was not

collected during the duration of this process.

For the heat-activated adhesives, 0.152 mm thick circular films were stacked to form 3.5 mm thick disks. The layers were compacted by pressing with a roller. Samples were placed in the chamber and further pressurized to mitigate delimitation and porosity. Prior to placing the sample in the chambers, the surfaces were coated with Frekote® 700-NC, a mold release, to allow for sample removal. The ultrasound wave propagation and Raman spectroscopy set-ups were then mounted to the desired chamber to begin a test.

5.2.3 Setup

The set-up included an ultrasonic system, a Raman spectroscope and a chamber to hold the sample and allocate the measurement devices. The ultrasound wave propagation equipment consisted of a set of ultrasonic transducers, a Panametrics pulse-receiver Model 500RP, and an oscilloscope Singlent SDS 1052DL. Two pairs of transducers were used, longitudinal wave transducers (Panametrics Model V102), 1 MHz, and shear wave transducers (Panametrics Model V153), 1 MHz. The Raman spectroscopy unit was composed of a HyperFlux U1 Spectrometer with an Andor iDus DU416A-LDC-CCD by Tornado Spectral Systems and an RFP-400 modular Raman probe by Hellma Axiom Inc. The laser wavelength used was 785 nm. Fig. 5.1 shows the two experimental arrangements. The ultrasonic set-up and Raman spectrometer were integrated to the chambers described below.

Low-Temperature Chamber

This chamber consisted of two acrylic disks and an aluminum ring. The inner diameter of the chamber was 70 mm. The dimensions were chosen such that the width was much larger than the wavelength. The thickness of the aluminum ring was between 2.5 and 4.2 mm. To compensate the shrinkage of the resin during curing before the gel point, a reservoir was designed as seen in Fig. 5.2. While the resin cured up to the gel point, resin flowed from the reservoir into the chamber through the opening. This chamber did not compensate for shrinkage after gelation.

High-Temperature Chamber

This chamber was designed as a mold-plunger similar to the PVT device by Nawab et al. and other equivalent dilatometric devices [128]. Fig. 5.3 shows a schematic sectional view of this setup. The

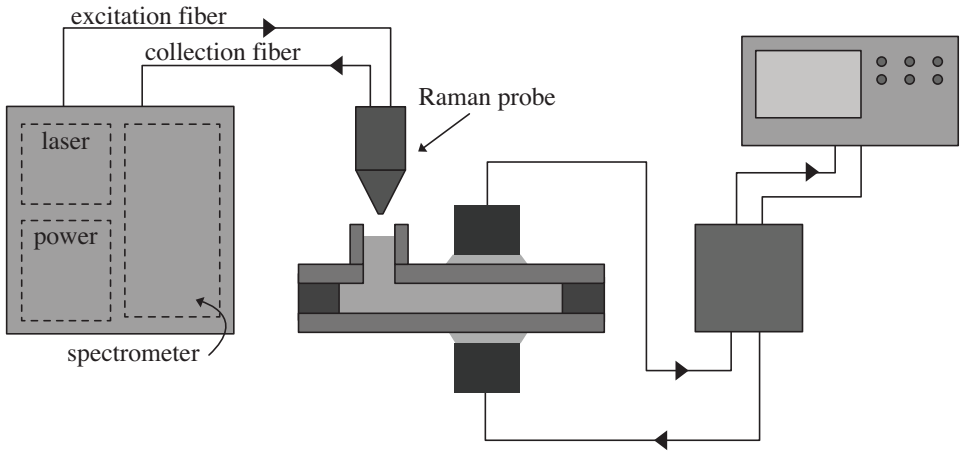

(a)

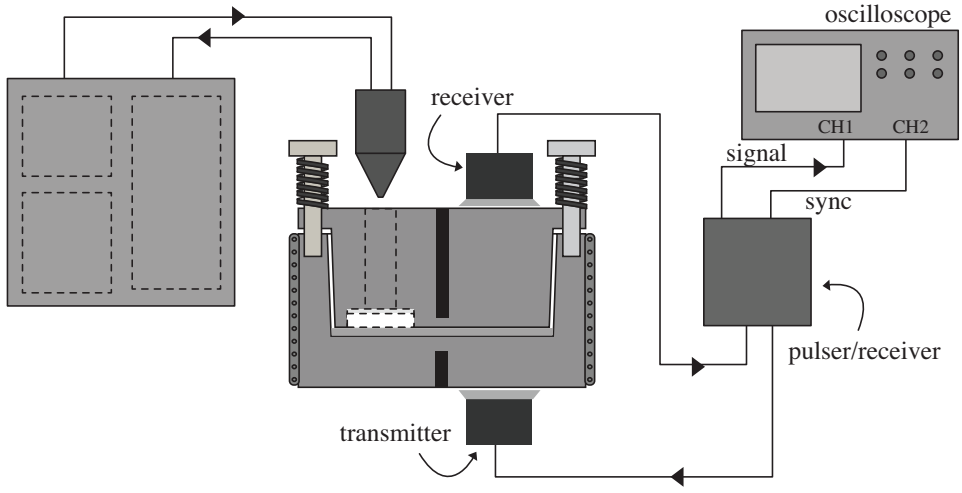

(b)

Figure 5.1: Schematic of experimental setups: (a) using an acrylic chamber and (b) using a high-temperature mold.

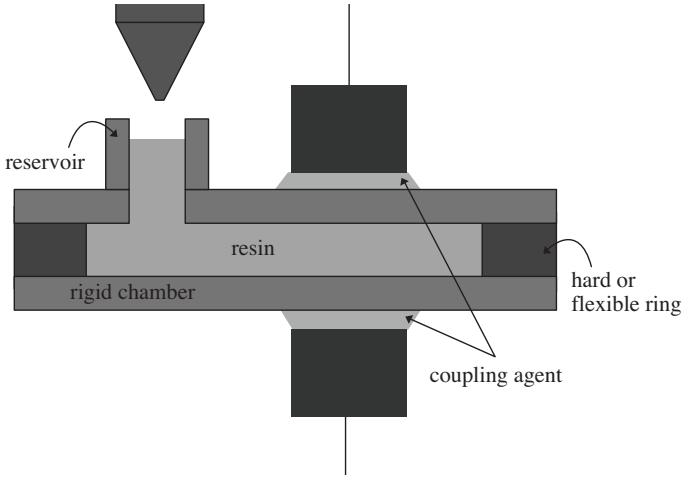

Figure 5.2: Schematic of the acrylic chamber for room temperature measurements.

mold cavity held a 78 mm in diameter and 3.5 mm thick disk specimen, and it had a demolding angle of 3°. The energy input was a ring-type heater band, M-25115-SP by Husky Injection Molding Systems Ltd, placed around the mold. The plunger had a flange with six screws, each equipped with a spring, that provided a constant pressure to compensate for the chemical shrinkage of the specimen. A counter-bored hole sealed by a quartz disk allowed the Raman probe to transmit the signal from the laser source to the sample at a fixed distance. The temperature profiles in the mold cavity and plunger were controlled by a PID-controller, CR 7800 by Omega Engineering, in combination with a thermocouple located in the mold's center hole. The ultrasound transducers (transmitter and receiver) were placed facing each other on the flat surface of the mold cavity and the plunger during testing. The transducers were aligned symmetrically to the Raman cavity to test the same curing conditions.

5.2.4 Protocol

After preparing and placing the sample in the chamber, the Raman and ultrasound setups were attached. The Raman spectroscopy settings for the three epoxies studied were a laser power of 400 mW, and an exposure time of 2000 μs averaging 10 measurements for each data point. The Raman probe was fixed normal to the top surface of the sample at 50 mm. The Raman analysis only captured the reaction at the top layer. It was assumed that the degree of cure in that layer was representative of the degree of cure of the 3.5 mm thick samples, where thermal gradients will

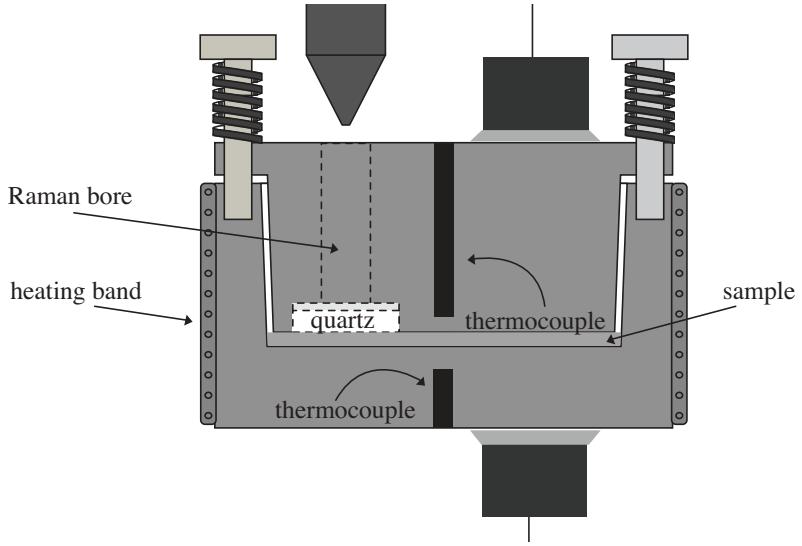

Figure 5.3: Schematic of the mold-type chamber for high-temperature measurements.

be small. It could be possible to measure the reaction at different thicknesses by modifying the height of the Raman probe but this was not explored in this study.

For the ultrasound unit, the two transducers mode (through transmission mode) was used in the experiments with both chambers. Epoxy 2000 and adhesives DA 408 and 409 had different ultrasound protocols according to their activation source—mix and heat activation for epoxy 2000 and DA 408 and 409 respectively—as described below.

For the low-temperature chamber, the ultrasound transducers were clamped to the chamber to assure a constant pressure and alignment throughout the test so that the transmission length remained constant and the coupling between the different interfaces was assured (see Fig. 5.2). For all tests, the first received signal was measured and the subsequent echoes were neglected. A thin layer of glycerol 96 % was used to couple the transducers and acrylic disks for the longitudinal wave tests. The zero offset of the transducer's response was measured before testing. This was done by recording the propagation time for the two transducers pressed together without any material in between. A highly viscous coupling agent is needed between the transducer and the specimen to transmit the transverse oscillations in the shear wave tests. Commercial coupling agents are available for shear tests, but preliminary experiments were performed with regular honey. The tests showed that honey worked as a good substitute and it was used for all subsequent tests.

For the high-temperature chamber, the transducers lost their piezoelectric properties above 50

°C. Based on the work of Ko et al. [133], 6.35 mm thick quartz disks were used as delay lines to insulate the transducers during testing at high temperatures. Ultrasound measurements were taken by placing the transducers with the delay lines on the mold for a period of 5 s. After the data was collected the ultrasonic transducers were removed and the delay lines cooled down for the next measurement. This process was repeated every three minutes to avoid transducer overheating and corruption of the piezoelectric signal. Glycerol 96 % was used as the coupling agent because it had a boiling point of 290 °C at atmospheric pressure. The maximum testing temperature was 120 °C.

The three-epoxy systems were tested using different temperature cycles. First, system epoxy 2000 was tested in the low-temperature chamber during 48 h at 22 °C. Lastly, adhesives DA 408 and 409 were tested under a non-isothermal and isothermal cycle. Samples were heated from 20 to 120 °C at a rate of 5 K/min and held there for 1 h. This temperature was above T_{g_1} for both adhesives—105.6 and 111.1 °C for adhesives DA 408 and 409 respectively (refer to section 3.3.2).

5.2.5 Signal Processing

Raman signal

Raman spectroscopy is based on inelastic scattering of monochromatic light, often from a laser source [132]. When a sample is exposed to laser light, it absorbs and reemits photons. Due to inelastic scattering, the frequency of photons reemitted is shifted up or down, and this is called the Raman effect [132]. Low-frequency transitions such as vibrations and rotation of the sample molecules are captured in the shift. The energy shift of the scattered photons can be directly correlated to a specific bond and is independent of the incoming photon's energy. The intensity of Raman scattered photons depends directly on the number of bonds in the evaluated volume [134]. Therefore, changes in the chemical constitution can be monitored directly. Due to energetic considerations, energy shifts to lower frequencies (Stokes effect) are more likely than upshifts (Anti-Stokes effect). Raman bands are usually reported in wavenumbers, being the inverse of wavelengths. The measurement of multiple Raman spectra over time in a reactive polymer can be used to quantify the degree of cure.

The measured spectral signal contained background and noise. To extract the Raman spectrum, the Baseline Estimation and Denoising with Sparsity (BEADS) developed by Ning et al. [135] was

applied to every measured signal. This algorithm, available in Matlab, fits the Raman signal as sparse peaks and optimizes their shape by comparing it to the original signal while using a high and low pass filter for the separation of the noise and baseline, respectively. Wruck adapted the Matlab algorithm to the epoxies studied and his methodology was used here [136].

The peak intensity, I, is directly correlated to the number of specific bonds. To compare different spectra intensities, every spectrum was normalized by the intensity of a peak stable through curing [10]. The intensity of the peak at 1186 cm^{-1}, I_{1186}, which corresponds to the CH-backbone vibration, was used for the three epoxies studied. This peak has been commonly used as the normalization peak in epoxy studies under the assumption that the scattering intensity of the backbone vibrations would not change due to the cure reaction exhibiting a constant intensity [9,11]. I_{1186} shifted slightly, therefore the BEADS algorithm was modified to determine the maximum value within a narrow range of $I_{1186} \pm 5$ wn and to average it with the data point before and after to compensate for shape changes. Equation 5.1 shows an example of the averaging process for any $I_n(wn)$—that includes I_{1186} and I_{1255} —where I_n is the peak intensity value of the n-wavenumber, wn. The maximum value coincided with I_{1186} in the example, but this was not always the case.

$$\bar{I}_n = \frac{3I_n}{I_{1185} + I_{1186} + I_{1189}} \tag{5.1}$$

I_{1255} that relates to the oxirane ring vibration was evaluated to define and quantify c. Equation 5.2 shows the definition of c in the Raman analysis, with $\bar{I}_0$ and $\bar{I_\infty}$ being the normalized (relative) peak intensity of the uncured and fully cured material respectively.

$$c = \frac{\bar{I}_{1255,0} - \bar{I}_{1255}(t)}{\bar{I}_{1255,0} - \bar{I}_{1255,\infty}} \tag{5.2}$$

Fig. 5.4 and 5.5 show examples of the data normalization implemented by Wruck using the Matlab algorithm by Ning et al. [135] for the spectra over time and the correction for the temperature effects [136]. Three aspects of the definition of c were further considered. First, several peaks including I_{1255} broaden when the materials were tested at elevated temperatures. This effect, also reported by Janarthan et al. [125], was offset using a cumulative peak intensity. $I_{1255} \pm 5$ cm^{-1} values were added up to define the cumulative peak intensity. $I_{1255,0}$ and $I_{1255,\infty}$ were also calcu-

lated as a cumulative peak intensity in a range of $\pm$ 5 cm^{-1} before the normalization step described in equation 5.1.

Second, I_∞ was quantified from the measurements of fully cured specimens in all the epoxies and normalized to get $\bar{I}_\infty$. Lastly, the quantification of I_0 depended on the epoxy system. For the adhesives DA 408 and 409, an uncured sample taken out of the freezer was measured at room temperature. The result was then normalized to get $\bar{I}_0$. The degree of cure during the storage before testing was not considered here, since it was found negligible in the kinetic analysis (see chapter 3, section 2.2.2). In contrast, the signal for I_0 of system 2000 epoxy resin was compounded based on the mix ratio proposed by Musto et al. [10]. Separate measurements of the epoxy 2000 and the hardener 2020 were used to get I_0 as seen in equation 5.3.

$$I_0(wn) = I_{ep} + \left(\frac{m_{ca}}{m_{ep} + m_{ca}}\right) I_{ca} \tag{5.3}$$

I_{ep} and I_{ca} are the spectral intensity of the epoxy and curing agent (hardener), and m_{ep} and m_{ca} the mass of the epoxy and curing agent respectively. The compounded I_0 signal was then normalized to get $\bar{I}_0$.

Ultrasound signal

Ultrasound wave propagation makes use of a piezoelectric disc to convert an electrical signal into a mechanical pulse and vice versa, generating and receiving waves. Piezoelectric materials like quartz can be polarized in a particular direction—e.g. longitudinal and transversal to the thickness direction—according to the cutting orientation of the crystal. Therefore, when an electrical signal is applied the material undergoes a small change in length in the polarized direction. In direct contact ultrasound, the energy is transferred to the sample using a coupling agent in the interface between the sensor and the specimen. Frequencies between 400 KHz and 12 MHz have been used in ultrasonic measurements of epoxy systems during cure. The waves generated by the ultrasonic transducers travel through the sample at the speed of sound, which changes based on the stiffness of the material. Ultrasonic waves attenuate as they travel through the medium of interest. Thermosets attenuate ultrasonic waves rapidly due to their viscoelastic nature. A tradeoff between achieving a better resolution at higher frequencies that lead to more attenuation is presented in ultrasonic

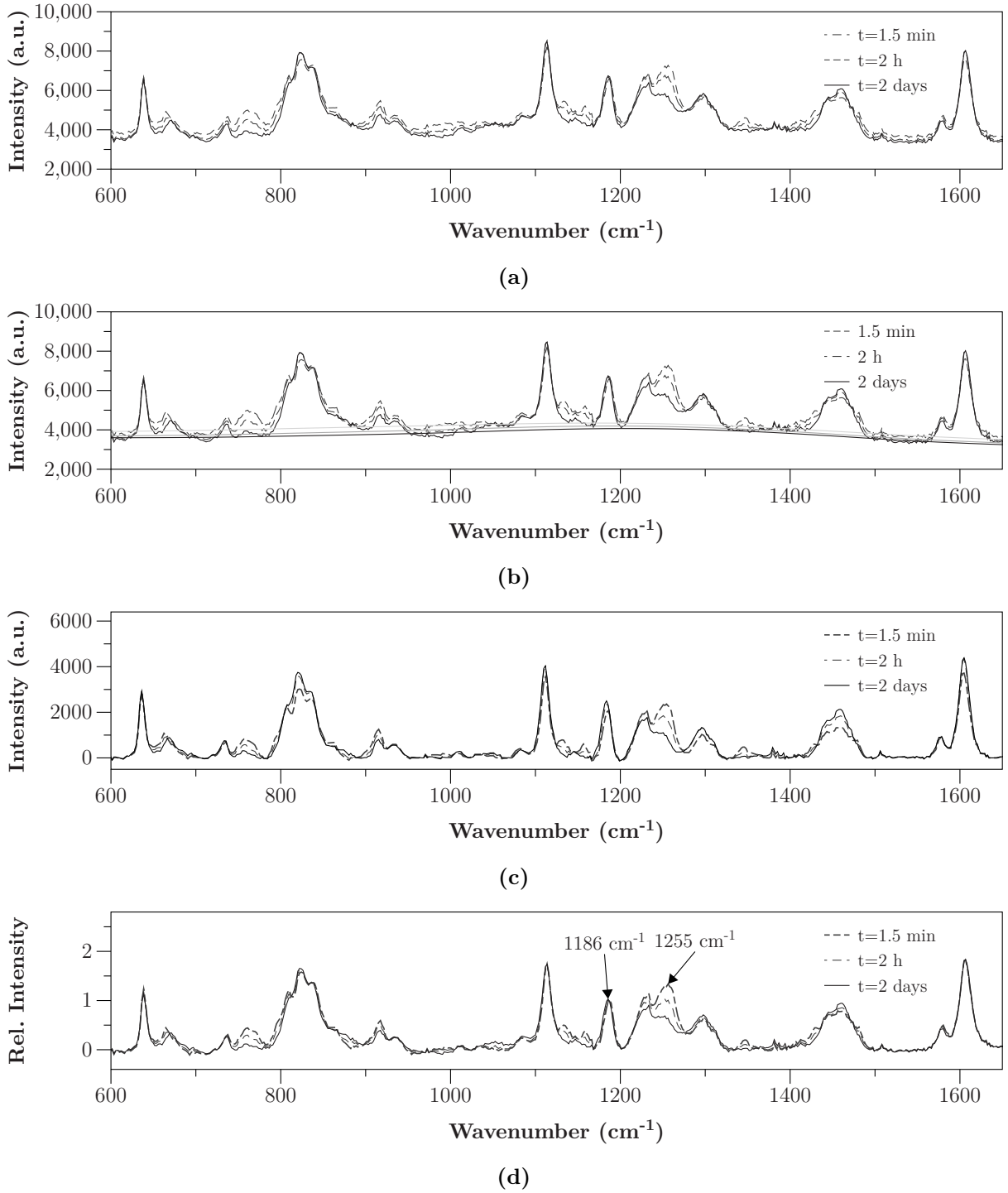

Figure 5.4: Raman signal post-processing of epoxy 2000 during cure in the low-temperature chamber. Data taken at 22 °C: (a) raw signal, (b) triangular correction and estimated baseline, (c) BEADS estimated signal, and (d) normalized (relative) intensity.

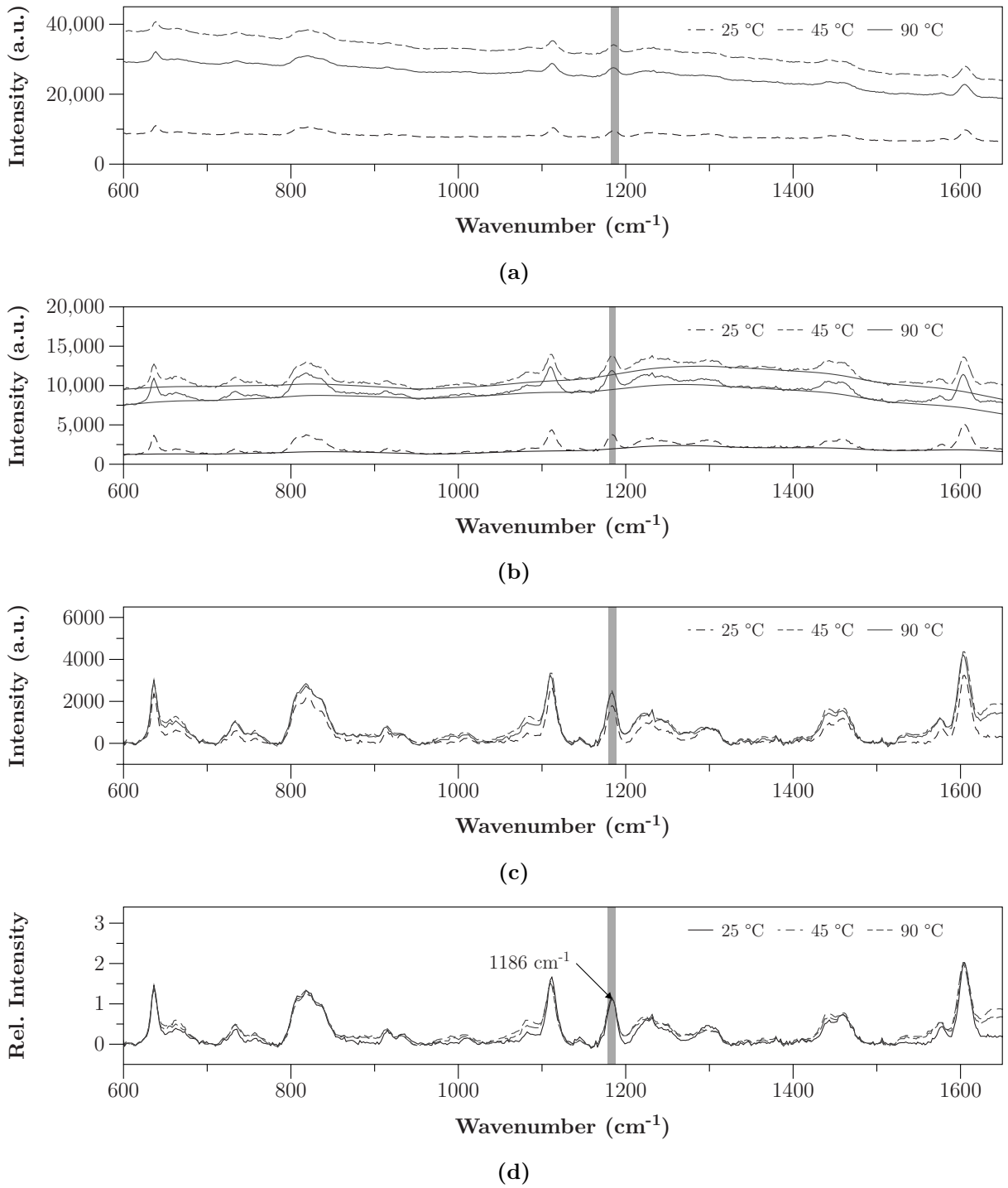

Figure 5.5: Post-processing of temperature influence in the Raman signal for fully cured EP 409. Data taken at 2 min for all temperatures: (a) raw signal, (b) triangle-corrected signal and baseline, (c) BEADS estimated signal, and (d) normalized (relative) intensity. Adapted from Wruck [136].

measurements.

The ultrasonic measurements give the time of flight of the longitudinal, t_L, or transversal, t_S, waves through the material. $t_{L,S}$ decreases during curing as the resin changes from the liquid to solid state. The density is taken as a constant in most DMA and ultrasonic studies. During curing, chemical shrinkage causes a volumetric contraction. Thus, the thickness decrease, $\rho(t)$, and density increase, $\rho(t)$, of the epoxies were included here (see Equations 5.4 and 5.5). The longitudinal, c_L, and transversal, c_T, wave speed are given by

$$c_L = \frac{L(t)}{t_L} \tag{5.4}$$

$$c_T = \frac{L(t)}{t_S} \tag{5.5}$$

The diameter of the specimens tested was larger than the longitudinal wave suppressing Poisson's expansion and contraction. Thus, the relation between c_L, ρ, and the tensorial modulus in the direction 1, C_{1111}, is defined as

$$c_L = \sqrt{\frac{C_{1111}}{\rho}} \tag{5.6}$$

including the volumetric contraction, the density changes with cure and Equation 5.7 becomes

$$c_L = \frac{L(t)}{t_L} = \sqrt{\frac{C_{1111}}{\rho(t)}} \tag{5.7}$$

For isotropic materials—a well-mixed epoxy system free of porosity and fillers—or when all values of C_{ijkl} are the same, C_{1111} is related to the Young's modulus, E, and Poisson's ratio, ν. For viscoelastic materials, each modulus is interpreted as the absolute value of the complex modulus [107]. Thus, the relationship becomes (the absolute value can be dropped since all the quantities studied are positive)

$$C^*_{1111} = E^* \frac{1-\nu^*}{(1+\nu^*)(1-2\nu^*)} \tag{5.8}$$

The shear or transversal wave speed, c_T, for isotropic viscoelastic materials is define as

$$c_T = \sqrt{\frac{G^*}{\rho}} \tag{5.9}$$

with G^* the absolute value of the complex shear modulus. The Poisson's ratio—interpreted as the absolute value of the complex Poisson's ratio—can then be calculated from

$$G^* = \frac{E^*}{2(1+\nu^*)} \tag{5.10}$$

which results in

$$\nu^* = \frac{1-2(c_T/c_L)}{2-2(c_T/c_L)^2} \tag{5.11}$$

During curing, the liquid resin solidifies and becomes solid. In the liquid state, the shear wave speed is zero. Thus, the Poisson's ratio is 1/2. For viscoelastic materials, tanδ assesses how a dynamic system will respond to an oscillating load. This property is calculated by looking at the decay of the highest peak in the first signal that gets returned for two different length samples. First, the attenuation, α, can be calculated from the amplitude, A_i, and length of two specimens in units of nepers per unit length

$$\alpha = \frac{ln(A_1/A_2)}{L_1 - L_2} \tag{5.12}$$

then, tanδ is related to the attenuation in the longitudinal tests by the following the mathematical relation

$$\alpha = \frac{\omega}{c_L} tan\frac{\delta}{2} \tag{5.13}$$

where ω is the angular velocity. It could also be possible to measure the height of later peaks in the same sample to obtain attenuation data.

During the experiments, $t_{L,S}$ was captured every 3 min. A voltage versus time spreadsheet was saved to calculate the longitudinal or shear time of flight, $t_{L,S}$, and the wave amplitude, A. $t_{L,S}$ was read from the pulse initiation to the beginning of the first peak. The measured ultrasound

signal included the information of all the different materials placed in between the transducers. To extract the data corresponding to the epoxy specimen, the superposed $t_{L,S}$ of the chamber and the coupling agent were subtracted from the original signal. The analysis of $tan\delta$ was not included in this study, but it will be considered in further studies.

In the high-temperature chamber, the temperature dependency of the aluminum, the glass delay lines and the coupling agent were measured from 20 to 90 °C in increments of 20 °C as seen in Fig. 5.6. The quartz disks were only characterized at room temperature neglecting the small temperature effects in the 5 s interval.

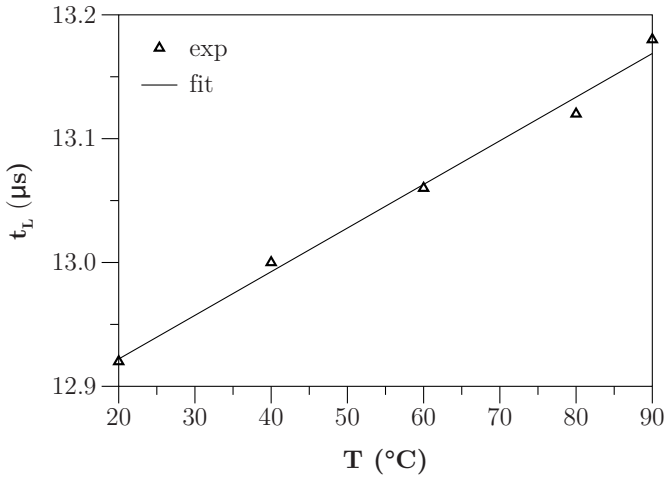

Figure 5.6: t_L of the ultrasound signal through the components of the high-temperature chamber.

5.3 Results and Discussion

5.3.1 Raman Spectroscopy

Low-Temperature Chamber

Fig. 5.7 compares c of system epoxy 2000 quantified via DSC and Raman spectroscopy. The reaction that occurred during mixing, degassing and assembling of the set-up was not included in both analyses to correlate results under the same conditions. Both definitions of c agreed with Raman spectroscopy reporting slightly higher values in the initiation and propagation stages. Cruz reported similar trends in his studies of unsaturated polyester and two-part epoxy systems [11,126,127]. Following the hypothesis from Cruz [126], Raman spectroscopy results showed a shift

in time compared to the DSC analysis. System epoxy 2000 exhibits a low and slow rate of reaction at room temperature. In the initial stage of the reaction, molecular changes are small but could cause vibrational displacements of the molecules which are an indication of curing. This curing development was captured by Raman spectroscopy, but since the heat released was not significant it was not captured by DSC. Raman spectroscopy was also more sensitive in the last stage of curing. c_∞ of epoxy 2000 was reported at 14.5 h in the DSC analysis whereas Raman spectroscopy gave a c of 98 % and reported a c_∞ value at 22.7 h.

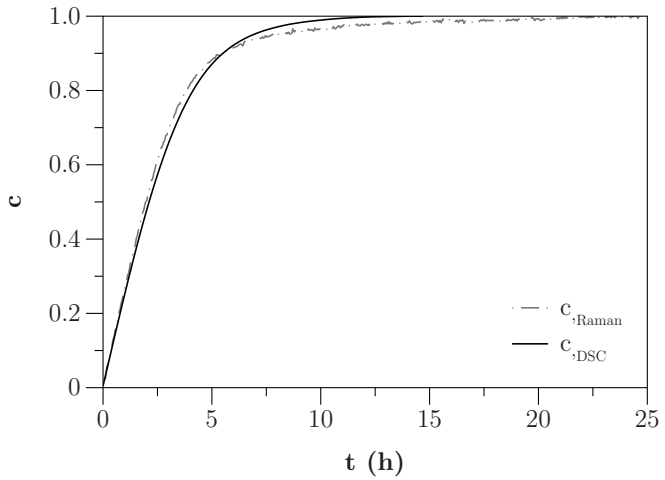

Figure 5.7: Comparison of c vs t at 22 °C quantified via Raman spectroscopy and DSC.

When considering this hypothesis, it is important to discuss three factors that could affect c of epoxy 2000 calculated from the Raman spectroscopy results. First, c_0 was defined from a composed signal of epoxy 2000 and hardener 2020 based on the work of Musto et al. [10]. Their rule of mixtures principle worked for a preliminary definition of c_0 of epoxy 2000. To validate this, c_0 was compared with the spectrum of the mixture after 2 min into the reaction (reached after mixing) and the values overlapped in most measurements with deviations for some experiments. Tuning the definition of c_0 could eliminate this deviation and give more repetitive and accurate results.

Second, c_∞ was initially defined as the degree of cure reached after 24 h. However, tests performed at prolonged times could more accurately quantify c_∞. This study did not include aging and no conclusions can be drawn about that phenomenon here. Further analysis measuring this material after accelerating the aging could assess if through the proposed methodology additional

cure due to aging can be capture. An aging analysis should be supported by measurements of T_{g_1}. Lastly, improper mixing could cause significant deviations when quantifying c.

High-Temperature Chamber

Figs. 5.8 and 5.9 compare the calculation of c using Raman spectroscopy and DSC for adhesives DA 408 and 409 respectively. The Raman spectroscopy signal exhibited significant scattering due to temperature effects [125]. The results agreed with Raman spectroscopy reporting higher degrees of cure in the initial stage and before reaching a plateau.

As shown in section 3.3.1, adhesive DA 408 exhibits a small exothermal heat released between 20 and 90 °C when subjected to a non-isothermal analysis using a 5 K/min ramp. In this region, DSC gave a c of 6.8 x 10^{-2} % whereas Raman spectroscopy gave a c value between 5.7 and 9.3 %. Similar to the results and hypotheses proposed by Cruz [11], the small molecular motion caused vibrational changes not reflected as exothermal released of energy. These vibrations were further accelerated during the beginning of the ramp compared to the previous analysis of epoxy 2000 at room temperature. However, the energy released was minimal.

The middle region showed a similar cure development with a time shift that could be visualized, for example, by looking at the time scale to reached the gel point, c_{gel}. During the isothermal step at 120 °C, Raman spectroscopy reported higher c values during the first 5-6 min up to a c value of 92 %. After this point, the curves overlapped reaching a fully cured state at the same time.

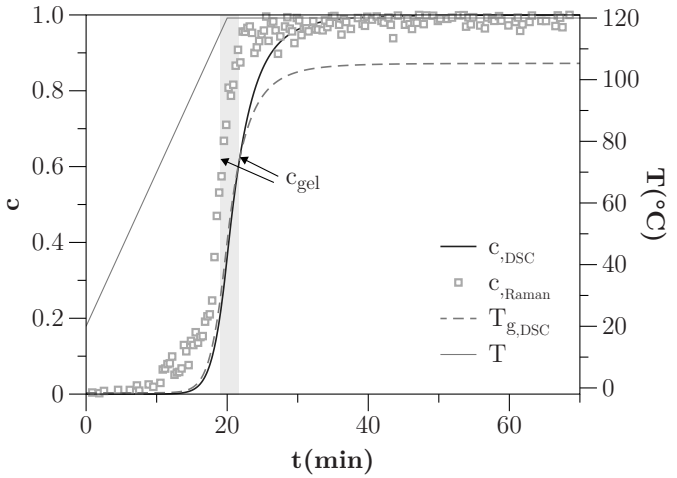

Figure 5.8: Comparison of c vs t of adhesive DA 408 modeled via Raman spectroscopy and DSC.

Adhesive DA 409 exhibited a similar trend at a different thermal history because of its higher T_{g_1} (111.1 C). The heat released captured during the 5 K/min ramp from 20 to 120 °C by DSC was 0.28 J/g that corresponds to a c of 0.1 % whereas Raman spectroscopy gave a c value between 15.1 and 19.2 %. This difference could be interpreted as curing that do not cause a significant exothermal reaction but could be revealed following the low frequency transitions in the molecules via Raman spectroscopy. The degree of cure is quantified in DSC assuming that the heat released during the exothermal reaction of a thermoset is directly proportional to the rate of cure, quantifying only the energy released during the bonding of molecules that form a 3D network [11]. Curves had a similar trend for c values between 26.0 and 53.2 %, after which Raman spectroscopy reported a faster reaction. The curves matched at a c value of 89.1 %.

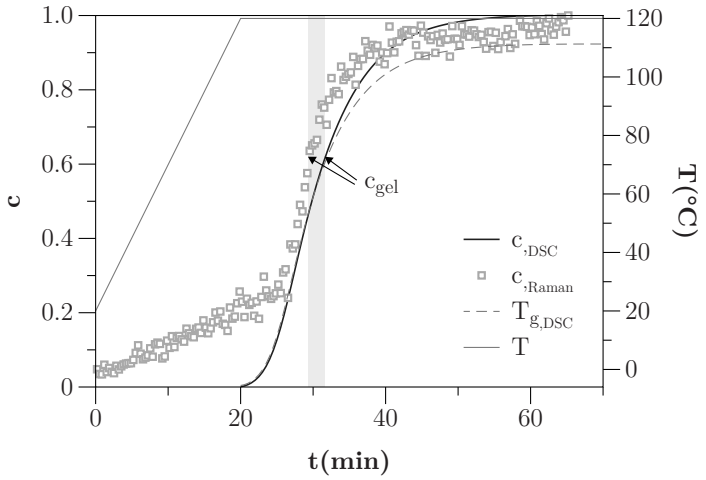

Figure 5.9: Comparison of c vs t of adhesive DA 409 modeled via Raman spectroscopy and DSC.

The influence of c_0, c_∞ and the mixing protocol in the calculation of c from Raman spectra were previously discussed. Other influential factors are the type of definition used to quantify c, the stability of the numerical algorithm, and experimental errors. The degree of cure can be quantified from Raman spectra following center shifts, peak height reduction, peak height increase, area reduction or a combination of multiple changes [11]. In this work, c was defined based on three factors: the disappearance of normalized peak $\bar{I}_{1255}$ and a $\pm$ 5 cm^{-1} area that compensated for center shifts and deviations of the peaks of interest.

The proposed definition compensated part of the peak broadening presented at high temperatures, but this is an ongoing topic of study that requires further evaluation. As reported in previous

literature [11], peak I_{1255} did not disappear completely compromising the accuracy of c_∞. Future efforts include the addition of intensity corrections to reach stronger peaks [137, 138]. This will allow the quantification of c using other peaks that almost disappear completely like peak I_{1350} which corresponds to CH_2 stretch interaction to oxygen before epoxy ring opening. This could improve accuracy in the definition of c_∞, reducing the scattering and deviations of c processed using the BEADS algorithm.

The implementation of the BEADS algorithm shown to be a valid post-processing technique to quantify c of thermosets. Instabilities were observed specially during testing at high temperatures for the heat activated adhesives, but overall the results agreed with reported literature analysis [11, 127].

5.3.2 Ultrasound Wave Propagation

The longitudinal and shear wave speeds shown in Fig. 5.10 were calculated from the data on the sample thickness and the time delay for a wave to travel through the epoxy 2000 specimen. The longitudinal wave speed at the beginning and end of the tests was 1532.2 and 2373.2 m/s respectively. Raman spectroscopy captured a c of 0.97 at that time reporting potential extra growth of the acoustic properties. The c development was reflected by the growth of c_L, which is often used to monitor the degree of cure. This is an example of the advantage of correlating these two techniques to assess the cure state and acoustic property development.

The c_S signal was first captured at 150 to 160 min and rose from 831 to 1331 m/s. A c of 0.6 was quantified from the Raman spectroscopy analysis at 151 min. Although no conclusions can be drawn about the sensitivity of shear waves to c_{gel} at room temperature measurements, at this point, the cure state at the beginning of shear transmission can be accurately determined with the combination of Raman spectroscopy and ultrasound wave propagation. c_S marked the beginning of the mechanical property analysis since both wave speeds were used to get the complex moduli in this work. The values obtained fit previous studies of epoxy systems, where c_L and c_S values at the fully cure state can be found between 2200 and 3100 m/s, and 800 and 1500 m/s respectively [139, 140].

Both wave speeds calculations including shrinkage after theoretical gelation (60 %), deviated 0.96 % to the results using a constant thickness. Assuming a constant thickness was valid for

the resin and conditions analyzed without compromising accuracy. Future trials involve validating the shrinkage compensation out of the reservoir and the use of a rubber ring membrane to allow the resin to shrink freely. However, resin systems are mostly manufactured under pressure which restricts free shrinkage growth. The mold type chamber presented in the second phase of this work would be a better alternative when attempting to measure conditions closer to a manufacturing application.

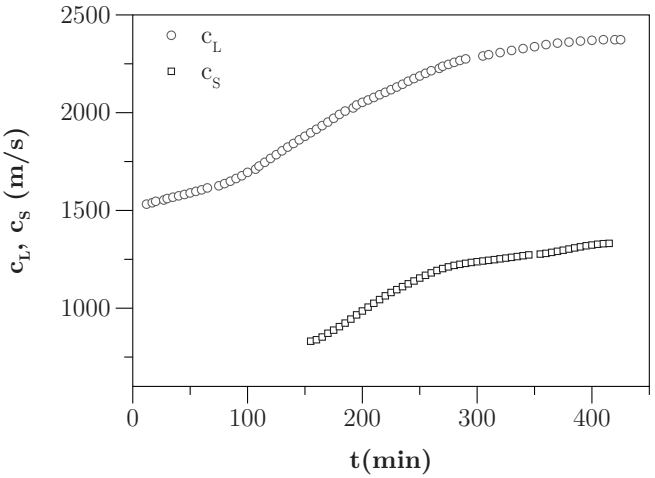

Figure 5.10: Longitudinal, c_L, and shear, c_S, wave speed of epoxy 2000 during cure. Test performed at 22 °C with a frequency of 1 MHz.

C^*_{1111} is shown in Fig. 5.11. This quantity was calculated for the whole curing range. However, this definition from elasticity is only valid for the solid viscoelastic region. This was represented with a continuous line starting at 148.2 min, assuming a theoretical gel point of 60 %. Similar to the wave speed analysis, calculations with a density modified due to shrinkage deviated less than 1 % to the results using a constant density value. C^*_{1111} gave a preliminary range of moduli values that will be lower than 6 GPa which fit previous reports of E^* and G^* values of about 5 and 2 GPa respectively. Fig. 5.12 shows the results for E^* and G^*. With this technique, a c value could be correlated to a direct value of the moduli and vice versa.

As mentioned before, the shear waves were detected at 150 to 160 min into the test. Further work is needed in this area validating the results with measurements of c_{gel}, which is a state independent of frequency. It was reported by McHugh that at high temperatures and at ultrasonic frequencies between 400 KHz and 5 MHz, vitrification occurs earlier at higher frequencies and can

overshadow gelation [141].

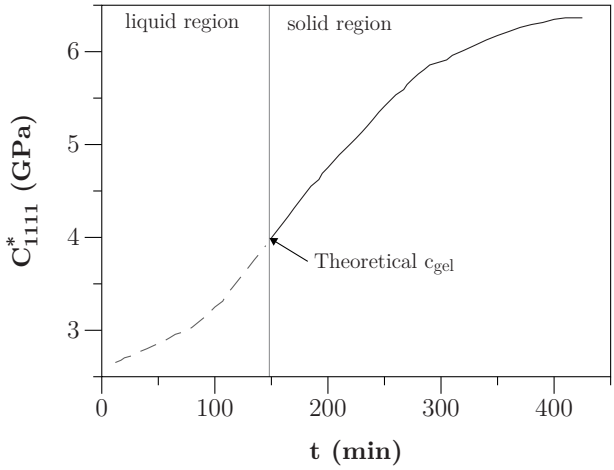

Figure 5.11: Tensorial modulus in the 1 direction, C^*_{1111} at 1 MHz. Notice that this definition is only valid in the solid region.

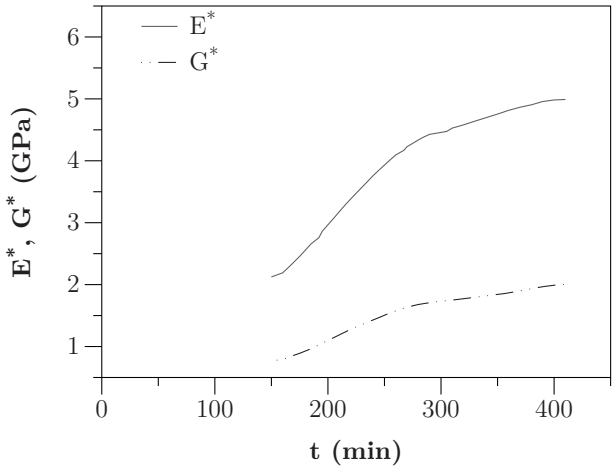

Figure 5.12: Complex moduli, E^*, and G^*, at 1 MHz.

Fig. 5.13 shows the behavior of ν^* after gelation, which decreased as the material solidified. ν^* leveled off at a value of 0.28. The wave results presented here only covered the first 450 min of the reaction. This corresponded to a c of 96.3 % calculated with the Raman spectroscopy method presented here, and this is observed as the measurements tend to plateau. Further iterations involve measuring the specimen up to 22.7 h (fully cured state) to better correlate the moduli and kinetic analysis. E^* was also calculated after 155 min, since the information from C^*_{1111} and ν^* are required.

The sensitivity of the ultrasound wave propagation technique to monitor moduli development was shown with the potential to follow Poisson's ratio change, which is mostly considered constant for predictions in manufacturing of thermoset composites.

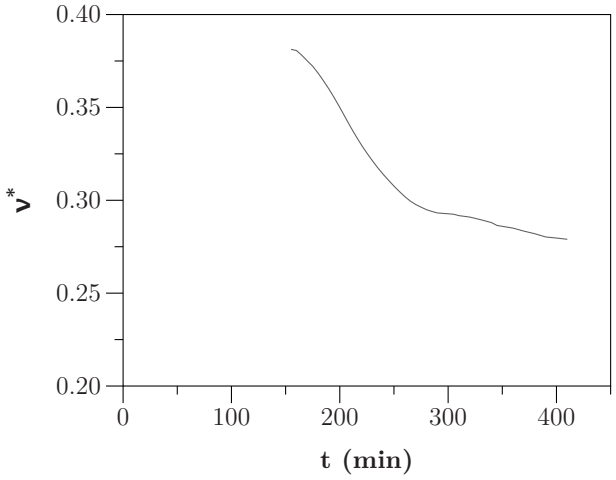

Figure 5.13: Complex Poisson's ratio, ν^*, at 1MHz.

Ultrasonic measurements were also performed for epoxy DA 408 and 409 in the high-temperature chamber. The initial and final stages of the reaction were captured for both films. However, when most of the reaction occurred based on the Raman spectroscopy and DSC analyses, no ultrasound signal was detected. Krautkramer et al. explained this phenomenon because of high testing temperatures and the exothermal heat generated due to the reaction [142]. The transducers used were limited to temperatures up to 50 °C. The beginning and end of the reaction were obtained using delay lines, and this was still valuable information in terms of assessing duration of a process, but the monitoring of the full cure cycle was not obtained. Suitable transducers like the ones reported by McHugh [141] could be implemented in this methodology expanding the full analysis to heat activated systems.

5.4 Conclusions

A testing protocol to simultaneously follow kinetic and mechanical development of thermosets was developed and evaluated. Longitudinal or shear wave ultrasonic transducers and a spectrometer with a laser source and a modular Raman probe were assembled to a chamber containing the sample. The experiments were executed in two phases. In phase one, a two-part epoxy was tested using an acrylic chamber with a reservoir to compensate for the shrinkage in the liquid state. Pressure and high temperatures were not included. In phase two, the two-part epoxy and two heat activated adhesives were tested in a mold-type chamber. Samples were tested up to 120 °C at a constant pressure of 0.25 MPa (36 psi). At high temperatures, delayed lines and stepwise measurements every 3 min were performed due to transducer limitations.

Preliminary results showed that with proper experimental practices and post-processing of the ultrasound and Raman signals, both techniques combined offered a closer interpretation of the curing behavior during the mechanical development of thermosets

The study detailed the main factors that impacted the accuracy of c quantified via Raman spectroscopy. The definition selected to quantify c, c_0 and c_∞ played a critical role. Here, the decreased of peak I_{1255}—oxirane vibration—normalized using peak I_{1188}—CH-backbone vibration—were used to define c. It was necessary to use a cumulative peak averaging over the maximum in a range of $\pm$ 5 cm^{-1} surrounding these two peaks to offset for height and width changes due to temperature effects. The influence of temperature in the area and shape of the peaks is still open to further evaluation. c_∞ was quantified using a spectrum after a long period of time since peak I_{1255} did not disappear completely. Another possibility could be to evaluate a peak that almost disappear completely like I_{1355}—CH_2-0 interaction with oxygen ring. c_0 of the two-part epoxy was defined based on a spectrum composed via rule of mixes of epoxy/hardener. This definition presented variations during different experiments. A more detailed analysis of the applicability of this definition could improve measurement accuracy. c_0 of the adhesives was defined as the spectrum for the unreacted network at room temperature neglecting pre-cure during the resin's production. This definition was more stable and presented a small variation.

The BEADS algorithm by Ning et al. [135] available in Matlab and adapted by Wruck for epoxy systems gave results that agreed with reported literature and showed good reproducibility. The

post-processing can be improved by additional analysis of the role of c_0, c_∞ and the temperature influence in peak changes.

The absolute values of the complex moduli and Poisson's ratio were interpreted using ultrasound wave propagation. The development of these properties over time was captured up to a c of 96.2 %. For this cure percentage, E^*, G^* and ν^* leveled off at 4.99 GPa, 2.02 GPa and 0.28 respectively. Examples of acoustic and mechanical properties correlated with the degree of cure growth showed the advantages of combining both techniques. The values obtained for the moduli and wave speeds fit previous studies validating the repetitiveness of the steps implemented here. The chamber design was critical in the implementation of ultrasonic sensors. For the conditions tested, the analysis for low-temperature was feasible, but limited at high temperatures by the ultrasonic sensors' sensitivity above 50 °C and the high attenuation presented during the exothermal released of energy.

Proper degassing of a mix-activated system is required to eliminate air bubbles. Delamination and porosity should be treated before testing in pressurized systems where ultrasound measurements are affected by voids and loss of contact between surfaces. Future efforts include implementing ultrasonic transducers for high temperatures like those used by McHugh. This will allow continuous measurements of heat activated systems. Lower frequency transducers can compensate the disparity in attenuation measurements and shear wave measurements at high temperatures. The use of a state of the art spectrometer developed by Tornado Spectral Systems that provides relative intensity correction, and Raman shift standard calibration will produce a cleaner signal increasing the accuracy of the analysis.

Chapter 6

Spring-Forward Effect Measured via Laser Scanner

The increase of residual stresses during the phase change of thermoset fiber-reinforced composites cause warpage. A manufacturing defect of interest is the angular distortion in curved fiber-reinforced thermoset parts, also referred to as the spring-forward effect or anisotropy-induced curvature change. One major challenge is to measure the effect of the profile thickness in the final angle change. Three major factors decrease the accuracy of warpage measurements of spring-forward effect as a function of thickness. First, the analytical models available for preliminary calculations assume the angle changes are independent from thickness. Second, most experimental techniques assume an ideal mold geometry and only measure the part. Third, the angle change is measured in one location rather than across the entire part.

Chapter 7 explores the use of a laser measurement technique to quantify warpage. The laser scans part surfaces creating a virtual point cloud. This is further post-processed into a 3D CAD file. By comparing a 3D representation of mold and part a more accurate warpage was measured. The angle was measured along the part averaging every 10 mm and compared to the dimensions of the mold in the same locations. The results showed that thickness has a big influence in the angle change of corner parts that cannot be captured with analytical models. This technique has the potential to measure warpage of complex mold and part geometries in real industrial settings.

6.1 Introduction

The spring-forward effect refers to the angle change in corners of thermally molded composite materials, see Fig. 6.1 [46]. In pre-impregnated materials (prepreg), glass/carbon fiber plies have

thermoset resin impregnated in an un-reacted state. After refrigerated storage, to avoid premature cross-linking, the prepreg is placed in the mold and cured under high temperature and pressure in an autoclave or out-of-clave manufacturing process.

The laminates are subjected to elevated temperatures for fast polymerization and cross-linking during processing, also referred to as curing. At the elevated temperature and before curing, the material has not yet developed residual stresses. However, during curing, phase change effects lead to formation of residual stresses, which can impact the dimensional stability of laminated structures. Upon cooling from the elevated cure temperature, residual stresses continue to develop in the component due to the thermal expansion mismatch along and across the fiber directions, which add to stress resulting from phase change as well as cure shrinkage of the epoxy resins. The shrinkage and residual stresses cause dimensional distortions upon release from the mold. Fig. 6.2 shows three of the causes of residual stresses [46].

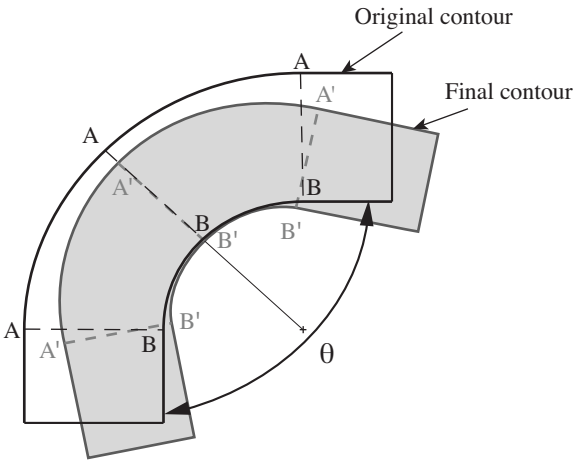

Figure 6.1: Spring forward effect in corners of thermally molded composites. Used with permission from Osswald [46].

A number of models have been developed to describe the macroscopic mechanical properties of continuous fiber reinforced thermosets. These models are closely related to the literature survey presented in Chapter 5. Some of the articles will be presented again from the perspective of residual stress build-up. Hahn and Kim [143] developed a model that approximated a linear correlation between the elastic modulus and the degree of cure. Bogetti and Gillespie [82] found a one-dimensional model to explain the effect of temperature gradients and degree of cure on residual stresses in thick

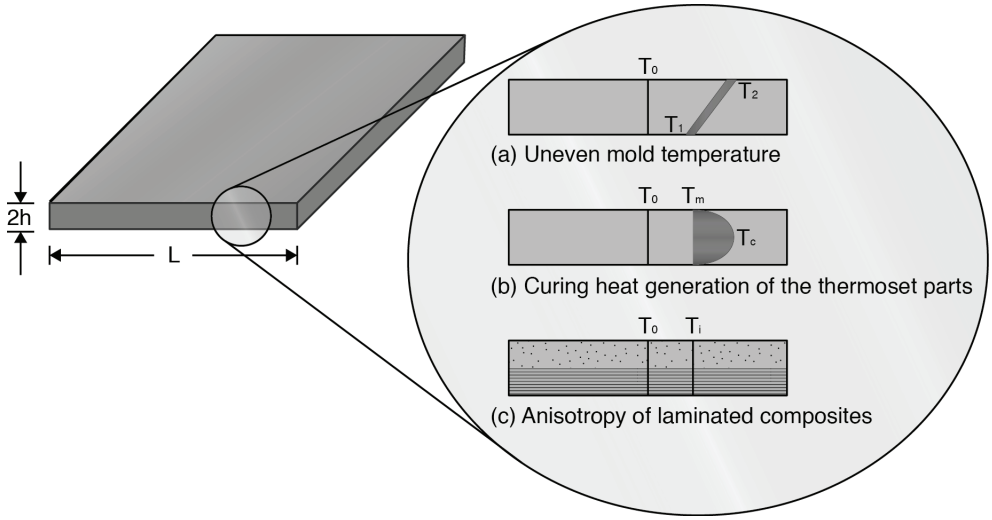

Figure 6.2: Possible causes of residual stresses build-up across the thickness of the part. Used with permission from Osswald [46].

laminates. In this model, cure kinetics, through-thickness energy balance, and elastic laminated plate theory were combined. White and Hahn also developed a model to predict residual stresses in composite materials during cure [93]. Their model combines cure kinetics coupled with the energy balance and viscoelastic material behavior. Later, White and Kim [97] showed the complexity in rheology of curing epoxy and developed a viscoelastic finite element model. A newer model has been provided by Prasatya et al. [101]; they predicted residual stresses in three-dimensional laminates using a thermo-viscoelastic model. Their results showed that elastic calculations significantly overestimate residual stresses and that viscoelastic effects cannot be ignored. Ersoy et al. conducted research on this topic using a simple two-step finite element model [106].

Analytical models to describe the spring-forward effect have also been proposed. O'Neill et al. proposed an elastic model where the warpage of angled composite parts was independent of both, shape and thickness [144]. Their model concluded that the spring-forward angle, $\Delta\theta$, was proportional to the difference between the in plane, α_L, and through thickness, α_L, thermal expansion coefficients, the temperature difference between the solidification temperature, T_s, and the temperature, T, and the initial angle, θ. The model is given by Eq. 6.1.

$$\Delta\theta = \theta \cdot (\alpha_T - \alpha_L)(T_s - T) \tag{6.1}$$

After O'Neill and coworkers work, many analytical models have tried to account for more geometrical, material and processing factors. Ganley et al. identified and quantified four causes of the spring-forward phenomenon in the area of filament wound composites [145]. Their study presented an analytical model derived from a moment balance, corroborated with experiments, which concluded that the coefficient of thermal expansion mismatch between the composite part and the mandrel is the main reason for the angle change. On the other hand, part compaction was concluded to play a minor role, whereas anisotropy with initial curvature and through thickness inhomogeneity were irrelevant in the distortion build-up. Eq. 6.2 shows the angle distortion that can be analytically predicted by knowing the residual strain or stress, which has to be experimentally determined. In Eq. 6.2, h is the part thickness, y is the distance from the neutral axis and $\varepsilon(y)$ is the residual strain.

$$\Delta\theta = \frac{\int_{-\frac{t}{2}}^{\frac{t}{2}} 12\varepsilon(y) \cdot y dy}{h^3} \tag{6.2}$$

Sprowitz et al. [146] and Dong in 2009 [147] used a model based on the influence of the coefficient of thermal expansion. The model has a correction factor when compared to O'Neill's model [144]. The model is written in Eq. 6.3.

$$\Delta\theta = \frac{\theta \cdot (\alpha_T - \alpha_L)(T_s - T)}{1 + \alpha_T \Delta T} \tag{6.3}$$

Further, Dong introduced into Eq. 6.3 a modified coefficient of thermal expansion α' to account for the chemical shrinkage effect [147]. The modified coefficient of thermal expansion α' is shown in Eq. 6.4, where ε_c is the strain due to chemical shrinkage.

$$\alpha' = \alpha - \frac{\varepsilon_c}{\Delta T} \tag{6.4}$$

Ersoy et al. [86] also used a correction factor in O'Neill's model including the effect of a thermal contraction due to chemical shrinkage in plane and through thickness β_L and β_T respectively (Eq. 6.5). This was a simplification of a previous model proposed by Ranford and Rennick which presented significant variation between non-thermoelastic spring forward predictions when compared

to their experimental results [86].

$$\Delta\theta = \theta \cdot (\alpha_T - \alpha_L)(T_s - T) + (\beta_L - \beta_T) \tag{6.5}$$

Despite the amount of work done in the understanding of this manufacturing defect, residual stresses caused during the phase change are not well understood.

While the mathematical or numerical model used for prediction of the spring-forward effect is important, it is equally important to experimentally verify such a model. Many experimental techniques to measure the warpage caused in the manufacturing of curved composites have been proposed. Spencer, Watson and Rogers approached the problem through a mathematical analysis [148]. Ersoy, Potter et al. [86] and many other authors used direct experimental measures to capture the displacement [146, 149]. An example of a different approach is that of Stair et al. who used a translation table and linear voltage displacement transducer to capture the warpage on a flat plate of composite [150].

Most methods focused on analyzing the final component and the results are compared to ideal values of the mold. This assumption could apply in simple geometries, but for complex parts, mold distortions should be included in warpage analysis to accurately determine the deviation with respect to the actual mold geometry. To this effort, this work proposes a laser measurement technique (Laser Diode Device) to capture the shape of the mold and sample into point clouds and measure the angle through CAD software. This technique allows the 3D modeling of the mold and final component, and subsequently a 3D quantification of the warpage. The laser presents point spacing on X from 121 to 282 μm and minimum of 20 μm on Y, depending on scan velocity. It is possible to scan from 18,000 pts/s up until 100,000 pts/s with an associated noise of 40 μm.

6.2 Materials and Methods

6.2.1 Material

Unidirectional carbon epoxy prepreg DA409U/ G35-150, was studied. Material properties for proper manufacturing practices were quantified in previous chapters and obtained from the MSDS.

6.2.2 Sample Preparation

High temperature tacky tape was first applied to the outer edge of an L-shaped mold, followed by three coating layers of mold release, Frekote® 700-NC, on the remaining mold surface (see Fig. 6.3). The 15.24 x 10.16 cm (6 x 4 in) prepreg plies were placed ply-by-ply after adjusting to room temperature from -18 °C for at least 3 hours. This protocol matched the steps used in Chapter 4 to manufacture the beam samples. This sample size allowed for two samples to be cured during one cycle.

The positions of the laminates on the mold were recorded for the purpose of comparing the angle of the final part with the exact location on the mold. A peel ply layer was laid on top of the laminate for easy removal, which was followed by a perforated air film and a layer of breather fabric. The vacuum gauge and outlet were positioned and the mold was sealed with the tacky tape and a heavy-duty vacuum bag. Vacuum was applied to the bag for 15 min to check for and fix any leaks until a 0.09 MPa (13.4 Psi) vacuum pressure was achieved. The assembly was placed in a convective oven Gruenerg B80C46M at a processing cycle based on the kinetics analysis as seen in Fig.6.4 (see also Fig. 4.2(b)). The values shown in Fig. 6.4 neglected the influence of processing pressure (recommended as 2 bar (30 psi)), and the results are not valid for thick parts, however the analysis was used as a baseline to manufacture the L-shaped profiles.

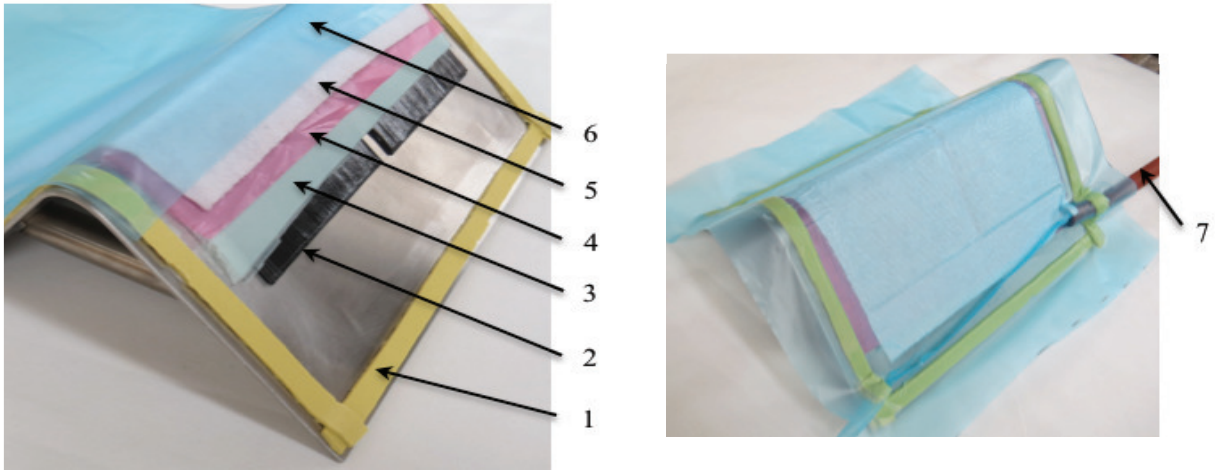

Figure 6.3: Layup in the prepreg-autoclave method: (1) High-Temperature Tacky-Tape, (2) DA 409 U/G35-150 Prepreg Laminate (A.P.C.M.), (3) Peel Ply, (4) Perforated Film, (5) Breather Fabric, (6) Bag Film, and (7) vacuum hose.

The temperature was monitored with a thermometer Fluke 52II during the test, registering a deviation of ± 4 °C. The assembly was removed from the oven once room temperature was reached. Six L-shaped parts with thickness 0.90, 1.80, 2.75, 3.80, 4.50 and 5.40 mm were manufactured in triplicate.

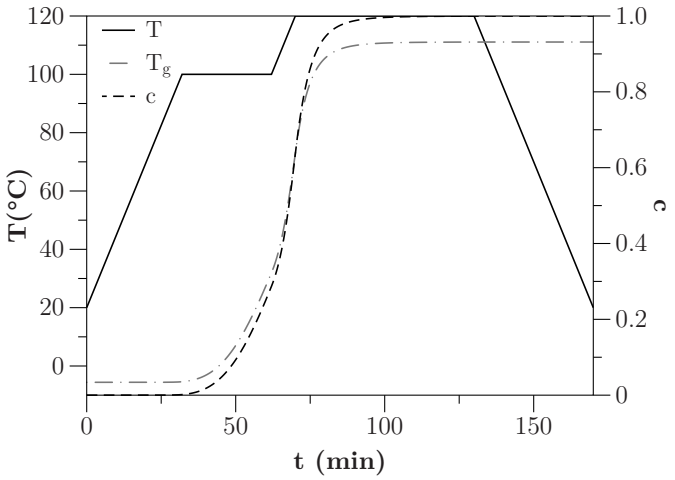

Figure 6.4: Temperature cycle used to manufacture L-shaped profiles.

6.2.3 Protocol

Warpage Measurement via Laser Scanner

The following measurement protocol was implemented using the scanner Shape Grabber^{TM}. The laser followed the part according to laser power, resolution, and laser length trajectory, and recorded the location of thousands of points. These points were processed and viewed on the Shape Grabber^{TM} software.

After capturing the sample shape, a file from the Shape Grabber^{TM} software was imported into Geomagic Studio 11^{TM}. This software was used to import the point cloud image and merge scans (in case of multiple) into a 3D set of images that can be treated to create a reliable virtual reflection of the object's real surface. Finally, the point cloud was transformed into a set of surfaces, and it was exported to SolidWorks^{TM} SPS Academic Version to quantify the 3D warpage of the components with respect to the mold. The mold angle was measured in 10 mm intervals to get a better accuracy of the deviation from the expected mold angle throughout the entire length.

6.3 Results and Discussion

The influence of the thickness on the angle distortion was analyzed to evaluate the accuracy of the proposed technique. The manufacturing process followed the recommendations by previous studies to reduce warpage [151]. Zhu et al. [151] reported that the mold type, mold material, part thickness and fiber orientation had a higher contribution to warpage in curved shapes, compared to dwell temperature, pressure or cooling rate, and this was considered in this work. In their study, Zhu et. al. showed that a female mold with a high thermal conductivity (aluminum mold) gave the lowest spring-forward angle, whereas a male mold with a high thermal conductivity gave the highest angle. Here a female mold was used but steel was preferred over aluminum because it is the standard in most manufacturing processes and for mold longevity.

Fig. 6.5 shows the step by step 3D representation of the mold and the composite L-shaped studied. By scanning several surfaces, a 3D representation of the object can be merged. One disadvantage of this technique is that the scanner fails to capture shiny surfaces. For example, the steel mold and glossy surface of the composite parts in this study. This was solved by covering the parts with a matte water soluble acrylic paint. Careful attention was paid to avoid dripping or excessive paint that can distort the measurements. As shown in Fig. 6.5 this technique captures all the details of the geometry.

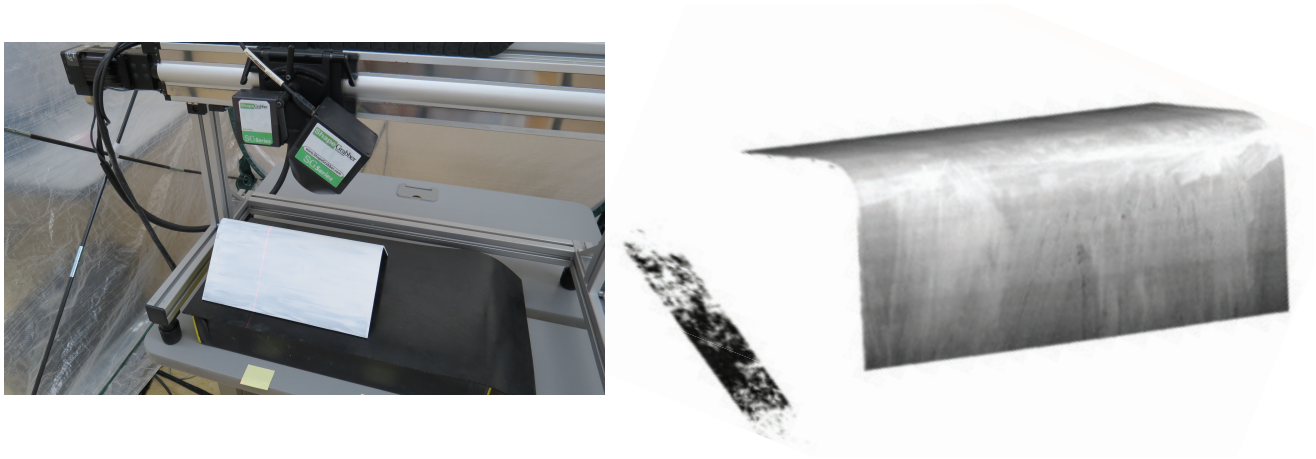

Figure 6.5: Point cloud image captured by the laser scanner and imported into Shape Grabber^{TM} Software.

Fig. 6.6 shows the 3D representation after post-processing the point cloud. Several benefits of this technique are accurate measurements of distances, angles, curvatures, and complex profiles with the use of accessible CAD technology. This technique can also be used as the input of numerical simulations to reverse engineer and optimize molds. The angle analysis presented in this study averaged angles along the length of top and bottom surfaces of the part. This is another advantage when assessing the influence of the mold surface and vacuum bagging in prepreg autoclave molding.

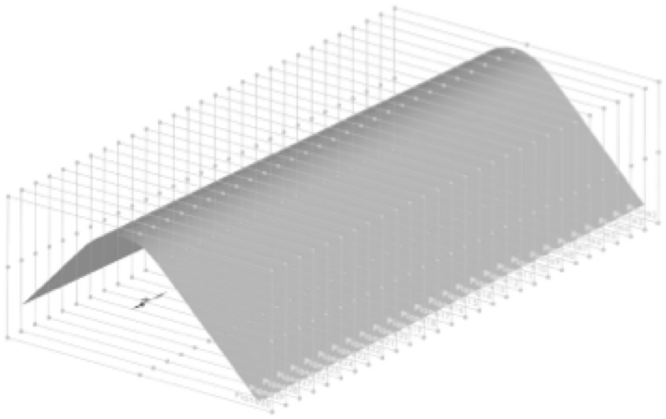

Figure 6.6: Measurement of angle in SolidWorks^{TM} dividing the sample into 10 mm sections.

Fig 6.7 shows the mismatch between our experimental results when compared to the prediction of O'Neill's analytical model that gave a constant angle of 0.24 ° for all parts. Thin profiles exhibited higher angle changes up to 1.25 ° for the 0.9 mm plate thickness. Increasing profile thickness up to 4 times (3.8 mm) reduced the angle change by 50.4 %. Although thickness changes are not always possible in a manufacturing process, this can be used as an aide to reduce warpage in curvature parts. One hypothesis is that the part compliance decreases with the increase of the thickness profile reducing the effect of residual stresses during processing, but this should be further validated with numerical modeling and further testing.

Analytical elastic models failed to predict the angle distortion in parts processed under the same conditions with variable thickness of this study. Similar to previous studies by Zhu et al. [151] and Ersoy et al. [86], our experimental results show that distortion of the L-shaped structure strongly depends on the number of layers, and consequently the thickness. The effect of thickness to warpage agreed with tendencies of three previous studies reported by Ersoy et al. as well as the results

founded in their own work [86].

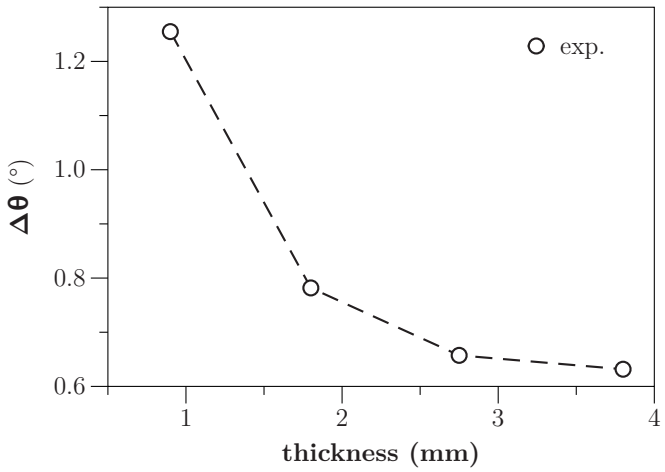

Figure 6.7: Angle average of the difference between mold and part geometry along the length. Measurements using the laser Shape Grabber technique.

6.4 Conclusions

A novel method to measure thermoset composite warpage was presented and evaluated. A laser scanner was used to create a 3D virtual representation of the mold and the part. Several L-shaped profiles of composite DA 409 with thickness between 0.9 and 3.8 mm were manufactured and their angle distortion was evaluated as a function of thickness. The results were compared to O'Neill's analytical model which neglects thickness effects. The results showed that as the thickness increases the angle change reduces. It was shown that preliminary analytical calculations cannot account for the complex composite behavior during manufacturing. Most analytical models reviewed in this work neglect phase change effects on the dimensional stability of curved laminated structures. This may be true for thin parts. However, thick parts cure unevenly, resulting in phase change effects that must be included in order to predict the shrinkage and warpage of the final product. Such effects become evident through experimental studies, which show a strong effect of thickness on warpage. Future efforts involve comparing these measurements with numerical modeling. The goal will be to quantify the most influential factors that affect angle changes as we change the thickness of a component.

Chapter 7

Future Work

The results obtained from the experiments and modeling presented here will be used in numerical studies of warpage in thick plates and L-shaped profiles. Although this is beyond the scope of the present work, preliminary efforts were made to setup a template in the FEA commercial sofware COMSOL Multiphysics. The aim was to validate the capability of current commercial software to model case studies that require coupling of several physical principles. The proper modeling of warpage in thermoset composites involves the anisotropic behavior, energy transfer, kinetic reaction, and the elastic/viscoelastic behavior of the material.

A 2D case study evaluated by many authors [82, 92, 93, 151, 152] was implemented in COMSOL Multiphysics. A thick composite plate of 15 cm in length and 25, 40, and 75 mm in thickness, manufactured via compression molding, was modeled (see Fig. 7.1).

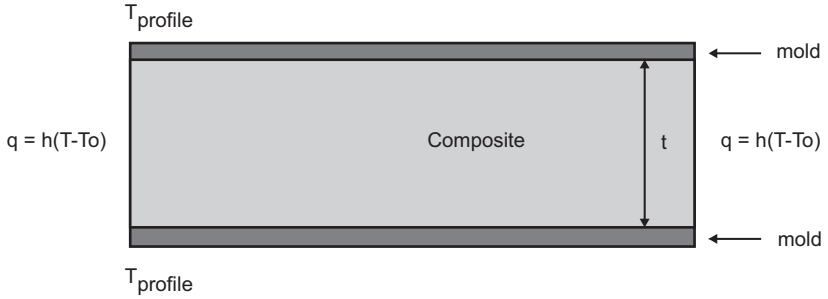

Figure 7.1: Component studied by H.S. Kim and Hahn in 1987 [80].

The dimensions were taken from the work of Hahn and Kim [152] to replicate and compare the accuracy of the software. A vertical symmetry constraint was put on the center of the part, to save computational cost. The rectangular geometry was split into 1 mm horizontal layers to represent the stocking on plies of composite. The number of plies varied from 25 to 75, as the thickness

evaluated was between 2.5 and 7.5 cm. Although a prepreg ply has a thickness of 0.157 mm, the 1 mm thickness was chosen to further reduce computational cost. This does not affect the results as shown by previous authors [82]. The material properties and processing cycle conditions were taken from the work published by Hahn and Kim [80], Bogetti and Gillespie [82], Kim and White [95], and by Zhu et al. [151]. These authors studied the same problem using different simulation methods, reaching similar results. Data includes the material properties of the epoxy, kinetic equation and parameters, temperature cycle, boundary conditions, and geometrical profile.

The solid mechanics, energy and kinetic analysis included the variables and parameters from Bogetti and Gillespie seen in the appendix in Tables 7.1 and 7.2. The following equations were coupled to the structural analysis. The heat transfer analysis included the transient, conductive and heat generation mechanisms.

$$d_z \rho c_p \frac{\partial T}{\partial t} + d_z \rho c_p u \cdot \nabla T = \nabla \cdot (d_z k \nabla T) + d_z Q \tag{7.1}$$

The kinetics reaction was coupled to the energy equation through the heat generation (since it is produce by the released of energy during the exothermal curing reaction) as follows:

$$\rho Q_T \frac{\partial c}{\partial t} = Q \tag{7.2}$$

$$\frac{\partial c}{\partial t} = (k_1 + k_2 c)(1 - c)(0.47 - c), c \leq 0.3 \tag{7.3}$$

$$\frac{\partial c}{\partial t} = k_3(1 - c), c \geq 0.3 \tag{7.4}$$

The simulation results obtained using COMSOL Multiphysics are shown in Figs. 7.2-7.4. The degree of cure and temperature profiles lined up closely with the results in all the previous studies. Overall the temperature gradients and cure mismatch in thick composites was captured. The use of this numerical setup in commercial software will be used in new studies of more complex geometric profiles and material property models, as part of the continuation of this project.

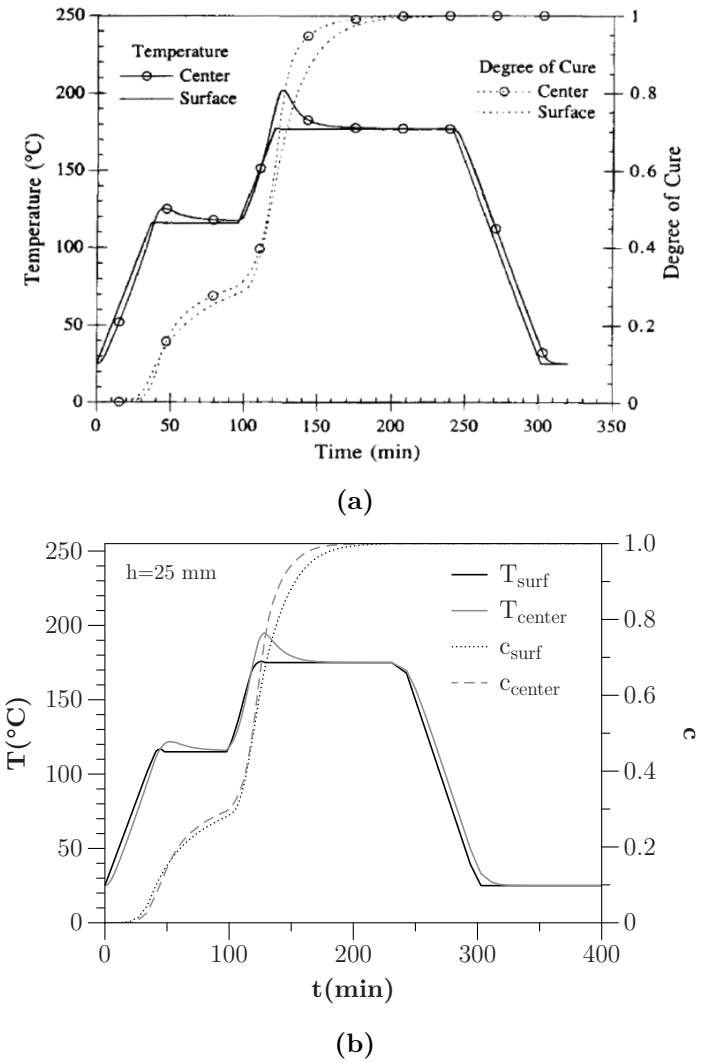

Figure 7.2: Temperature and cure history of a 25 mm thick plate made of CF/EP AS4/3501: (a) results by Y.K. Kim and S.R. White (1991) [93], and (b) comparison using COMSOL Multiphysics.

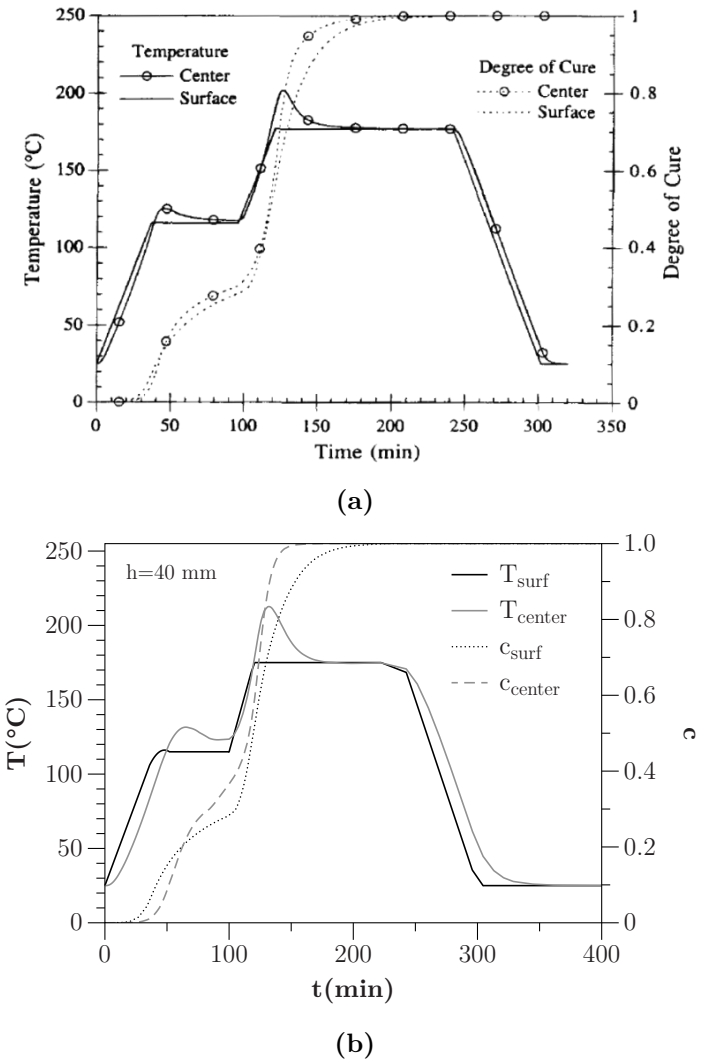

Figure 7.3: Temperature and cure history of a 40 mm thick plate made of CF/EP AS4/3501: (a) results by Zhu et al. (2001) [151], and (b) comparison using COMSOL Multiphysics.

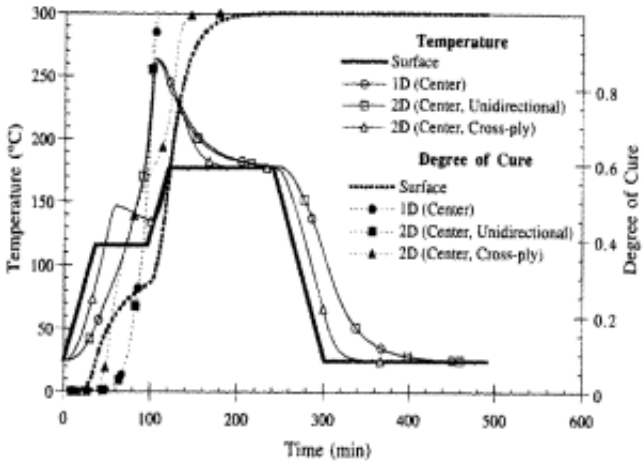

(a)

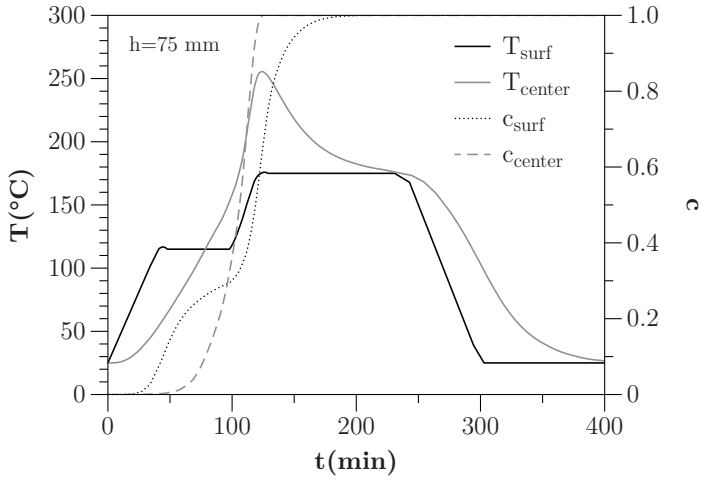

(b)

Figure 7.4: Temperature and cure history of a 75 mm thick plate made of CF/EP AS4/3501: (a) results by Y.K. Kim and S.R. White, 1991 [92], and (b) comparison using COMSOL Multiphysics.

7.1 Appendix

Table 7.1: Parameters used to validate the implementation of residual stresses in COMSOL Multiphysics®.

T_∞	298.15 (K)	$G_{23,f}$	6.894 (MPa)
ρ	1520 $\left(\frac{kg}{m^3}\right)$	$G_{13,f}$	$G_{12,f}$
C_p	0.942 $\left(\frac{kJ}{kg\cdot^oC}\right)$	$E_{1,f}$	206.8 (GPa)
k_z	0.446 $\left(\frac{W}{m\cdot^oC}\right)$	$E_{2,f}$	20.68 (GPa)
Q_T	198.9 $\left(\frac{kJ}{kg}\right)$	$\nu_{12,m}$	ν_m
$E_a, 1$	80.7 $\left(\frac{kJ}{mol}\right)$	$\nu_{13,m}$	ν_m
$E_a, 2$	77.8 $\left(\frac{kJ}{mol}\right)$	$\nu_{23,m}$	ν_m
$E_a, 3$	56.6 $\left(\frac{kJ}{mol}\right)$	$\nu_{12,f}$	0.2
E_m^o	3.447 (MPa)	$\nu_{23,f}$	0.5
E_m^∞	3.447 (GPa)	$\nu_{13,f}$	0.2
γ	0	ν_f	0.67
$c_{mod,gel}$	0	$\alpha_{1,m}$	5.76e-5 $(\frac{1}{K})$
$c_{mod,dif}$	1	$\alpha_{2,m}$	$a_{1,m}$
R	8.314 $\left(\frac{J}{mol\cdot K}\right)$	$\alpha_{1,f}$	-9e-7 $(\frac{1}{K})$
t	0 (s)	$\alpha_{2,f}$	7.2e-6$(\frac{1}{K})$
ν_m	0.35	$\Delta\upsilon$	1 %
$G_{12,f}$	27.58 (GPa)	$G_{23,f}$	6.89 (GPa)

Table 7.2: Variables used used to validate the implementation of residual stresses in COMSOL Multiphysics® Simulation

k_1	$A_1 exp\left(\frac{-E_{a,1}}{RT}\right)$
k_2	$A_2 exp\left(\frac{-E_{a,2}}{RT}\right)$
k_3	$A_3 exp\left(\frac{-E_{a,3}}{RT}\right)$
E_m	$(1-c_{mod})E_m^o + a_{mod} * E_m^\infty + \gamma * c_{mod} * (1-c_{mod})(E_m^\infty - E_m^o)$
c_{mod}	$\frac{c-c_{mod,gel}}{c_{mod,dif}-c_{mod,gel}}$
A_1	2.105e9 (1/min)
A_2	-2.014e9 (1/min)
A_3	1.960e5 (1/min)
G_m	$E_m/(2(1+\nu_m))$
$G_{12,m}$	G_m
$G_{13,m}$	G_m
$G_{23,m}$	G_m
$E_{1,m}$	E_m
$E_{2,m}$	E_m
k_f	$\frac{E_{1,f}}{2(1-\nu_{12,f}-2(\nu_{12,f}^2))}$
E_1	$\frac{E_{1,f}*\nu_f*E_{1,m}*(1-\nu_f)+((4*(\nu_{12,m}-\nu_{12,f}^2)*k_f*k_m*G_{23,m}*(1-\nu_f)*\nu_f))}{((k_f+G_{23,m})*k_m+(k_f-k_m)*G_{23,m}*\nu_f))}$
ν_{12}	$\frac{\nu_{12,f}*\nu_f*\nu_{12,m}*(1-\nu_f)+(((\nu_{12,m}-\nu_{12,f})*(k_m-k_f)*G_{23,m}*(1-\nu_f)*\nu_f))}{((k_f+G_{23,m})*k_m+(k_f-k_m)*G_{23,m}*\nu_f))}$
ν_{23}	$\frac{2*E_1*k_r-E_1*E_2-4(\nu_{12}^2)*k_r*E_2}{2*E_1*k_r}$
ν_{13}	ν_{12}
G_{12}	$\frac{G_{12m}*((G_{12f}+G_{12m})+(G_{12f}-G_{12m})*\nu_f)}{((G_{12f}+G_{12m})-(G_{12f}-G_{12m})*\nu_f)}$
G_{13}	G_{12}
G_{23}	$\frac{(G_{23,m}*(k_m*(G_{23,m}+G_{23,f})+2*G_{23,f}*G_{23,m}+k_m*(G_{23,f}-G_{23,m})*\nu_f))}{(k_m*(G_{23,m}+G_{23,f})+2*G_{23,f}*G_{23,m}-(k_m+2*G_{23,m})*(G_{23,f}-G_{23,m})*\nu_f)}$
E_2	$\frac{1}{\frac{1}{4*k_r}+\frac{1}{4*G_{23}}+\frac{\nu_{12}^2}{E_1}}$
E_3	E_2
k_r	$\frac{((k_f+G_{23,m})*k_m+(k_f-k_m)*G_{23,m}*\nu_f)}{((k_f+G_{23,m})-(k_f-k_m)*\nu_f)}$
ϵ_1	$\frac{(\epsilon_{1,f}*E_{1,f}*\nu_f+\epsilon_{1,m}*E_{1,m}*(1-\nu_f))}{(E_{1,f}*\nu_f+E_{1,m}*(1-\nu_f))}$
ϵ_2	$\frac{(\epsilon_{2,f}+\nu_{12,f}*\epsilon_{1,f})*\nu_f+(\epsilon_{2,m}+\nu_{12,m}*\epsilon_{1,m})*(1-\nu_f)-(\nu_{12,f}*\nu_f+\nu_{12,m}*(1-\nu_f))*((\epsilon_{1,f}*E_{1,f}*\nu_f+\epsilon_{1,m}*E_{1,m}*(1-\nu_f))}{(E_{1,f}*\nu_f+E_{1,m}*(1-\nu_f))}$
ϵ_3	ϵ_2

References

[1] T. A. Osswald and G. Menges, "Historical Background," in *Material Science of Polymers for Engineers (Third Edition)*, pp. 21–47, Hanser, 2012. DOI: 10.3139/9781569905241.002.

[2] Staff, "Resins for the fast zone," *CW, CompositesWorld*, July 2015.

[3] Composites World, "At JEC Europe 2015: Hexcel," Mar. 2015.

[4] Composites World, "Unidirectional carbon fiber prepreg tapes just 15 gsm," June 2015.

[5] S. Black, "Automotive composites. Thermosets for the fast zone.," *CW, CompositesWorld*, Aug. 2015.

[6] S. Goris, J. Puentes, and T. A. Osswald, "Chapter 33: Continuous Fiber-Reinforced Composites Prepreg Layup," in *Manufacturing engineering handbook* (e.-i.-c. Hwaiyu Geng, ed.), New York : McGraw-Hill,, 2nd edition ed., 2015.

[7] U. M. Vakil and G. C. Martin, "Crosslinked epoxies: Network structure characterization and physicalmechanical properties," *J. Appl. Polym. Sci.*, vol. 46, pp. 2089–2099, Dec. 1992.

[8] B. G. Min, Z. H. Stachurski, and J. H. Hodgkin, "Cure kinetics of elementary reactions of a DGEBA/DDS epoxy resin: 1. Glass transition temperature versus conversion," *Polymer*, vol. 34, no. 23, pp. 4908–4912, 1993.

[9] R. E. Lyon, K. E. Chike, and S. M. Angel, "In situ cure monitoring of epoxy resins using fiber-optic Raman spectroscopy," *J. Appl. Polym. Sci.*, vol. 53, pp. 1805–1812, Sept. 1994.

[10] P. Musto, M. Abbate, G. Ragosta, and G. Scarinzi, "A study by Raman, near-infrared and dynamic-mechanical spectroscopies on the curing behaviour, molecular structure and viscoelastic properties of epoxy/anhydride networks," *Polymer*, vol. 48, pp. 3703–3716, June 2007.

[11] J. C. Cruz and T. A. Osswald, "Monitoring epoxy and unsaturated polyester reactions under pressureReaction rates and mechanical properties," *Polym Eng Sci*, vol. 49, pp. 2099–2108, Nov. 2009.

[12] G. A. Kuznetsov, N. I. Nikiforov, R. A. Potekhin, B. A. Kalinin, and O. G. Tarakanov, "Crosslinking density and its effect on the dynamic mechanical properties of rigid polyurethane foams," *Polymer Science U.S.S.R.*, vol. 17, pp. 2824–2831, Jan. 1975.

[13] G. A. Sofer and E. A. Hauser, "A new tool for determination of the stage of polymerization of thermosetting polymers," *J. Polym. Sci.*, vol. 8, pp. 611–620, June 1952.

[14] G. Wisanrakkit, J. K. Gillham, and J. B. Enns, "The glass transition temperature (tg) as a parameter for monitoring the cure of an amine/epoxy system at constant heating rates," *J. Appl. Polym. Sci.*, vol. 41, pp. 1895–1912, Jan. 1990.

[15] I. Alig, M. Fedtke, K.-G. Husler, W. Tnzer, and S. Wartewig, "Modified epoxies as studied by ultrasonic methods," in *Relationships of Polymeric Structure and Properties* (I. Chudek, ed.), no. 78 in Progress in Colloid & Polymer Science, pp. 54–58, Steinkopff, 1998.

[16] W. Stark, M. Jaunich, W. Bohmeyer, and K. Lange, "Investigation of the crosslinking behaviour of ethylene vinyl acetate (EVA) for solar cell encapsulation by rheology and ultrasound," *Polymer Testing*, vol. 31, no. 7, pp. 904–908, 2012.

[17] J. B. Enns and J. K. Gillham, "Timetemperaturetransformation (TTT) cure diagram: Modeling the cure behavior of thermosets," *J. Appl. Polym. Sci.*, vol. 28, pp. 2567–2591, Aug. 1983.

[18] C. C. Riccardi, H. E. Adabbo, and R. J. J. Williams, "Curing reaction of epoxy resins with diamines," *J. Appl. Polym. Sci.*, vol. 29, pp. 2481–2492, Aug. 1984.

[19] M. Opaliki, J. M. Kenny, and L. Nicolais, "Cure kinetics of neat and carbon-fiber-reinforced TGDDM/DDS epoxy systems," *J. Appl. Polym. Sci.*, vol. 61, pp. 1025–1037, Aug. 1996.

[20] S. Swier, G. V. Assche, A. V. Hemelrijck, H. Rahier, E. Verdonck, and B. V. Mele, "Characterization of Reacting Polymer Systems by Temperature-Modulated Differential Scanning Calorimetry," *Journal of Thermal Analysis and Calorimetry*, vol. 54, pp. 585–604, Nov. 1998.

[21] X. Ramis, A. Cadenato, J. Morancho, and J. Salla, "Curing of a thermosetting powder coating by means of DMTA, TMA and DSC," *Polymer*, vol. 44, pp. 2067–2079, Mar. 2003.

[22] R. A. Fava, "Differential scanning calorimetry of epoxy resins," *Polymer*, vol. 9, pp. 137–151, Jan. 1968.

[23] J. P. Creedon, "Thermal Methods for Determination of Degree of Cure of Thermosets," in *Analytical Calorimetry* (R. S. Porter and J. F. Johnson, eds.), pp. 185–199, Springer US, 1970. DOI: 10.1007/978-1-4615-8621-0_17.

[24] M. R. Kamal and S. Sourour, "Kinetics and thermal characterization of thermoset cure," *Polym Eng Sci*, vol. 13, pp. 59–64, Jan. 1973.

[25] S. Sourour and M. R. Kamal, "Differential scanning calorimetry of epoxy cure: isothermal cure kinetics," *Thermochimica Acta*, vol. 14, pp. 41–59, Jan. 1976.

[26] J. Mijovi, "Cure kinetics of neat versus reinforced epoxies," *J. Appl. Polym. Sci.*, vol. 31, pp. 1177–1187, Apr. 1986.

[27] S. Swier and B. Van Mele, "In situ monitoring of reaction-induced phase separation with modulated temperature DSC: comparison between high-Tg and low-Tg modifiers," *Polymer*, vol. 44, pp. 2689–2699, Apr. 2003.

[28] S. Hadiprajitno, J. Hernandez, and T. A. Osswald, "Developing time-temperature-transformation diagrams for unsaturated polyesters using DSC data.," in *2003 Annual Technical Conference of Plastic Engineers*, (Nashville, TN), pp. 818–822, May 2003.

[29] J. P. Hernandez-Ortiz and T. A. Osswald, "A Novel Cure Reaction Model Fitting Technique Based on DSC Scans," *Journal of Polymer Engineering*, vol. 25, no. 1, pp. 23–38, 2005.

[30] N. C. RestrepoZapata, T. A. Osswald, and J. P. Hernndez-Ortiz, "MODELING AND ANALYSIS OF CURE KINETICS OF ALIPHATIC EPOXY RESIN WITH AND WITHOUT DIFFUSION," in *ANTEC-12*, (Orlando, FL), SPE, 2012.

[31] N. C. Restrepo-Zapata, T. A. Osswald, and J. P. Hernndez-Ortiz, "Method for timetemperaturetransformation diagrams using DSC data: Linseed aliphatic epoxy resin," *J. Appl. Polym. Sci.*, vol. 131, Aug. 2014.

[32] N. C. Restrepo-Zapata, T. A. Osswald, and J. P. Hernndez-Ortiz, "Vulcanization of EPDM rubber compounds with and without blowing agents: Identification of reaction events and TTT-diagram using DSC data," *Polym Eng Sci*, vol. 55, pp. 2073–2088, Sept. 2015.

[33] N. Restrepo-Zapata, B. Eagleburger, T. Saari, T. A. Osswald, and J. Hernandez, "Chemo-rheological time-temperature-transformation-viscosity diagram: foamed EPDM rubber compound," *J. Appl. Polym. Sci.*, 2016.

[34] C. Strasser, "Fast Cooling Rates for a Lower Degree of Crystallinity of Polymers," *Application Sheet Thermoplastics-DSC 214 Polyma*, vol. 255, 2013.

[35] C. Strasser, "Simulation of the Crystallization Behavior During Injection Molding by Means of Heat-Flux DSC: Isothermal Crystallization Tests," *Application Sheet Thermoplastics-DSC 214 Polyma*, vol. 255, 2013.

[36] C. Strasser, "High Sensitivity or High Resolution? The Choice of the Heating Rate," *Application Sheet Thermoplastics-DSC 214 Polyma*, vol. 259, 2013.

[37] C. Strasser, "How to Create Amorphous PET in a DSC The Importance of Fast Cooling Rates," *Application Sheet Thermoplastics-DSC 214 Polyma*, vol. 257, 2013.

[38] A. A. Minakov, D. A. Mordvintsev, and C. Schick, "Melting and reorganization of poly(ethylene terephthalate) on fast heating (1000 K/s)," *Polymer*, vol. 45, pp. 3755–3763, May 2004.

[39] Y. Furushima, S. Kumazawa, H. Umetsu, A. Toda, E. Zhuravlev, A. Wurm, and C. Schick, "Crystallization kinetics of poly(butylene terephthalate) and its talc composites," *J. Appl. Polym. Sci.*, vol. 134, pp. n/a–n/a, Apr. 2017.

[40] G. Vanden Poel and V. B. F. Mathot, "High performance differential scanning calorimetry (HPer DSC): A powerful analytical tool for the study of the metastability of polymers," *Thermochimica Acta*, vol. 461, pp. 107–121, Sept. 2007.

[41] M. Rakotomalala, S. Wagner, and M. Dring, "Recent Developments in Halogen Free Flame Retardants for Epoxy Resins for Electrical and Electronic Applications," *Materials*, vol. 3, pp. 4300–4327, Aug. 2010.

[42] H. J. Flammersheim and J. R. Opfermann, "Investigation of Epoxide Curing Reactions by Differential Scanning Calorimetry Formal Kinetic Evaluation," *Macromol. Mater. Eng.*, vol. 286, pp. 143–150, Mar. 2001.

[43] J. Puentes, B. LaQua, L. Iervolino, K. Dahl, M. Knott, and T. A. Osswald, "Review of Analytical Models of Anisotropy Induced Curvature Change via FEA Simulation and an Experimental Study," in *2013 Annual Technical of the Society of Plastic Engineers (ANTEC)*, (Las Vegas, NV), pp. 2630–2637, SPE, May 2014.

[44] H. Janeschitz-Kriegl, H. Wippel, C. Paulik, and G. Eder, "Polymer crystallization dynamics, as reflected by differential scanning calorimetry. Part 1: On the calibration of the apparatus," *Colloid Polym Sci*, vol. 271, pp. 1107–1115, Dec. 1993.

[45] G. W. Ehrenstein, G. Riedel, and P. Trawiel, "Differential Scanning Calorimetry (DSC)," in *Thermal Analysis of Plastics*, pp. 1–110, Carl Hanser Verlag GmbH & Co. KG, Sept. 2004.

[46] T. A. Osswald and G. Menges, "Solidification of Polymers," in *Material Science of Polymers for Engineers (Third Edition)*, pp. 295–337, Hanser, 2012.

[47] H. J. Flammersheim and J. Opfermann, "Formal kinetic evaluation of reactions with partial diffusion control," *Thermochimica Acta*, vol. 337, no. 12, pp. 141 – 148, 1999.

[48] M. Haider, P. Hubert, and L. Lessard, "Cure shrinkage characterization and modeling of a polyester resin containing low profile additives," *Composites Part A: Applied Science and Manufacturing*, vol. 38, pp. 994–1009, Mar. 2007.

[49] N. Rabearison, C. Jochum, and J. C. Grandidier, "A cure kinetics, diffusion controlled and temperature dependent, identification of the Araldite LY556 epoxy," *J Mater Sci*, vol. 46, pp. 787–796, Aug. 2010.

[50] H. L. Friedman, "Kinetics of thermal degradation of char-forming plastics from thermogravimetry. Application to a phenolic plastic," *Journal of Polymer Science Part C: Polymer Symposia*, vol. 6, no. 1, pp. 183–195, 1964.

[51] T. Ozawa, "A New Method of Analyzing Thermogravimetric Data," *Bulletin of the Chemical Society of Japan*, vol. 38, 1965.

[52] A. International, "ASTM E698-16 Standard Test Method for Kinetic Parameters for Thermally Unstable Materials Using Differential Scanning Calorimetry and the Flynn/Wall/Ozawa Method," in *ASTM E698-16*, ASTM International, 2016.

[53] I. V. Arkhangel'skii, A. V. Dunaev, I. V. Makarenko, N. A. Tikhonov, and A. V. Tarasov, *Non-Isothermal Kinetic Methods*. Edition Open Access, Apr. 2013.

[54] E. Rabinowitch, "Collision, coordination, diffusion and reaction velocity in condensed systems.," *Trans. Faraday Soc.*, vol. 33, pp. 1225–1233, 1937.

[55] M. T. Aronhime and J. K. Gillham, "Time-temperature-transformation (TTT) cure diagram of thermosetting polymeric systems," in *Epoxy Resins and Composites III* (K. Duek, ed.), no. 78 in Advances in Polymer Science, pp. 83–113, Springer Berlin Heidelberg, 1986.

[56] J. K. Gillham, "Formation and properties of thermosetting and high Tg polymeric materials," *Polym Eng Sci*, vol. 26, pp. 1429–1433, Nov. 1986.

[57] S. L. Simon and J. K. Gillham, "Thermosetting cure diagrams: Calculation and application," *J. Appl. Polym. Sci.*, vol. 53, pp. 709–727, Aug. 1994.

[58] X. Wang and J. K. Gillham, "TGTemperature property (TgTP) diagram for thermosetting systems: Anomalous behavior of physical properties vs. extent of cure," *J. Appl. Polym. Sci.*, vol. 47, pp. 425–446, Jan. 1993.

[59] G. Kalogiannakis, D. V. Hemelrijck, and G. V. Assche, "Measurements of Thermal Properties of Carbon/Epoxy and Glass/Epoxy using Modulated Temperature Differential Scanning Calorimetry," *Journal of Composite Materials*, vol. 38, pp. 163–175, Jan. 2004.

[60] M. Knott, author, *Development of properties during cure of thermoset polymers*. M.S., The University of Wisconsin-Madison, The University of Wisconsin-Madison, Madison, WI, 2014.

[61] N. C. Restrepo-Zapata and T. A. Osswald, "Cintica de curado de un caucho EPDM y una resina epoxdica aliftica. Modelamineto y anlisis sin y con difusin," *Revista Iberoamericana de polmeros*, vol. 14, pp. 245–254, July 2012.

[62] N. C. RestrepoZapata, T. A. Osswald, and J. P. HernndezOrtiz, "Vulcanization of EPDM rubber compounds with and without blowing agents: Identification of reaction events and TTT diagram using DSC data," *Polymer Engineering & Science*, vol. 55, no. 9, pp. 2073–2088, 2015.

[63] I. M. Hodge, "Physical aging in polymer glasses," *Science*, vol. 267, p. 1945, Mar. 1995.

[64] A. International, "ASTM E228-11 Standard Test Method for Linear Thermal Expansion of Solid Materials With a Push- Rod Dilatometer1," in *ASTM E228-11*, ASTM International, 2011.

[65] A. International, "Standard Test Method for Transition Temperatures and Enthalpies of Fusion and Crystallization of Polymers by Differential Scanning Calorimetry 1," in *ASTM D3418-15*, ASTM International, 2015.

[66] A. T. DiBenedetto, "Prediction of the glass transition temperature of polymers: A model based on the principle of corresponding states," *Journal of Polymer Science Part B: Polymer Physics*, vol. 25, no. 9, pp. 1949–1969, 1987.

[67] C. W. Wise, W. D. Cook, and A. A. Goodwin, "Chemico-diffusion kinetics of model epoxy-amine resins," *Polymer*, vol. 38, pp. 3251–3261, Jan. 1997.

[68] M. Levitsky and B. W. Shaffer, "Thermal Stresses in Chemically Hardening Elastic Media With Application to the Molding Process," *J. Appl. Mech*, vol. 41, pp. 647–651, Sept. 1974.

[69] B. W. Shaffer and M. Levitsky, "Thermoelastic Constitutive Equations for Chemically Hardening Materials," *J. Appl. Mech*, vol. 41, pp. 652–657, Sept. 1974.

[70] A. M. Lindrose, "Ultrasonic wave and moduli changes in a curing epoxy resin," *Experimental Mechanics*, vol. 18, pp. 227–232, June 1978.

[71] M. R. Barone and D. A. Caulk, "A Model for the Flow of a Chopped Fiber Reinforced Polymer Compound in Compression Molding," *J. Appl. Mech.*, vol. 53, pp. 361–371, June 1986.

[72] T. A. Osswald, "Berechnung von Schwindung und Verzug fr SMC- und GMT- Formteile," 1988.

[73] T. A. Osswald, "Berechnung von Schwindung und Verzug fr SMC- und GMT- Formteile.," in *22nd internationale AVK Tagung*, vol. 20, (Mainz, Germany), pp. 1–10, 1989.

[74] O. Specker, T. A. Osswald, and W. Michaeli, "Methoden zur Vorausberechnung der Faserorientierung beim Pressen von SMC mit geschnittenen Glasfasern: Teil1 - Unverrippte Bauelemente; Teil2 - Verrippte Bauelemente.," *Forschungsvereinigung Automobiltechnik*, vol. 87, 1990.

[75] I. Spiriadis, *Berechnung von Schwindung und Verzug fr SMC- und GMT- PreBteilen*. PhD thesis, IKV, RWTH Aachen University, Aachen, 1988.

[76] S.-C. Tseng and T. A. Osswald, "Predicting shrinkage and warpage of thin compression molded fiber reinforced thermoset parts," *Society for the Advancement of Material and Process Engineering*, vol. 24, no. 4, pp. 40–48, 1993.

[77] S.-C. Tseng and T. A. Osswald, "Prediction of Shrinkage and Warpage of Fiber Reinforced Thermoset Composite Parts," *Journal of Reinforced Plastics and Composites*, vol. 13, pp. 698–721, Aug. 1994.

[78] H. Golestanian and A. S. El-Gizawy, "Cure Dependent Lamina Stiffness Matrices of Resin Transfer Molded Composite Parts with Woven Fiber Mats," *Journal of Composite Materials*, vol. 31, pp. 2402–2423, Dec. 1997.

[79] E. Ruiz and F. Trochu, "Thermomechanical Properties during Cure of Glass-Polyester RTM Composites: Elastic and Viscoelastic Modeling," *Journal of Composite Materials*, vol. 39, pp. 881–916, May 2005.

[80] K. S. Kim and H. T. Hahn, "Residual stress development during processing of graphite/epoxy composites," *Composites Science and Technology*, vol. 36, no. 2, pp. 121–132, 1989.

[81] W. I. Lee, A. C. Loos, and G. S. Springer, "Heat of Reaction, Degree of Cure, and Viscosity of Hercules 3501-6 Resin," *Journal of Composite Materials*, vol. 16, pp. 510–520, Nov. 1982.

[82] T. A. Bogetti and J. W. Gillespie, "Process-Induced Stress and Deformation in Thick-Section Thermoset Composite Laminates," *Journal of Composite Materials*, vol. 26, pp. 626–660, May 1992.

[83] A. A. Johnston, *An integrated model of the development of process-induced deformation in autoclave processing of composite structures*. PhD thesis, University of British Columbia, 1997.

[84] T. J. Chapman, J. W. Gillespie, R. B. Pipes, J.-a. E. Manson, and J. C. Seferis, "Prediction of Process-Induced Residual Stresses in Thermoplastic Composites," *Journal of Composite Materials*, vol. 24, pp. 616–643, June 1990.

[85] G. Fernlund, N. Rahman, R. Courdji, M. Bresslauer, A. Poursartip, K. Willden, and K. Nelson, "Experimental and numerical study of the effect of cure cycle, tool surface, geometry, and lay-up on the dimensional fidelity of autoclave-processed composite parts," *Composites Part A: Applied Science and Manufacturing*, vol. 33, pp. 341–351, Mar. 2002.

[86] N. Ersoy, T. Garstka, K. Potter, M. R. Wisnom, D. Porter, and G. Stringer, "Modelling of the spring-in phenomenon in curved parts made of a thermosetting composite," *Composites Part A: Applied Science and Manufacturing*, vol. 41, pp. 410–418, Mar. 2010.

[87] T. M. Curiel and G. Fernlund, "Stress Build-up in Bonded Composite Patch Repair," in *20th technical conference of the American Society for Composites*, (Philadelphia), 2005.

[88] T. Curiel and G. Fernlund, "Deformation and stress build-up in bi-material beam specimens with a curing FM300 adhesive interlayer," *Composites Part A: Applied Science and Manufacturing*, vol. 39, pp. 252–261, Feb. 2008.

[89] L. Khoun, T. Centea, and P. Hubert, "Characterization Methodology of Thermoset Resins for the Processing of Composite Materials - Case Study: CYCOM 890rtm Epoxy Resin," *Journal of Composite Materials*, Dec. 2009.

[90] S. H. Dillman and J. C. Seferis, "Kinetic Viscoelasticity for the Dynamic Mechanical Properties of Polymeric Systems," *Journal of Macromolecular Science: Part A - Chemistry*, vol. 26, pp. 227–247, Jan. 1989.

[91] J. W. Lane, J. C. Seferis, and M. A. Bachmann, "Dielectric studies of the cure of epoxy matrix systems," *J. Appl. Polym. Sci.*, vol. 31, pp. 1155–1167, Apr. 1986.

[92] S. R. White and H. T. Hahn, "Process Modeling of Composite Materials: Residual Stress Development during Cure. Part II. Experimental Validation," *Journal of Composite Materials*, vol. 26, pp. 2423–2453, Jan. 1992.

[93] S. R. White and H. T. Hahn, "Process Modeling of Composite Materials: Residual Stress Development during Cure. Part I. Model Formulation," *Journal of Composite Materials*, vol. 26, pp. 2402–2422, Jan. 1992.

[94] R. A. Schapery, "A method of viscoelastic stress analysis using elastic solutions," *Journal of the Franklin Institute*, vol. 279, no. 4, pp. 268 – 289, 1965.

[95] Y. K. Kim and S. R. White, "Stress relaxation behavior of 3501-6 epoxy resin during cure," *Polym Eng Sci*, vol. 36, pp. 2852–2862, Dec. 1996.

[96] Y. K. Kim and S. R. White, "Viscoelastic Analysis of Processing-Induced Residual Stresses in Thick Composite Laminates," *Mechanics of Composite Materials and Structures*, vol. 4, pp. 361–387, Oct. 1997.

[97] S. R. White and Y. K. Kim, "Process-Induced Residual Stress Analysis of as4/3501-6 Composite Material," *Mechanics of Composite Materials and Structures*, vol. 5, pp. 153–186, Apr. 1998.

[98] Y. K. Kim and S. R. White, "Cure-Dependent Viscoelastic Residual Stress Analysis of Filament-Wound Composite Cylinders," *Mechanics of Composite Materials and Structures*, vol. 5, pp. 327–354, Jan. 1999.

[99] T.-M. Wang, I. M. Daniel, and J. T. Gotro, "Thermoviscoelastic Analysis of Residual Stresses and Warpage in Composite Laminates," *Journal of Composite Materials*, vol. 26, pp. 883–899, June 1992.

[100] D. J. O'Brien, P. T. Mather, and S. R. White, "Viscoelastic Properties of an Epoxy Resin during Cure," *Journal of Composite Materials*, vol. 35, pp. 883–904, May 2001.

[101] P. Prasatya, G. B. McKenna, and S. L. Simon, "A Viscoelastic Model for Predicting Isotropic Residual Stresses in Thermosetting Materials: Effects of Processing Parameters," *Journal of Composite Materials*, vol. 35, pp. 826–848, May 2001.

[102] T. Instruments, *Manual: RSA III Rheometric system analyzer*. T.A. Instruments, 2005.

[103] T. Instruments, *Manual: ARES Rheometer*. T.A. Instruments, 2006.

[104] A. Osmeda, "Measurements of strain induced by chemical shrinkage in polymer composites," *Journal of Polymer Engineering*, vol. 36, no. 4, pp. 431–440, 2015.

[105] T. Garstka, N. Ersoy, K. D. Potter, and M. R. Wisnom, "In situ measurements of through-the-thickness strains during processing of AS4/8552 composite," *Composites Part A: Applied Science and Manufacturing*, vol. 38, pp. 2517–2526, Dec. 2007.

[106] N. Ersoy and M. Tugutlu, "Cure kinetics modeling and cure shrinkage behavior of a thermosetting composite," *Polym Eng Sci*, vol. 50, pp. 84–92, Jan. 2010.

[107] R. Lakes, "Viscoelastic measurement techniques," *Rev. Sci. Instrum.*, vol. 75, pp. 797–810, Apr. 2004.

[108] R. P. Chartoff, J. D. Menczel, and S. H. Dillman, "Dynamic Mechanical Analysis (DMA)," in *Thermal Analysis of Polymers* (J. D. Menczel and R. B. Prime, eds.), pp. 387–495, John Wiley & Sons, Inc., 2009.

[109] C.-Y. M. Tung and P. J. Dynes, "Relationship between viscoelastic properties and gelation in thermosetting systems," *J. Appl. Polym. Sci.*, vol. 27, pp. 569–574, Feb. 1982.

[110] H. H. Winter and F. Chambon, "Analysis of Linear Viscoelasticity of a Crosslinking Polymer at the Gel Point," *Journal of Rheology (1978-present)*, vol. 30, pp. 367–382, Apr. 1986.

[111] H. H. Winter, "Can the gel point of a cross-linking polymer be detected by the G"-G" crossover?," *Polymer engineering and science*, vol. 27, no. 22, pp. 1698–1702, 1987.

[112] J. M. Castro and C. W. Macosko, "Kinetics and Rheology of Typical Polyurethane Reaction Injection Molding Systems," SPE, 1980.

[113] D. U. Shah and P. J. Schubel, "Evaluation of cure shrinkage measurement techniques for thermosetting resins," *Polymer Testing*, vol. 29, pp. 629–639, Sept. 2010.

[114] Y. Nawab, S. Shahid, N. Boyard, and F. Jacquemin, "Chemical shrinkage characterization techniques for thermoset resins and associated composites," *J Mater Sci*, vol. 48, pp. 5387–5409, Apr. 2013.

[115] J. Kay, K. Fahrang, K. Hsiao, and G. Fernlund, "Effect of process conditions on porosity in out-of-autoclave prepreg laminates," in *International Conference on Composite Materials*, (JeJu Island, South Korea), Aug. 2011.

[116] J. Wang, M.-P. G. Laborie, and M. P. Wolcott, "Application of beam mechanics to sensing the cure development of wood-phenolic joints by dynamic mechanical analysis," *Thermochimica Acta*, vol. 465, pp. 18–24, Dec. 2007.

[117] R. D. Adams and A. S. Weinstein, "Flexural Stiffness of Sandwich Beams," *J. Eng. Mater. Technol*, vol. 97, pp. 264–270, July 1975.

[118] A. W. Nolle, "Methods for Measuring Dynamic Mechanical Properties of RubberLike Materials," *Journal of Applied Physics*, vol. 19, pp. 753–774, Aug. 1948.

[119] A. Maffezzoli, E. Quarta, V. a. M. Luprano, G. Montagna, and L. Nicolais, "Cure monitoring of epoxy matrices for composites by ultrasonic wave propagation," *J. Appl. Polym. Sci.*, vol. 73, pp. 1969–1977, Sept. 1999.

[120] F. Lionetto, F. Montagna, and A. Maffezzoli, "Ultrasonic dynamic mechanical analysis of polymers," *Applied Rheology*, vol. 15, no. 5, pp. 326–335, 2005.

[121] F. Lionetto and A. Maffezzoli, "Monitoring the cure state of thermosetting resins by ultrasound," *Materials*, vol. 6, no. 9, pp. 3783–3804, 2013.

[122] R. Meier, S. Zaremba, F. Springl, K. Drechsler, F. Gaille, and C. Weimer, "ONLINE PROCESS MONITORING SYSTEMSBENCHMARK AND TEST STUDY," in *Flow Processes in Composites Materials-11*, (Auckland, New Zeland), July 2012.

[123] M. Frigione, A. Maffezzoli, D. Acierno, V. a. M. Luprano, and G. Montagna, "Nondestructive and in-situ monitoring of mechanical property buildup in epoxy adhesives for civil applications by propagation of ultrasonic waves," *Polym Eng Sci*, vol. 40, pp. 656–664, Mar. 2000.

[124] J. Mc Hugh, *Ultrasound technique for the dynamic mechanical analysis (DMA) of polymers.* Bundesanstalt fr Materialforschung und-prfung (BAM), 2008.

[125] V. Janarthanan and G. Thyagarajan, "Temperature and radiation effects on the Raman bands of epoxy resin," *J Chem Sci*, vol. 102, pp. 721–723, Oct. 1990.

[126] J. C. Cruz, M. Kemper, and T. A. Osswald, "Precise curing analysis of accelerated unsaturated polyester reactions under Raman spectroscopy," in *2006 Annual Technical of the Society of Plastic Engineers (ANTEC)*, (Charlotte, NC), pp. 2828–2832, SPE, May 2006.

[127] J. C. Cruz, M. Kemper, and T. A. Osswald, "Monitoring curing reactions of thermosets under high pressure by use of Raman spectroscopy," in *2007 Annual Technical of the Society of Plastic Engineers (ANTEC)*, (Cincinnatti, OH), pp. 2129–2133, SPE, May 2007.

[128] Y. Nawab, P. Casari, N. Boyard, and F. Jacquemin, "Characterization of the cure shrinkage, reaction kinetics, bulk modulus and thermal conductivity of thermoset resin from a single experiment," *J Mater Sci*, vol. 48, pp. 2394–2403, Nov. 2012.

[129] M. K. Saraswat, K. M. B. Jansen, and L. J. Ernst, "Cure Shrinkage and Bulk Modulus Determination for Moulding Compounds," in *2006 1st Electronic Systemintegration Technology Conference*, vol. 2, pp. 782–787, Sept. 2006.

[130] J. Puentes, L. Wruck, A. Chaloupka, N. Rudolph, and T. A. Osswald, "Combining Wave and Spectroscopic Techniques To Monitor The Development Of Thermosets During Cure," in *European Conference on Composite Materials*, (Munich, Germany), June 2016.

[131] T. J. Rmer, J. F. Brennan, G. J. Puppels, A. H. Zwinderman, S. G. v. Duinen, A. v. d. Laarse, A. F. W. v. d. Steen, N. A. Bom, and A. V. G. Bruschke, "Intravascular Ultrasound Combined With Raman Spectroscopy to Localize and Quantify Cholesterol and Calcium Salts in Atherosclerotic Coronary Arteries," *Arterioscler Thromb Vasc Biol*, vol. 20, pp. 478–483, Feb. 2000.

[132] P. Instruments, "Raman spectroscopy basics," 2016.

[133] R. T. Ko, C. W. Lee, T. Storage, and M. Y. Chen, "Ultrasonic measurements of polyimide materials during heating," in *AIP Conference Proceedings*, vol. 1430, pp. 1699–1706, AIP Publishing, May 2012.

[134] L. Yadav, *Organic Spectroscopy*. Springer Science & Business Media, 2005.

[135] X. Ning, I. W. Selesnick, and L. Duval, "Chromatogram baseline estimation and denoising using sparsity (BEADS)," *Chemometrics and Intelligent Laboratory Systems*, vol. 139, pp. 156–167, Dec. 2014.

[136] L. Wruck, *Development of a measuring chamber to characterize the cure dependent properties of thermosets using ultrasound and Raman-spectroscopy*. M.S., University of Wisconsin-Madison, Madison, WI, 2016.

[137] A. International, "Standard Guide for Raman Shift Standards for Spectrometer Calibration," in *ASTM E1840 - 96*, ASTM International, 2014.

[138] S. J. Choquette, E. S. Etz, W. S. Hurst, D. H. Blackburn, and S. D. Leigh, "Relative intensity correction of Raman spectrometers: NIST SRMs 2241 through 2243 for 785 nm, 532 nm, and 488 nm/514.5 nm excitation," *Appl Spectrosc*, vol. 61, pp. 117–129, Feb. 2007.

[139] Dring, J., Bartush, J., McHugh, J., and Stark, W., "Contribution to Ultrasound Cure Control for Composite Manufacturing," (Roma (Italy)), The International Committee for Non-Destructive Testing ICNDT, Oct. 2000.

[140] D. W. Van Krevelen and K. Te Nijenhuis, "Chapter 14 - Acoustic Properties," in *Properties of Polymers (Fourth Edition)*, pp. 505–522, Amsterdam: Elsevier, 2009. DOI: 10.1016/B978-0-08-054819-7.00014-5.

[141] J. McHugh, *Ultrasound Technique for the Dynamic Mechanical Analysis (DMA) of Polymers*. PhD thesis, Technical University of Berlin, Berlin, Germany, 2008.

[142] D. r. n. J. Krautkrmer and D. r. n. H. Krautkrmer, "Attenuation of Ultrasonic Waves in Solids," in *Ultrasonic Testing of Materials*, pp. 107–118, Springer Berlin Heidelberg, 1983. DOI: 10.1007/978-3-662-02357-0_7.

[143] C. D. Han and K.-W. Lem, "Chemorheology of thermosetting resins. IV. The chemorheology and curing kinetics of vinyl ester resin," *J. Appl. Polym. Sci.*, vol. 29, pp. 1879–1902, May 1984.

[144] J. M. O'Neill, T. G. Rogers, and A. J. M. Spencer, "Thermally induced distortions in the moulding of laminated channel sections," *Mathematical Engineering in Industry*, vol. 2, no. 1, pp. 65–72, 1988.

[145] J. M. Ganley, A. K. Mawi, and S. Huybrechts, "Explaining Spring-In in Filament Wound Carbon Fiber/Epoxy Composites," *Journal of Composite Materials*, vol. 34, pp. 1216–1239, July 2000.

[146] T. Sprwitz, T. Wille, M. Kleineberg, and J. Tessmer, "Spring-In Simulation in Fiber-Composite Manufacturing," in *13th European Conference for Composites Materials*, (Stockholm, Sweden), June 2008.

[147] C. Dong, "Modeling the Dimensional Variations of Composites Using Effective Coefficients of Thermal Expansion," *Journal of Composite Materials*, Aug. 2009.

[148] A. J. M. Spencer, P. Watson, and T. G. Rogers, "Mathematical analysis of the springback effect in laminated thermoplastic channel sections," *Composites Manufacturing*, vol. 2, no. 3, pp. 253 – 258, 1991.

[149] N. Ersoy, K. Potter, M. R. Wisnom, and M. J. Clegg, "Development of spring-in angle during cure of a thermosetting composite," *Composites Part A: Applied Science and Manufacturing*, vol. 36, pp. 1700–1706, Dec. 2005.

[150] S. Stair, R. W. Mailen, T. Vo, and D. A. Jack, "Manufacturing induced curvature of carbon fiber laminates: experimental observation and model validation," in *Annual Technical Conference of Plastic Engineers*, (Las Vegas, NV), Apr. 2013.

[151] Q. Zhu, P. H. Geubelle, M. Li, and C. L. Tucker, "Dimensional Accuracy of Thermoset Composites: Simulation of Process-Induced Residual Stresses," *Journal of Composite Materials*, vol. 35, pp. 2171–2205, Dec. 2001.

[152] H. T. Hahn and N. J. Pagano, "Curing Stresses in Composite Laminates," *Journal of Composite Materials*, vol. 9, pp. 91–106, Jan. 1975.